NAVAL POSTGRADUATE SCHOOL
MONTEREY, CALIFORNIA

THESIS

PROPAGATION LOSS STUDY AND ANTENNA DESIGN FOR THE MICRO-REMOTELY POWERED VEHICLE (MRPV)

by

Thad B. Gibson

September 1995

Thesis Advisor: David Jenn

Approved for public release; distribution is unlimited.

REPORT DOCUMENTATION PAGE

Form Approved
OMB No. 0704-0188

1.AGENCY USE ONLY *(Leave blank)*	2.REPORT DATE	3.REPORT TYPE AND DATES COVERED
	September 1995	Master's Thesis

4.TITLE AND SUBTITLE
PROPAGATION LOSS STUDY AND ANTENNA DESIGN FOR THE MICRO-REMOTELY POWERED VEHICLE (MRPV)

5.FUNDING NUMBERS

6.AUTHOR(S)
GIBSON, Thad B.

7.PERFORMING ORGANIZATION NAME(S) AND ADDRESS(ES)
Naval Postgraduate School
Monterey CA 93943-5000

8.PERFORMING ORGANIZATION REPORT NUMBER

9.SPONSORING/MONITORING AGENCY NAME(S) AND ADDRESS(ES)

10.SPONSORING/MONITORING AGENCY REPORT NUMBER

11.SUPPLEMENTARY NOTES
The views expressed in this thesis are those of the author and do not reflect the official policy or position of the Department of Defense or the U.S. Government.

12a.DISTRIBUTION/AVAILABILITY STATEMENT
Approved for public release; distribution is unlimited.

12b. DISTRIBUTION CODE

This thesis presents a propagation study and antenna design for the Micro-Remotely Powered Vehicle (MRPV). A propagation loss study was conducted to determine the attenuation of various building walls and to select an optimum frequency band for antenna design. An approximate ray tracing model for loss determination was developed and programmed in MATLAB. The computed losses from the model are presented for comparison with measured results. One possible antenna configuration for the MRPV, a circumferential slot, is analyzed and design parameters varied to obtain optimum antenna gain. A prototype of the slot antenna was developed. The antenna patterns, efficiency, and Voltage Standing Wave Ratio (VSWR) are presented.

14. SUBJECT TERMS Propagation loss, modeling, antenna design			15.NUMBER OF PAGES 117
			16.PRICE CODE
17. SECURITY CLASSIFICATION OF REPORT	18. SECURITY CLASSIFICATION OF THIS PAGE	19.SECURITY CLASSIFICATION OF ABSTRACT	20.LIMITATION OF ABSTRACT
Unclassified	Unclassified	Unclassified	UL

NSN 7540-01-280-5500

Standard Form 298 (Rev. 2-89)
Prescribed by ANSI Std. 239-18
298-102

Approved for Public release; distribution is unlimited

PROPAGATION LOSS STUDY AND ANTENNA DESIGN FOR THE MICRO-REMOTELY POWERED VEHICLE (MRPV)

Thad B. Gibson
Electronics Engineer, Department of Navy
B.S., The University of Texas at El Paso, 1990

Submitted in partial fulfillment of the
requirements for the degree of

MASTER OF SCIENCE IN ELECTRICAL ENGINEERING

from the

NAVAL POSTGRADUATE SCHOOL
SEPTEMBER, 1995

Author: _____
Thad B. Gibson

Approved by: _____
David C. Jenn, Thesis Advisor

_____
Gurnam S. Gill, Second Reader

_____
Michael A. Morgan, Chairman
Department of Electrical and Computer Engineering

ABSTRACT

This thesis presents a propagation study and antenna design for the Micro-Remotely Powered Vehicle (MRPV). A propagation loss study was conducted to determine the attenuation of various building walls and to select an optimum frequency band for antenna design. An approximate ray tracing model for loss determination was developed and programmed in MATLAB. The computed losses from the model are presented for comparison with measured results. One possible antenna configuration for the MRPV, a circumferential slot, is analyzed and design parameters varied to obtain optimum antenna gain. A prototype of the slot antenna was developed. The antenna patterns, efficiency, and Voltage Standing Wave Ratio (VSWR) are presented.

TABLE OF CONTENTS

I. INTRODUCTION 1

A. BACKGROUND 1

1. Beamed Microwave Power 1

2. Micro-Remotely Powered Vehicle (MRPV) 3

B. OBJECTIVE 4

II. PROPAGATION LOSS MEASUREMENTS 7

A. MEASUREMENT SYSTEM 7

1. Transmitting and Receiving Stations 8

2. Transmit and Receive Antennas 9

3. Equipment Listing 10

B. MEASUREMENTS 10

1. Building Walls 11

2. Measured Data 12

III. PROPAGATION LOSS MODELING 13

A. BACKGROUND 13

1. Spherical and Planar Electromagnetic Waves 13

2. Plane Waves at Oblique Incidence on an Interface 14

3. Plane Waves at Oblique Incidence on a Double Interface 17

B. PROPAGATION OF A SPHERICAL WAVEFRONT 19

1. Direct Path 19

2. Geometric Relationships for the Direct Path 22

3. Reflected Path 25

4. Beam Shaping 29
5. Total Received Field 30
C. MODELING RESULTS 31
1. Overview 31
2. Comparison of Computed and Measured Data 31
3. Summary 35

IV. ANTENNA DESIGN 37
A. BACKGROUND 37
1. Configurations 37
2. Circumferential Slot 38
B. SIMULATION 39
1. Method of Moments 39
2. Antenna Model 40
3. Results 44
C. ANTENNA PROTOTYPE 49

V. ANTENNA MEASUREMENTS 51
A. Antenna Parameters 51
B. Pattern Measurement 53
1. Test Set-Up 54
2. Far-Field Measurements 55
C. RF TO DC POWER CONVERSION 58
1. Antenna Efficiency 58
2. Rectenna Efficiency 62

VI. CONCLUSIONS....63
A. Summary....63
B. Future Considerations....64

APPENDIX A - WALL LOSS DATA....67
APPENDIX B - MATLAB PROGRAM....77
APPENDIX C - SINGLE FREQUENCY PLOTS....87
APPENDIX D - ANTENNA PARAMETER PLOTS....93

LIST OF REFERENCES....95

INITIAL DISTRIBUTION LIST....97

LIST OF FIGURES

Figure 1. Beamed power transmission 2

Figure 2. MRPV geometry 4

Figure 3. Propagation loss measurement system 7

Figure 4. Measurement system block diagram 8

Figure 5. Parabolic reflector antennas with log periodic feed 9

Figure 6. Test set-up 11

Figure 7. Loss measurements of typical building walls 12

Figure 8. Local plane wave approximation 14

Figure 9. Plane wave at oblique incidence - single interface 14

Figure 10. Plane wave at oblique incidence - double interface 17

Figure 11. Locally plane sections of a spherical wave 20

Figure 12. Equivalent source location 21

Figure 13. Equivalent source and antenna integration grid 22

Figure 14. Direct rays 23

Figure 15. Antenna grid - incident angle 24

Figure 16. Equivalent image source - reflected waves 27

Figure 17. Insertion loss of .25" glass pane 32

Figure 18. Insertion loss of 1.75" wood doors 32

Figure 19. Insertion loss of 5.5" wall w/ chalkboard 33

Figure 20. Insertion loss of 10.75" cement wall 33

Figure 21. Insertion loss of 1.75" metal doors 34

Figure 22. Possible antenna configurations 38

Figure 23. Voltage source excitation with PATCH 40

Figure 24. Edge fed slot antenna - isotropic view 41
Figure 25. Edge fed slot antenna - profile view 42
Figure 26. Center fed slot antenna - isotropic view 43
Figure 27. Center fed slot antenna - profile view 43
Figure 28. E-plane of edge fed slot antenna 45
Figure 29. H-plane of edge fed slot antenna 46
Figure 30. E-plane of center fed slot antenna 47
Figure 31. H-plane of center fed slot antenna 48
Figure 32. Prototype antenna 49
Figure 33. Circumferential slot antenna - prototype 50
Figure 34. Scattering parameter measurement 51
Figure 35. Smith chart of slot antenna 52
Figure 36. NPS X-band anechoic chamber 54
Figure 37. Far-field pattern measurements 55
Figure 38. Measured E-plane pattern 56
Figure 39. Measured H-plane pattern 57
Figure 40. Polynomial approximation to E plane data 61
Figure 41. Loss measurement of .25" glass pane, 2 to 2.9 GHz 67
Figure 42. Loss measurement of .25" glass pane, 2.9 to 6 GHz 68
Figure 43. Loss measurement of 1.75" wood doors, 2 to 2.9 GHz 69
Figure 44. Loss measurement of 1.75" wood doors, 2.9 to 6 GHz 70
Figure 45. Loss measurement of 5.5" wall w/ chalkboard, 2 to 2.9 GHz 71
Figure 46. Loss measurement of 5.5" wall w/ chalkboard, 2.9 to 6 GHz 72
Figure 47. Loss measurement of 10.75" cement wall, 2 to 2.9 GHz 73
Figure 48. Loss measurement of 10.75" cement wall, 2.9 to 6 GHz 74

Figure 49. Loss measurement of 1.75" metal doors, 2 to 2.9 GHz.....75
Figure 50. Loss measurement of 1.75" metal doors, 2.9 to 6 GHz.....76
Figure 51. Magnitude of direct rays at 2.5 GHz.....87
Figure 52. Phase of direct rays at 2.5 GHz.....88
Figure 53. Magnitude of reflected rays at 2.5 GHz.....89
Figure 54. Phase of reflected rays at 2.5 GHz.....90
Figure 55. Magnitude of combined rays at 2.5 GHz.....91
Figure 56. Phase of combined rays at 2.5 GHz.....92
Figure 57. Slot antenna impedance measurement - 8 to 12 GHz.....93
Figure 58. Slot antenna reflection loss measurement - 8 to 12 GHz.....94

LIST OF TABLES

Table 1. Equipment listing 10

Table 2. Typical building walls 12

Table 3. Summary of propagation loss measurements and calculations 35

ACKNOWLEDGEMENTS

I would like to extend my sincere gratitude to my thesis advisor, Prof. David Jenn, for his patience and guidance on this project. He provided me with the knowledge and insight necessary to complete this thesis.

I would also like to thank Prof. Rama Janaswamy and Prof. Gurnam Gill for their assistance in reviewing this thesis. In addition, I would like to thank Bob Vitale and ET1(SW) Mark Schooley for the technical assistance provided to me during tests conducted in the microwave lab and anechoic chamber.

I would also like to extend a special thanks to my parents for their un-ending support and encouragement in furthering my education.

Lastly, and foremost, I would like to thank my wife Martha for her love and support throughout my education at the Naval Postgraduate School. I extend to her my deepest appreciation for enduring the long hours of study that were required to complete my coursework and thesis research in one year.

I. INTRODUCTION

A. BACKGROUND

1. Beamed Microwave Power

The concept of beamed microwave power transmission was first introduced in the 1960's. Under U.S. Air Force funding, the Raytheon Company led the pioneering research efforts which resulted in an S-band (2.45 GHz) power beamed helicopter platform in 1964 [Ref. 1]. The demonstration of a beam riding helicopter soon followed in 1969. The beam riding helicopter guided itself using a microwave beam as a position reference for roll, pitch, yaw, and x and y translation. As a means of transferring energy, the main advantage of beamed microwave power transmission is in placement of the power source on the ground. A ground based microwave power source allows for the design of a very small platform with unlimited duration. Due to the large mass to power ratio required for batteries and internal combustion devices, it is not possible to design very small airborne platforms for even short ranges given current technology. A diagram of the principal elements for beamed power transmission is shown in Figure 1.

The beamed power transmission consists of a dc to microwave power conversion, transmitting antenna, free space transmission with possible blockage, and the microwave power reception and conversion to dc. The theoretical maximum efficiencies for each element of transmission are typically: dc to microwave power conversion - 90%, antenna efficiency - 97%, reception and conversion to dc - 92%. Therefore, a maximum overall dc to dc efficiency of

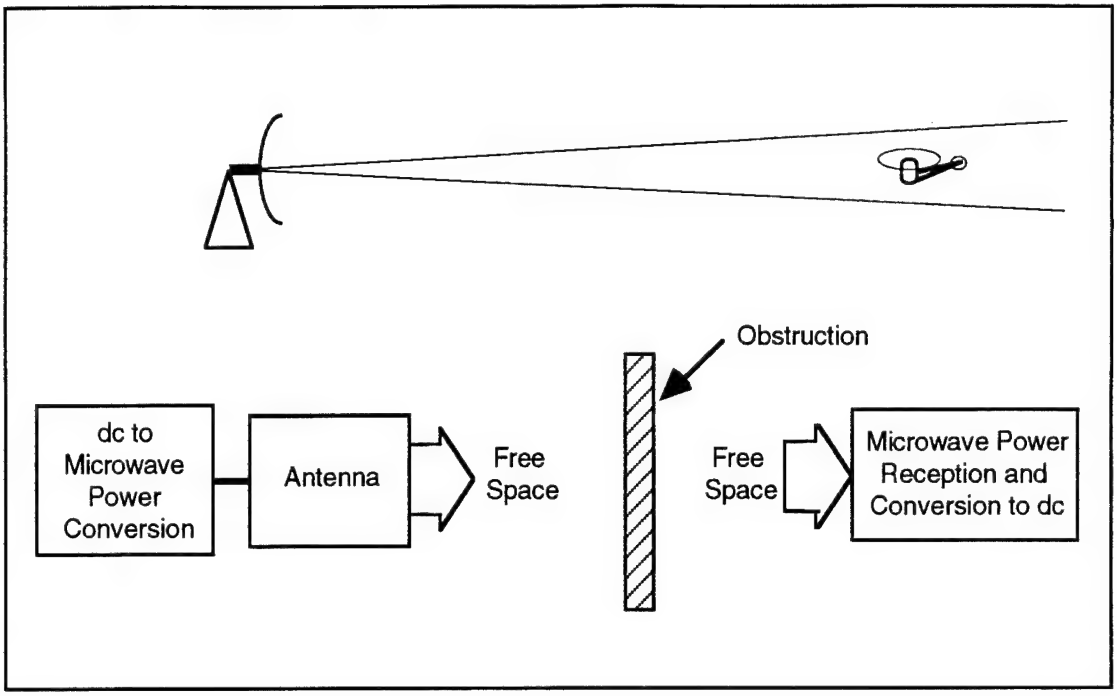

Figure 1. Beamed power transmission

76% is possible. A certified experimental overall dc to dc efficiency of 54% has been achieved in the laboratory [Ref. 2].

The beamed power is limited in transmission by the loss resulting from the spreading of the electromagnetic wave front as it propagates with distance and the loss due to any blockage encountered. The spreading loss is a function of distance, and beyond that, can only be improved by increasing the directivity of the antenna field pattern. The blockage loss depends on the electrical properties and physical characteristics of the obstruction. Therefore, the transmitted power must be determined from the required receive power and losses expected during the propagation of the beamed microwave power.

The reception and conversion from beamed microwave power to dc is performed by a device known as the "rectenna." The rectenna, as its name

suggests, consists of an antenna and a rectifier. In its simplest form, the device can be a half-wave dipole with impedance matching circuitry, terminating into a rectifying diode.

2. Micro-Remotely Powered Vehicle (MRPV)

The MRPV is a microwave power beamed surveillance helicopter currently under development with the Advanced Research Projects Agency (ARPA). The system requirements for the MRPV are as follows:

1) Provide immediate, continuous, video surveillance of the inside of any desired building or volume to a nearby unit.

2) Remain inexpensive and be covert.

3) Maintain Department of Defense (DOD), Department of Justice (DOJ), and commercial applications.

The MRPV is a very small (~2 cm^2), quiet, rotary wing aircraft with unlimited mission duration using a video camera for both real-time platform control and telemetry. The MRPV will be able to fly out at ranges greater than 50 m and monitor a scene with unlimited mission duration. The small size will also make the MRPV difficult to detect or destroy. The applications for MRPV will include: indoor building surveillance, monitoring of disputed borders, tactical military surveillance, and commercial remote monitoring. The MRPV geometry is shown in Figure 2.

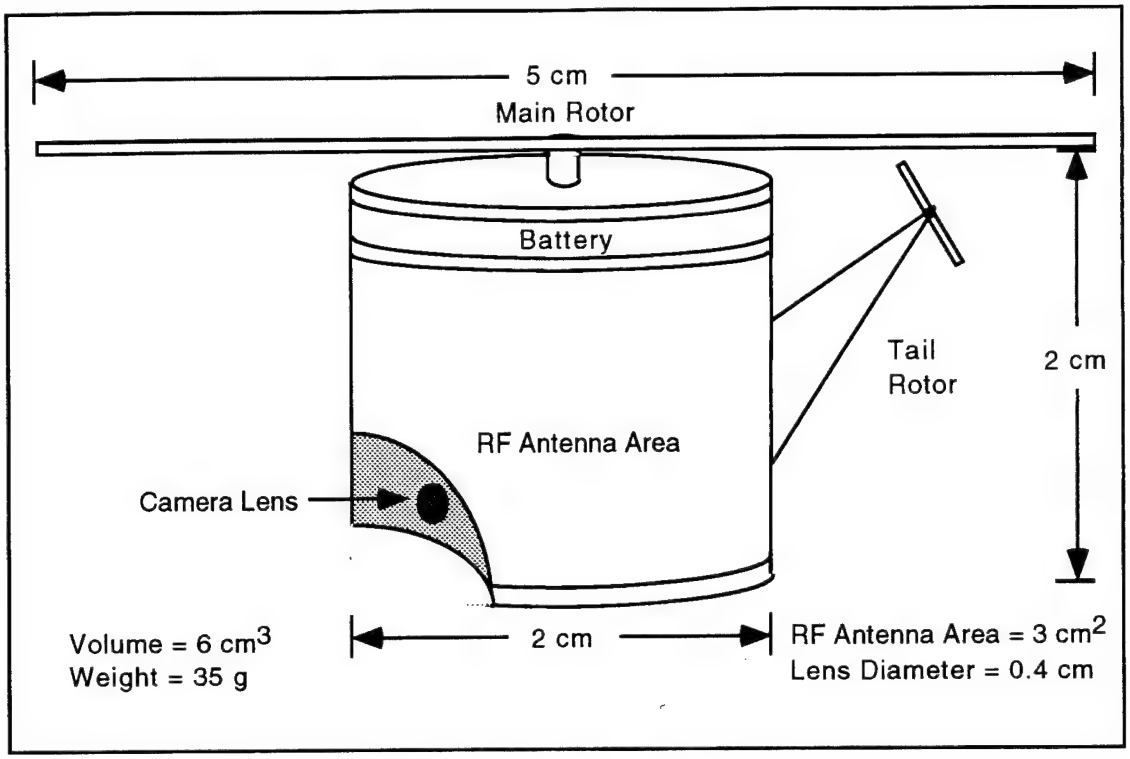

Figure 2. MRPV geometry

B. OBJECTIVE

The objectives of this research are: 1) to investigate the propagation losses of typical building walls, and 2) to design, build and test a prototype antenna for reception of beamed microwave power for the MRPV.

The propagation loss study will quantify the losses of a microwave power beam through typical building walls, the results of which will be used to select a system operating frequency and transmit power level. The type and location of the building walls used in this study are presented with the actual loss measurements. The loss measurements were taken using a HP 8350B signal generator and a HP 9562A spectrum analyzer. There are two primary frequencies of interest which arise from requirements to use existing off the

shelf hardware for the transmitter. These are 2.5 GHz (scientific and commercial band) and 5.5 GHz (satellite uplink frequency). The loss measurements were taken over a frequency band from 2 to 6 GHz.

An approximate model is presented for the propagation of a spherical electromagnetic wave front through a wall. This model is based on the method of images and geometrical optics. The propagation of locally plane sections of a spherical wave front are used to derive an equivalent free space source (i.e., with the wall removed) to account for the phase change and loss differences along the spherical wave front. Because of the locally plane assumption, the Fresnel transmission coefficients for a plane electromagnetic wave front passing through a lossy dielectric can be used. The transmission through a wall includes both the direct and floor reflected components of the wave. An equivalent source is derived for the direct waves and an equivalent image source is derived for the reflected waves. The complex values of the direct and reflected fields are computed at points representing the antenna aperture. The resulting array of field points is then integrated to find the total field received by the antenna.

The results of the MRPV antenna design are also presented. The primary antenna configuration of interest for a vertically polarized electric field is the circumferential slot. Calculations of far-field patterns and surface currents are simulated using the PATCH computer code which uses the method-of-moments (MM) solution to the electric field integral equation. Based on the PATCH code results, a prototype antenna was designed and built. The far-field patterns and efficiency were measured in the Naval Postgraduate School (NPS) anechoic chamber for a scaled model of the antenna. An approximate

antenna efficiency of 67.5% was measured. Using known values for power conversion efficiency, a possible rectenna configuration is shown with an overall microwave to dc power conversion efficiency of 61%.

The remainder of this thesis consists of four chapters. Chapter II discusses the first part of the propagation loss study. The measurement system for determining the propagation loss of various walls is presented, followed by a description of the walls tested and loss measurements. Chapter III continues the propagation loss study presenting the approximate ray tracing model that is derived for comparison with measured results. The model is based on the method of images and geometrical optics and approximates the propagation of a spherical wave front through a lossy dielectric boundary. Chapter IV presents the antenna design. A simulation of the prototype antenna is performed to determine the optimum feed point. Chapter V presents the results of measurements performed on the antenna. This includes the antenna parameters and the far-field measurements taken in the anechoic chamber. Chapter VI provides conclusions and any recommendations for follow on research in this area are also noted.

II. PROPAGATION LOSS MEASUREMENTS

A. MEASUREMENT SYSTEM

The wall loss is estimated by measuring the power received from a transmitter when the wall is present and comparing it to the received power without the wall. The propagation loss measurements were taken using the system depicted in Figure 3. The system consists of transmitting and receiving stations each with parabolic reflector antennas. The transmit signal is provided by a HP 8350B signal generator operating in the frequency sweep mode. The signal is received using a HP 8562A spectrum analyzer utilizing the trace hold feature. Used in this configuration, the transmitter sweeps through a specified frequency range with the receiver storing a trace of the resultant signal strength. Baseline free space measurements are taken to serve as a reference. The free space reference data was measured at separation distances of 10 and 15 ft.

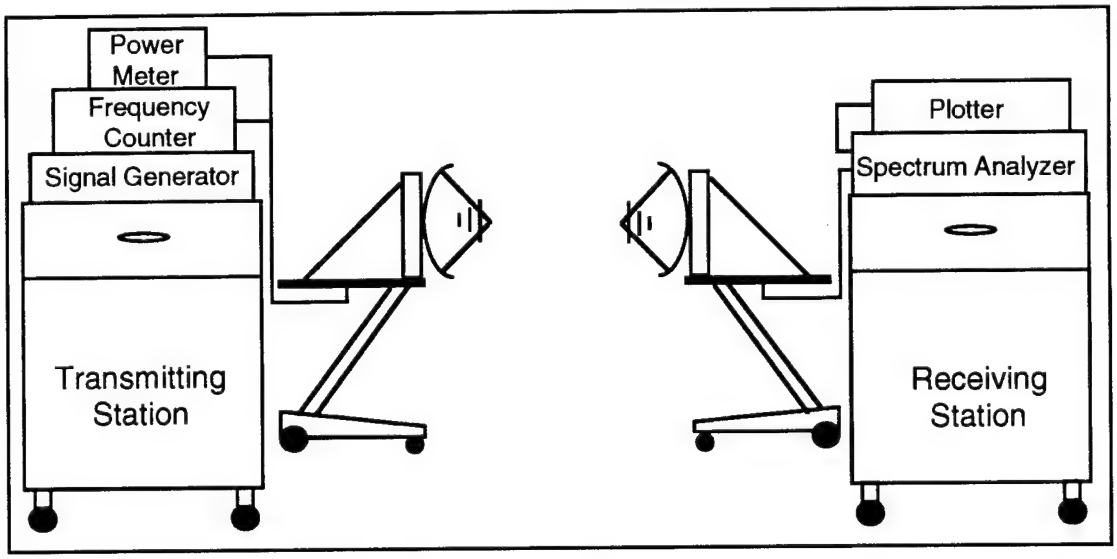

Figure 3. Propagation loss measurement system

1. Transmitting and Receiving Stations

Block diagrams of the transmitting and receiving stations are given in Figure 4.

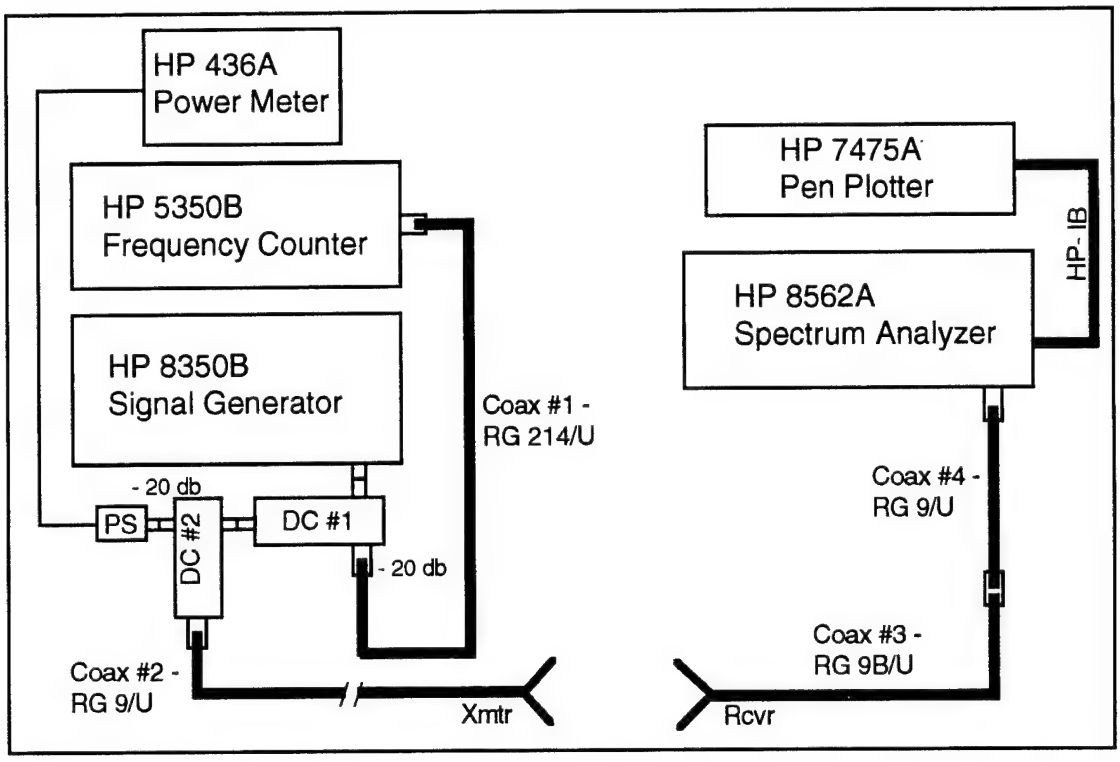

Figure 4. Measurement system block diagram

As shown, the transmitter station includes a HP 8350B signal generator, HP 5350B frequency counter, and a HP 436A power meter. The readings for frequency and power are obtained using 20 dB directional couplers as shown. The transmitting antenna is connected to the system using approximately 6 ft of 50 ohm coaxial cable. The receiving station consists of an HP 8562A spectrum analyzer and HP 7475A pen plotter connected together on a standard HP-IB interface. The receiving antenna is connected to the system using

approximately 7 ft of 50 ohm coaxial cable. The transmit and receive antennas are both parabolic reflectors with log periodic feeds.

The free space reference data is stored in the HP 8562A spectrum analyzer for subtraction with the blockage measurement. It is stored using the A-B-->A math function of the spectrum analyzer. The spectrum analyzer is also set in a maximum hold state for the A-B-->A trace. The trace records the measured propagation loss as the transmitter sweeps across the set range of frequencies.

2. Transmit and Receive Antennas

Identical transmit and receive antennas were assembled using American Electronic Laboratories (AEL) model APN102C parabolic reflectors with AEL model APII-101B log periodic feeds. The antennas were designed to be portable using modified Tektronix K212 instrument carts. The design and set-up of the portable parabolic reflector antennas is shown in Figure 5. In this figure, the antenna dimensions and electric field orientation with respect to the log periodic feed are also provided.

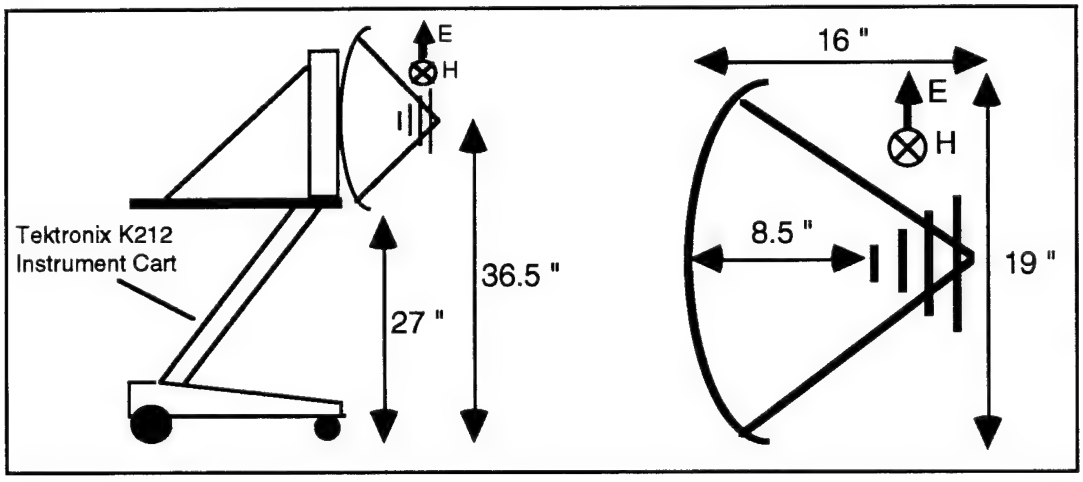

Figure 5. Parabolic reflector antenna with log periodic feed

3. Equipment Listing

A listing of all equipment used for both the transmitting and receiving stations is provided in Table 1.

	Model #	Serial #	Description
Transmitter			
Signal Generator	HP 8350B	2726A01436	0.005 - 12 GHz CW, -2 to +18 dbm
Frequency Counter	HP 5350B	2728A00933	X-band counter
Power Meter	HP 436A	1803A02841	-20 to +20 dbm
AEL Reflector	APN102C	350	parabolic reflector - 1 to 11 GHz
AEL Feed	APII 101B	950	log periodic - 1 to 12.4 GHz
Power Sensor	HP 8481A	-	50 ohm .05 to 18 GHz
Coax # 1	RG 214/U	CC2637-24	26" 50 ohm silver coated copper
Coax # 2	RG 9/U	8242	48" 50 ohm silver coated copper
Directional Coupler #1	HP 779D	1144A06099	-20 dbm directional coupler
Directional Coupler #2	HP 779D	1144A02899	-20 dbm directional coupler
Receiving			
Spectrum Analyzer	HP 9562A	3006A04767	9 kHz to 18 GHz, -120 to +18 dbm
Plotter	HP 7475A	2807V78367	pen plotter
AEL Reflector	APN102C	350	parabolic reflector - 1 to 11 GHz
AEL Feed	APII 101B	950	log periodic - 1 to 12.4 GHz
Coax # 3	RG 9B/U	92194	40" 50 ohm silver coated copper
Coax # 4	RG 9/U	8242	42" 50 ohm silver coated copper
Interface Connection	HPIB	-	analyzer to plotter interface

Table 1. Equipment listing

B. MEASUREMENTS

The system described in Chapter II, Section A, was used to measure propagation loss of a microwave power beam through several building walls. The measurements were taken using carefully chosen reference marks on the antennas for equipment alignment. With a standardized alignment of the antenna platforms and procedures, accurate comparisons can be made between measurements taken with and without the wall. The loss

measurements were collected over a frequency band of 2 to 6 GHz. The test measurement configuration is depicted in Figure 6. The distances d_1 and d_2 are those from the wall to the transmitter and receiver, respectively. The wall has thickness L, and material constants ε_r (dielectric constant), μ_o (permeability), and tan δ (loss tangent). The distances from each antenna to the wall were set equal ($d_1=d_2$) yielding a total distance d_1+L+d_2. Transmit and receive distances of 10 and 15 feet were used. These distances were the maximum possible given the confinement of building halls and rooms.

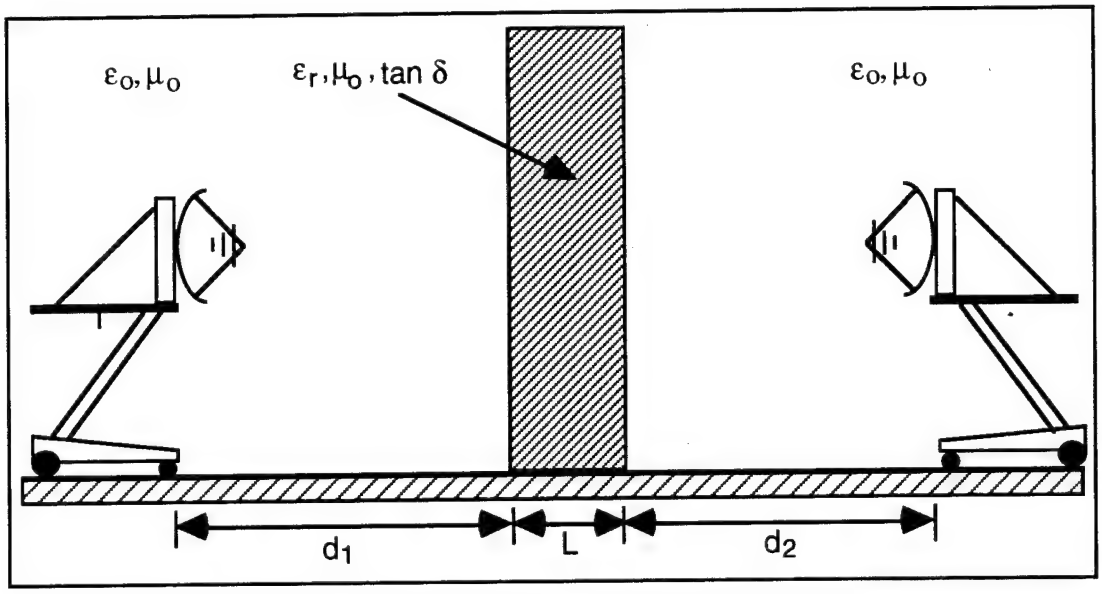

Figure 6. Test set-up

1. Building Walls

The walls measured in this test are located on the campus at the Naval Postgraduate School. A brief description of each wall is given in Table 2. The exact composition of the walls is unknown. The descriptions in Table 2 are based solely on visual inspection.

	Building Wall	Material Type	Location
A	.25 " Glass Pane	Glass	King Hall, Front Entrance
B	1.75 " Double Doors	Wood	Spanagel Hall, Room 429
C	5.5" Classroom Wall w/ Chalkboard	Sheetrock, metal, cement	Spanagel Hall, Room 408
D	10.75 " Classroom Wall	Cement, metal	Spanagel Hall, Room 421
E	1.75 " Double Doors	Metal covered, with glass windows	Spangel Hall, Roof exit doors

Table 2. Typical building walls

2. Measured Data

The measured losses for the materials listed in Table 2 are provided in Figure 7. The measured data for each wall was plotted using the HP 7475A pen plotter and the raw data is included in Appendix A.

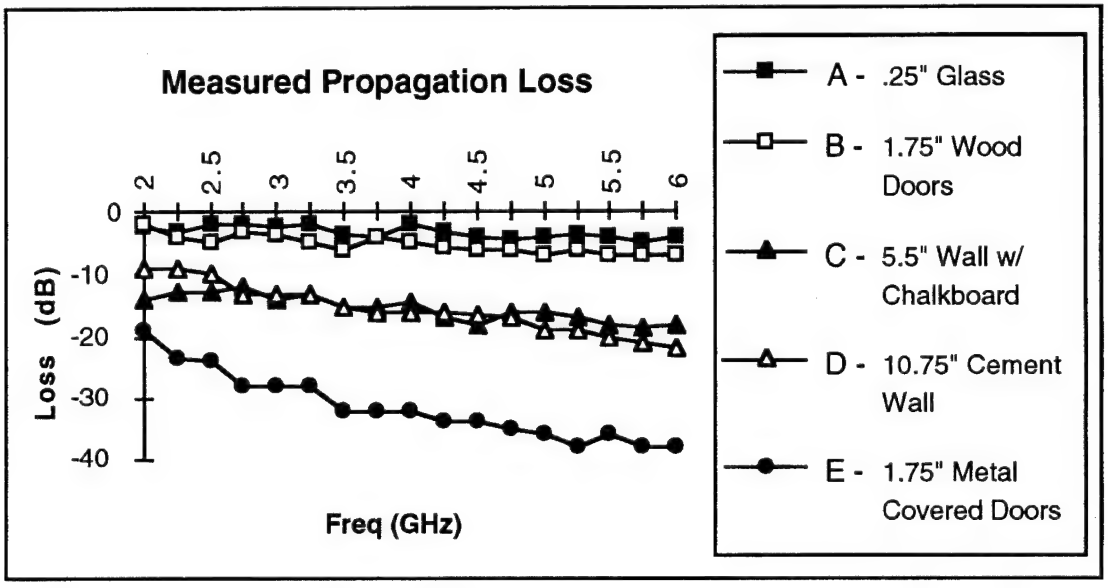

Figure 7. Loss measurements of typical building walls

III. PROPAGATION LOSS MODELING

A. BACKGROUND

An approximate model was developed for the propagation of a spherical electromagnetic wave through a building wall of known material properties. This model is based on the method of images and geometrical optics. The propagation of locally plane sections of a spherical wave front is used to determine the signal at the receive antenna that includes the phase and amplitude changes introduced by the wall. Based on the received signal, an equivalent free space source can be defined and the wall removed. A similar process is used to determine a free space image source located below the floor. Thus, these two sources radiate in free space and their superposition yields a solution that includes both the direct and reflected transmit waves. The complex values of the direct and reflected fields are computed at points representing the antenna aperture. The resulting array of field points is then integrated to find the total received field of the antenna. This approximate model is shown to be in good agreement with measured results.

1. Spherical and Planar Electromagnetic Waves

A spherical electromagnetic wave front emanates from an ideal point source. The ideal point source refers to an element of uniform amplitude current which is of infinitesimal length. The electric field vector of all realizable antennas contains $\hat{r}$, $\hat{\theta}$, and $\hat{\phi}$ field components. The $\hat{r}$ component of $\vec{E}$ cannot be assumed negligible when operating in the near-field region of the antenna. In the far field the radiated electromagnetic wave is spherical. Furthermore, only the $\hat{\theta}$ and $\hat{\phi}$ components are significant and they vary as $1/r$. Locally the

spherical wave can be considered to be a plane wave, when r is large as shown in Figure 8.

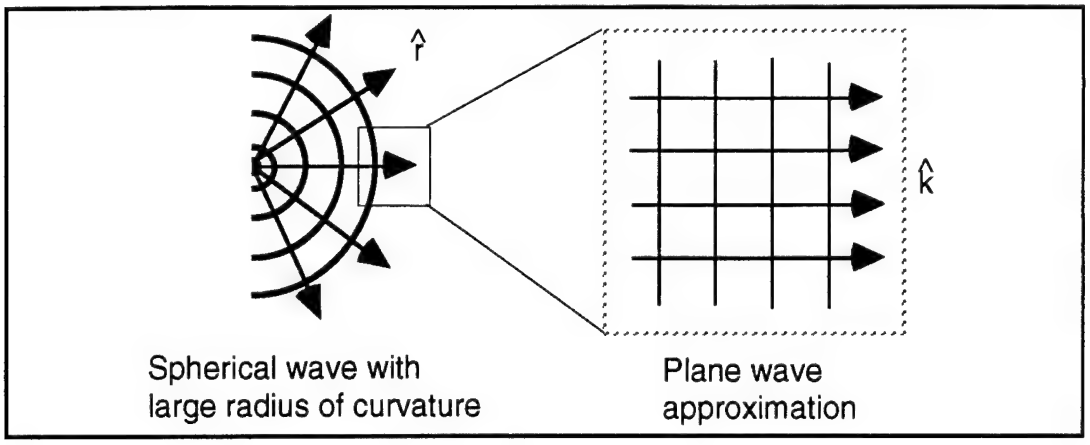

Figure 8. Local plane wave approximation

2. Plane Waves at Oblique Incidence on an Interface

The transmission and reflection of a plane wave at oblique incidence to a boundary is shown in Figure 9. In this derivation the boundary is assumed to be between free space and a lossy dielectric. The medium is characterized by ε_r, μ_r, and tan δ.

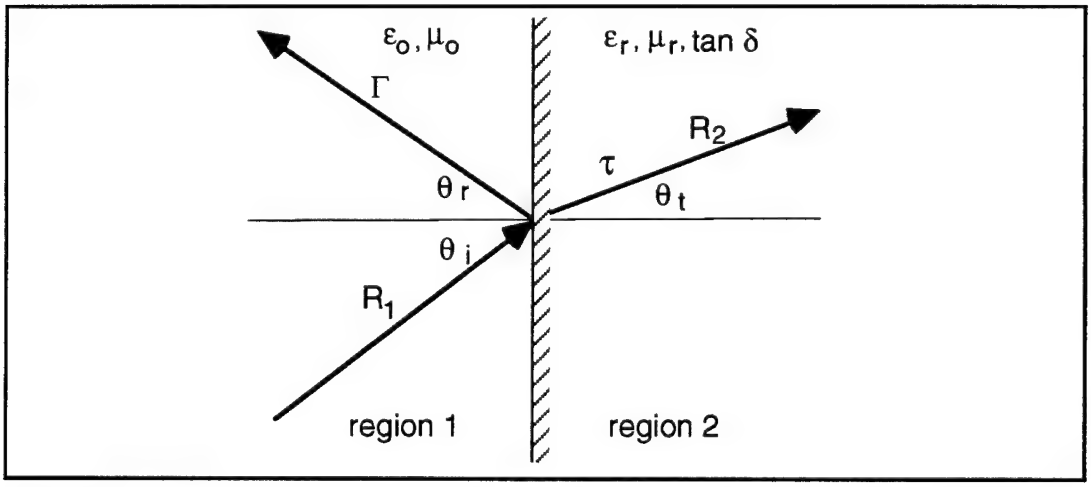

Figure 9. Plane wave at oblique incidence - single interface

The perpendicularly polarized wave, consisting of $\vec{E}$ in the plane of incidence and $\vec{H}$ parallel to the boundary, is impinging on a boundary at an angle of incidence θ_i. The boundary condition requires that [Ref. 3]

$$\beta_o \sin\theta_i = \beta_o \sin\theta_r = \beta_2 \sin\theta_t \tag{3.1}$$

or, $\theta_r = \theta_i$, which is Snell's Law. The phase constants are given by $\beta_o = 2\pi/\lambda_o$ and $\beta_2 = 2\pi/\lambda_2$. The wavelengths in free space and the medium are denoted λ_o and λ_2, respectively. Knowing that the intrinsic impedance of the dielectric regions are given by [Ref. 1]

$$\eta_o = \sqrt{\frac{\mu_o}{\varepsilon_o}} \qquad \text{(region 1)} \tag{3.2}$$

$$\eta_2 = \frac{\sqrt{\frac{\mu_o}{\varepsilon_o \varepsilon_r}}}{\sqrt{(1 - j\tan\delta)}} \qquad \text{(region 2)} \tag{3.3}$$

the reflection coefficient Γ and the transmission coefficient τ are given by

$$\Gamma = \frac{\eta_2 \cos\theta_t - \eta_o \cos\theta_i}{\eta_2 \cos\theta_t + \eta_o \cos\theta_i} \tag{3.4}$$

$$\tau = \frac{2\eta_2 \cos\theta_t}{\eta_2 \cos\theta_t + \eta_o \cos\theta_i} \tag{3.5}$$

These preceding equations are known as Fresnel's formulas for parallel polarization [Ref. 3]. The phase constants for the material on each side of the boundary can be written as

$$\beta_o = \omega\sqrt{\mu_o\varepsilon_o} \tag{3.6}$$

$$\beta_2 = \omega\sqrt{\frac{\mu_o\varepsilon_o\varepsilon_r}{2}\left[\sqrt{1+(\tan\delta)^2}+1\right]} \tag{3.7}$$

where $\omega = 2\pi f$ (f=frequency in Hertz). The term $\tan\delta$ in Equation (3.7) is the loss tangent of the material in region 2. The attenuation constant for a lossy dielectric material is given by

$$\alpha_2 = \omega\sqrt{\frac{\mu_o\varepsilon_o\varepsilon_r}{2}\left[\sqrt{1+(\tan\delta)^2}-1\right]} \quad . \tag{3.8}$$

Refering to Figure 9, given a distance to the boundary of R_1 and the distance from the boundary to the point of interest R_2, the electric field is given by

$$E(R_T) = \frac{\tau}{4\pi(R_T)}e^{-(\alpha_2 R_2 + j(\beta_o R_1 + \beta_2 R_2))} \quad . \tag{3.9}$$

The transmission coefficient τ accounts for the loss due to the reflection at the interface, the attenuation constant α_2 accounts for the loss due to the material dielectric and loss tangent, and the phase constants β_o and β_2 account for the changing phase with respect to a free space path. The total transmit/receive

distance of R_1 and R_2 is denoted as R_T. The value $E(R_T)$ represents the total transmitted field of an oblique planar wave incident at an angle θ_i.

3. Plane Waves at Oblique Incidence on a Double Interface

The transmission and reflection of a plane wave at oblique incidence to a two boundary interface is shown in Figure 10. The regions on both sides of the lossy dielectric panel are assumed to be free space. In this case the transmission of the plane wave must include the multiple reflections between the two faces. The transmission through each boundary is governed by the equations previously shown for the single interface. In the two interface problem, refraction causes the apparent location of the source as viewed in

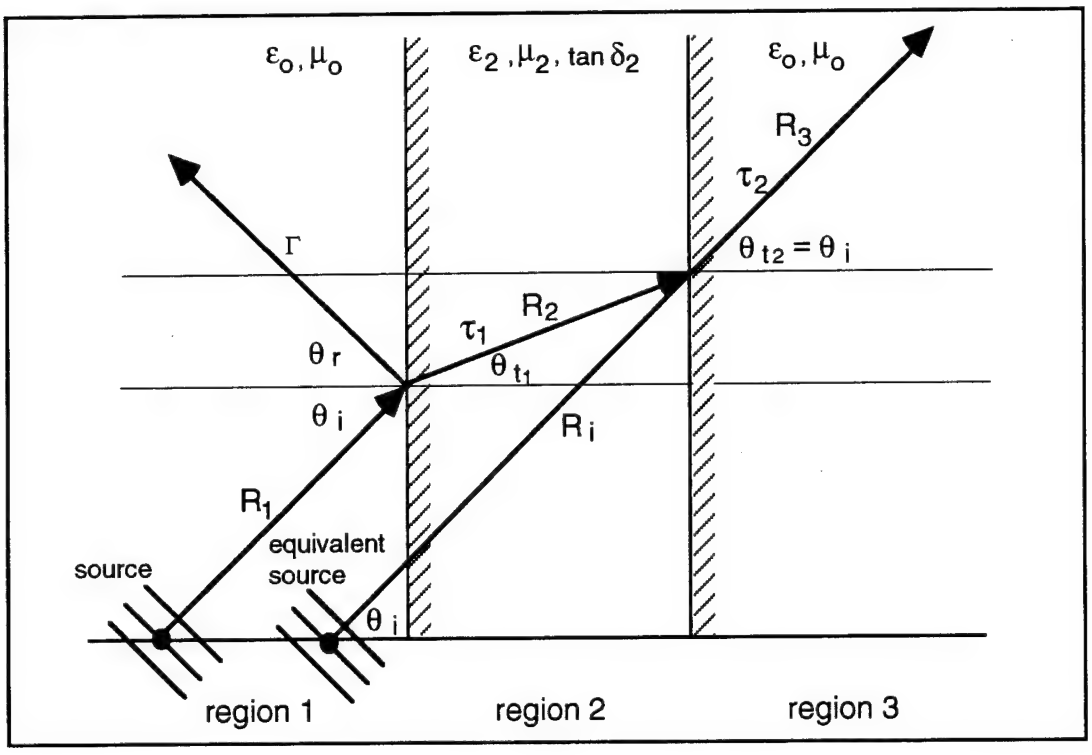

Figure 10. Plane wave at oblique incidence - double interface

region 3 to move as shown. The original source can be replaced by an equivalent source which is located closer to the wall and modified to account for the effects of the wall. The equivalent source takes into account the transmission coefficients of each region based on the original source and geometry. The equivalent source will also take into account the phase change and attenuation due to the wall. The wall can be removed and the equivalent source will radiate in free space. In this model, multiple reflections inside of the wall are neglected. Note that the equivalent source method can be expanded to include multiple reflections. An additional equivalent source can be defined for each multiple reflection added.

The transmission coefficient τ_1 is given by

$$\tau_1 = \frac{2\eta_2 \cos\theta_t}{\eta_2 \cos\theta_t + \eta_o \cos\theta_i} \tag{3.10}$$

and the transmission coefficient τ_2 is given by

$$\tau_2 = \frac{2\eta_o \cos\theta_i}{\eta_o \cos\theta_i + \eta_2 \cos\theta_t} \tag{3.11}$$

The phase and attenuation constants of the lossy dielectric are given by

$$\beta_2 = \omega\sqrt{\frac{\mu_2\varepsilon_2}{2}\left[\sqrt{1+(\tan\delta_2)^2}+1\right]} \tag{3.12}$$

$$\alpha_2 = \omega\sqrt{\frac{\mu_2\varepsilon_2}{2}\left[\sqrt{1+(\tan\delta_2)^2}-1\right]} \quad . \tag{3.13}$$

The electric field to the right of the second boundary can then be thought of as originating from an equivalent point source of the form

$$E(R_i) = \frac{\tau_1\tau_2}{4\pi(R_i)} e^{-(\alpha_2 R_2 + j(\beta_o(R_1+R_3)+\beta_2 R_2))} \tag{3.14}$$

which radiates in free space with the wall removed. The distance to the boundary is R_1, the distance traveled through the material is R_2, the distance traveled outside the second boundary is R_3, and the equivalent source distance is R_i. The transmission coefficients account for the loss due to the reflection at each interface. The phase constants account for the changing phase with respect to the transmitting reference.

B. PROPAGATION OF A SPHERICAL WAVEFRONT

1. Direct Path

The propagation of a spherical wave through a wall can be modeled by assuming that the radius of curvature is large and the wave front is locally plane. This is the standard assumption for geometrical optics [Ref. 4]. As shown in Figure 11, the propagation of a local portion of the wave front can be represented by a single ray at an angle θ_i.

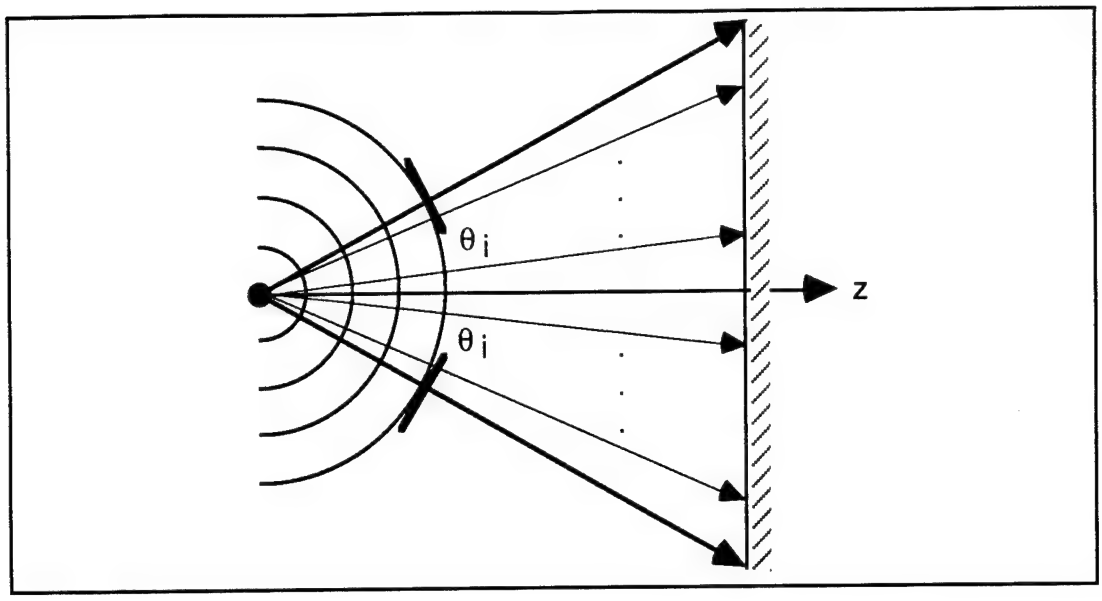

Figure 11. Locally plane sections of a spherical wave

The maximum and minimum angles that intercept the edges of the receive antenna can be traced back to the point where the lines intersect as shown in Figure 12. This point is the location of an equivalent spherical source radiating in free space, and provides the geometrical optics divergence factor ($1/R_i$). Every ray with angle of incidence θ_i will trace back through the intersection point. Each locally plane section corresponding to a particular angle of incidence is traced through the wall and the transmission coefficient and phase and attenuation constants calculated in each region. The rays coming from the equivalent source will contain the transmission coefficient and phase and attenuation constants from the path followed by the original rays.

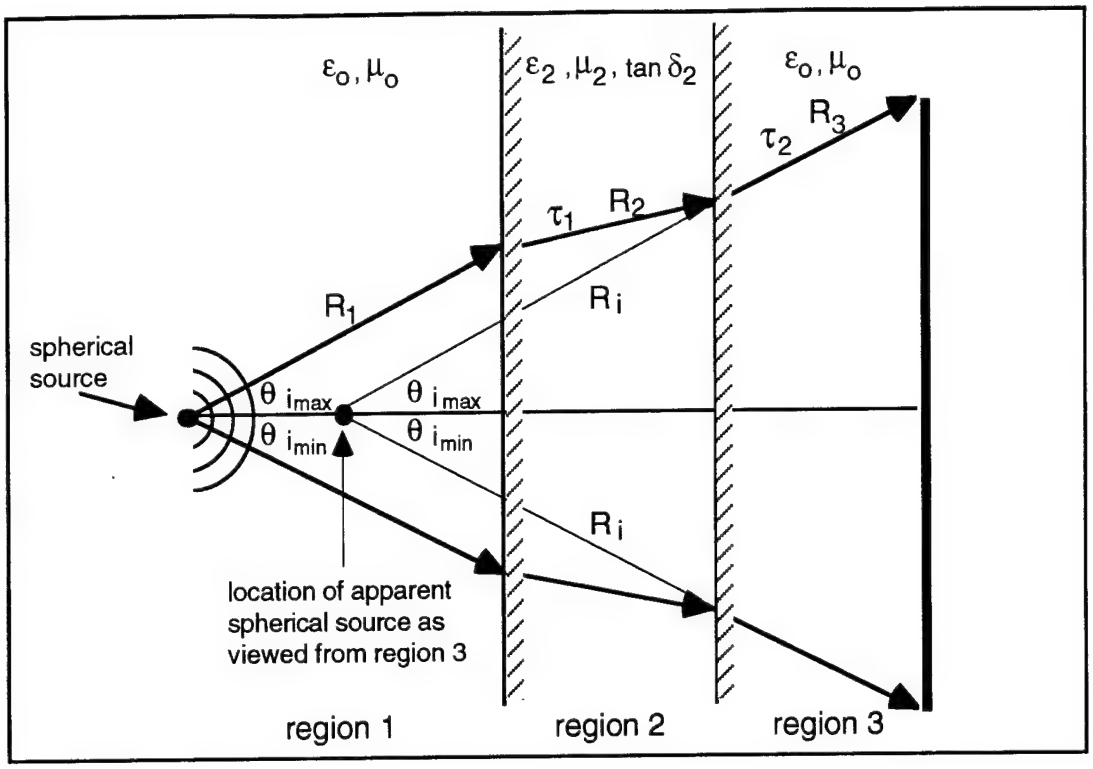

Figure 12. Equivalent source location

Using this approach the equivalent source includes the loss due to spreading along a single straight path R_i with no wall present as shown in Figure 13. The radiation pattern of the equivalent source E_i is given by Equation (3.14). Each variable in the equation is a function of the incidence angle. The transmission coefficient, phase constant, attenuation constant, and distances R_1, R_2, and R_3 are based on the ray paths from the original source. The distance R_i is the distance from the equivalent source to the point on the antenna grid, as indicated in Figure 13. The incident angle increment is chosen such that the spacing between each point on the receive aperture plane is approximately one tenth of a wavelength (.1λ). The total received field is found by integrating the field over the aperture [Ref 5].

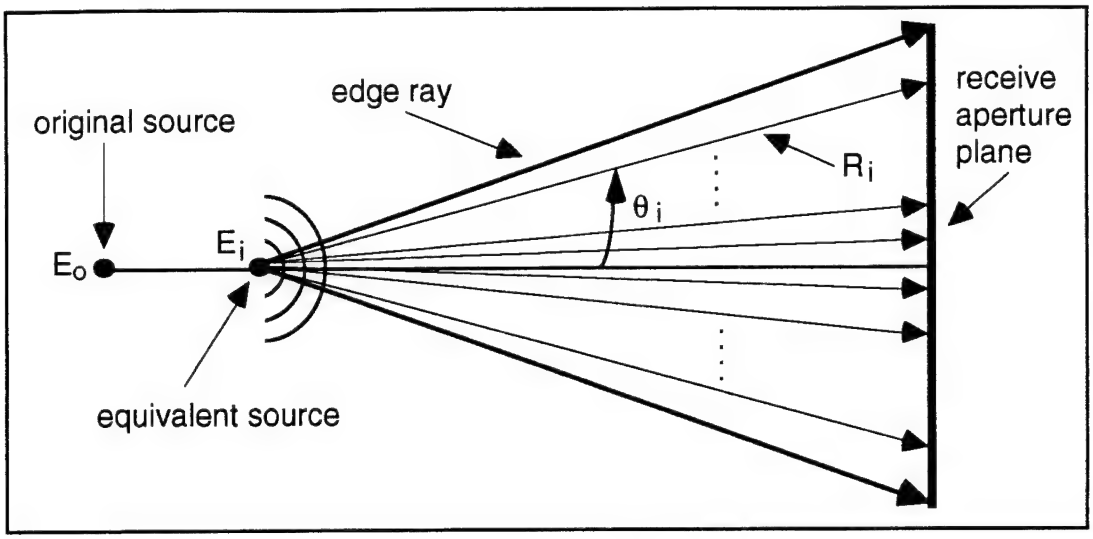

Figure 13. Equivalent source and antenna integration grid

2. Geometric Relationships for the Direct Path

Using the ray tracing concept, a building wall propagation loss model was formulated. In this section, formulas for the quantities appearing in Equation (3.14) are derived. As shown in Figure 14, the source is located at a height h above the floor and at a distance d_1 from a wall of thickness L. The receive location d_2 is assumed equal to d_1. The regions on either side of the wall are free space. A typical direct ray is shown in Figure 14.

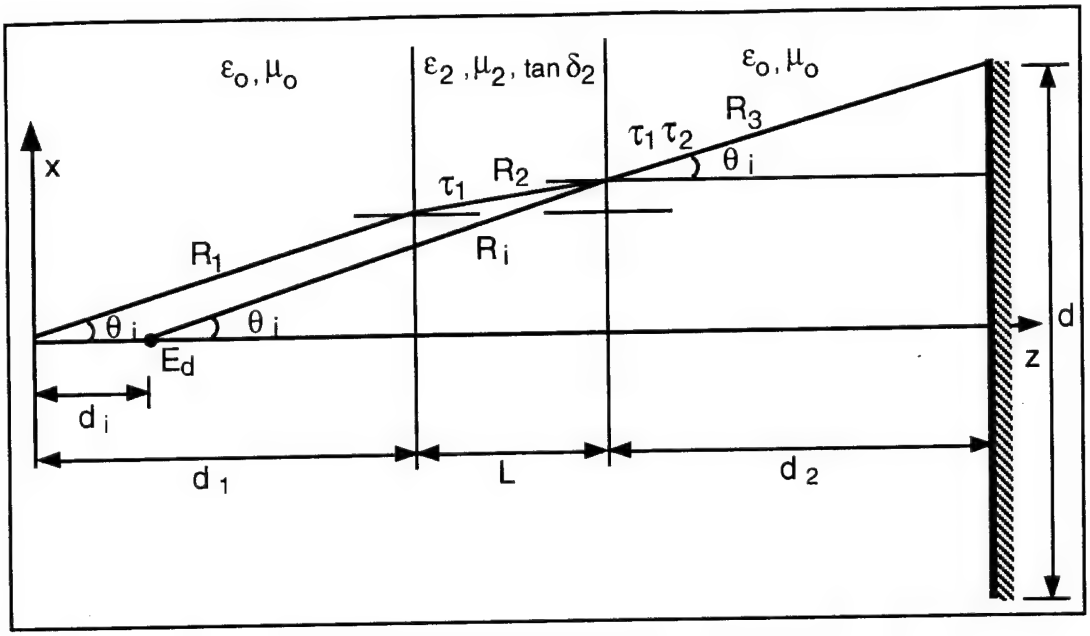

Figure 14. Direct rays

Given that θ_i is known, the distances R_1, R_2, R_3 and R_i can be calculated as

$$R_1 = \frac{d_1}{\cos\theta_i} \tag{3.15}$$

$$R_2 = \frac{L}{\cos\theta_t} = \frac{L}{\sin^{-1}(\frac{\beta_o}{\beta_2}\sin\theta_i)} \tag{3.16}$$

$$R_3 = \frac{d_2}{\cos\theta_i} \tag{3.17}$$

$$R_i = \frac{d_1 + L + d_2 - d_i}{\cos\theta_i} \tag{3.18}$$

The phase and attenuation constants of the wall are given by Equations (3.7) and (3.8). The transmission coefficients as a function of θ_i are given by Equations (3.10) and (3.11). The intrinsic impedance of free space η_o and the material η_2 are given by Equations (3.2) and (3.3). Thus, all of the quantities in Equation (3.14) are known, and the electric field at the aperture can be computed. Using a subscript d to denote the direct path, Equation (3.14) can be written as

$$E_d(R_i) = \frac{\tau_1\tau_2}{4\pi(R_i)} e^{-(\alpha_2 R_2 + j(\beta_o(R_1+R_3)+\beta_2 R_2))} \qquad (3.19)$$

The incident angle is determined by discretizing the receive aperture into a grid of points. Each location within the aperture of diameter d can be expressed as the magnitude of Δx_m and Δy_n, shown in Figure 15.

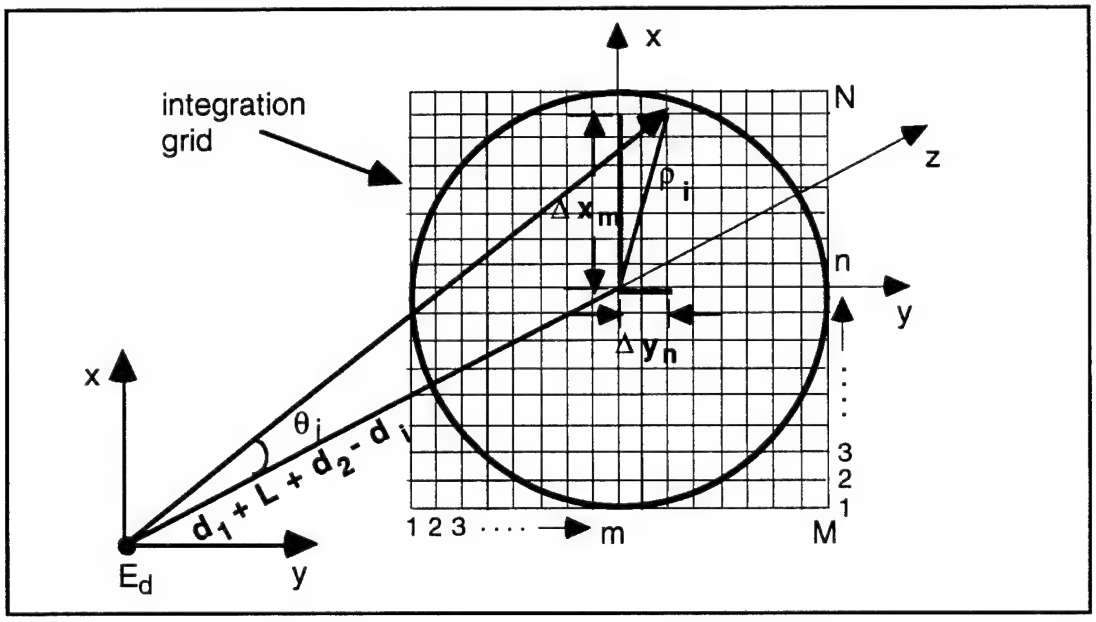

Figure 15. Antenna grid - incident angle

The magnitude ρ_i is used to calculate the incident angle $\theta_{i_{mn}}$.

$$\theta_{i_{mn}} = \tan^{-1}\left(\frac{\rho_{i_{mn}}}{d_1 + L + d_2 - d_i}\right) = \tan^{-1}\left(\frac{\sqrt{\Delta x_m + \Delta y_n}}{d_1 + L + d_2 - d_i}\right) \qquad (3.20)$$

The equivalent replacement source given by Equation (3.19) will create a field at each of the points on the antenna grid. In determining the received field for a vertically polarized antenna, only the x component is required. The E_x field component of an x-directed electric dipole $I_o l$ in the far-field can be expressed in terms of spherical coordinates as

$$E_x = \frac{-jk\eta I_o l e^{-jkr}}{4\pi r}\left[1 - \sin^2\theta\cos^2\phi\right] \quad . \qquad (3.21)$$

Therefore, the electric field of the equivalent source is normalized to include only the polarization factor $(1\text{-}\sin^2\theta\cos^2\phi)$ for an x directed infinitesimal dipole,

$$E_d(R_i) = \frac{(1 - \sin^2\theta\cos^2\phi)\tau_1\tau_2}{4\pi(R_i)} e^{-(\alpha_2 R_2 + j(\beta_o(R_1+R_3)+\beta_2 R_2))} \qquad (3.22)$$

Equation (3.22) is the equivalent spherical source with no wall present for the direct path of propagation.

3. Reflected Path

The floor reflection is included using an equivalent image source. The location of the original image is directly below the source. Since the floor is not a perfect conductor, the image is not of equal intensity, but reduced by a factor

Γ_r. With the image present, the floor is removed while the wall remains. This step is not entirely accurate, because it assumes that rays hitting the wall below floor level pass through the wall medium. However, for the geometry under consideration (equal antenna heights and equal distances from the wall) the approximation is accurate.

The original source is traced to the receiving antenna to determine the maximum and minimum angles of incidence of the reflected rays, $\theta_{r_{min}}$ and $\theta_{r_{max}}$. The rays corresponding to the maximum and minimum angles of incidence are traced back to the point of intersection, as shown in Figure 16. This is the location of the equivalent floor reflected source. The geometrical relationships are similar to those for the direct rays. The distances R_{1_r}, R_{2_r}, and R_{3_r} are

$$R_{1_r} = \frac{d_1}{\cos\theta_r} \quad . \tag{3.23}$$

$$R_{2_r} = \frac{L}{\cos\theta_r} = \frac{L}{\sin^{-1}(\frac{\beta_o}{\beta_2}\sin\theta_r)} \tag{3.24}$$

$$R_{3_r} = \frac{d_2}{\cos\theta_r} \quad . \tag{3.25}$$

The equivalent image source is determined by finding the point where the straight path lines $R_r\,(\theta_{r_{min}})$ and $R_r\,(\theta_{r_{max}})$ intersect. Due to the non-symmetry, the lines will intersect off of the z axis. An equation for each line is used to find the intersection point in d_{r_x} and d_{r_z}. The straight path length R_r for each reflected

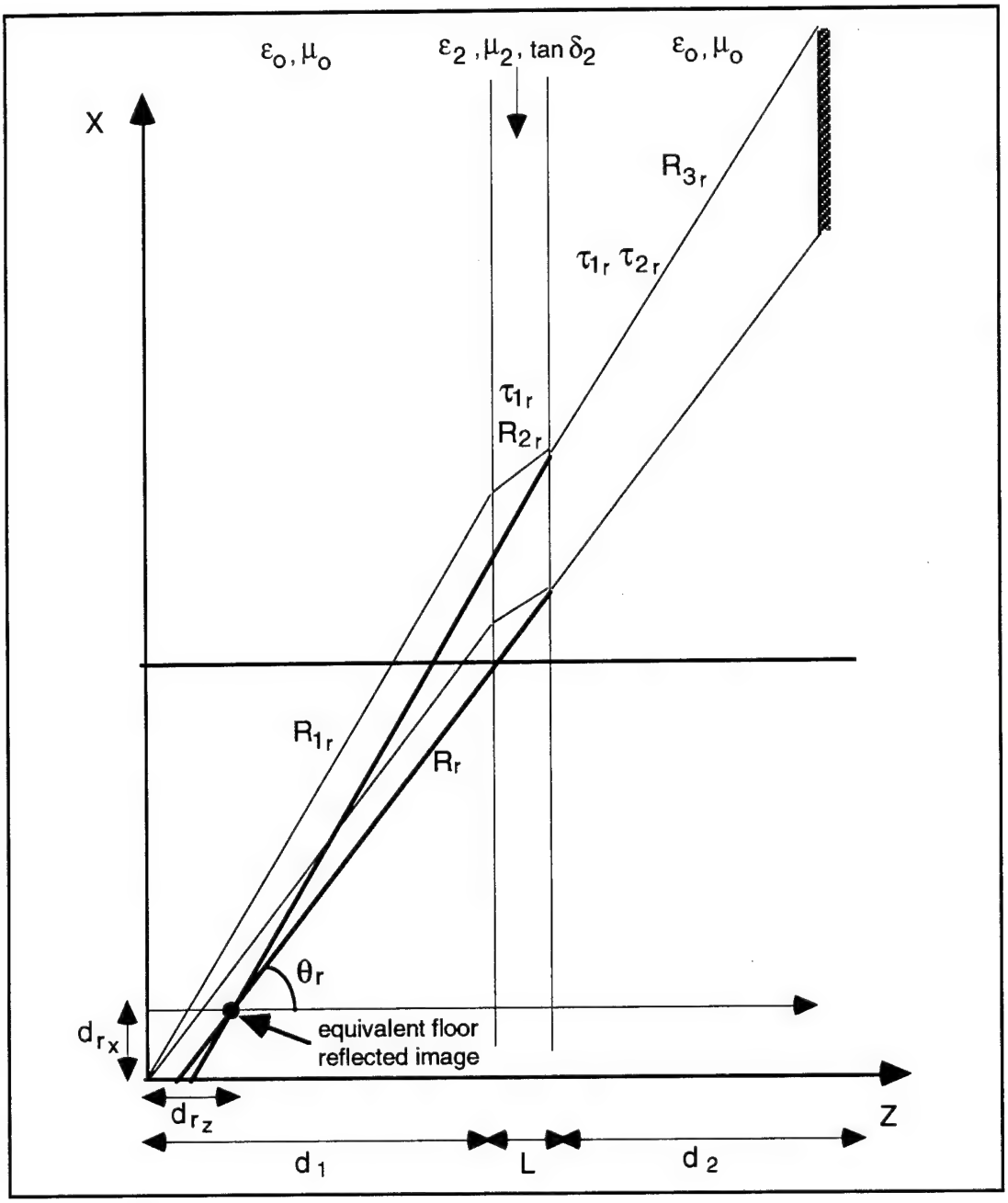

Figure 16. Equivalent image source - reflected waves

angle θ_r is given by,

$$R_r = \frac{d_1 + L + d_2 - d_{r_z}}{\cos\theta_r} \quad . \tag{3.26}$$

The phase and attenuation constants due to the wall are the same as for the directs rays given by Equations (3.7) and (3.8). The image beneath the floor will have less intensity than the source because the floor is not a perfect conductor. Thus, a reflection coefficient must be included to account for the reduced intensity of the floor image

$$\Gamma_r(\theta_r) = \frac{\eta_f \cos\theta_{t_f} - \eta_o \cos\theta_f}{\eta_f \cos\theta_{t_f} + \eta_o \cos\theta_f} \tag{3.27}$$

where η_f is the intrinsic impedance of the floor given by

$$\eta_f = \frac{\sqrt{\frac{\mu_o}{\varepsilon_o \varepsilon_f}}}{\sqrt{(1 - j\tan\delta_f)}} \tag{3.28}$$

and θ_f and θ_{t_f} are given by

$$\theta_f = \left(\pi/2 - \theta_r\right) \tag{3.29}$$

$$\theta_{t_f} = \sin^{-1}\left(\beta_o/\beta_f \sin\theta_f\right) \quad . \tag{3.30}$$

The electric field resulting from the floor reflected rays which includes the loss due to floor reflection is

$$E_r(R_r) = \frac{\Gamma_r \tau_{1_r} \tau_{2_r}}{4\pi(R_r)} e^{-(\alpha_2 \beta_{2_r} + j(\beta_o(R_{1_r} + R_{3_r}) + \beta_2 R_{2_r}))} \quad (3.31)$$

An equivalent image source with a pattern given by Equation (3.31) radiating in free space will create the same field at each of the points on the antenna grid as the original problem. Again, as in Equation (3.22), the source is modified to include only the polarization factor ($1-\sin^2\theta\cos^2\phi$) for an x directed infinitesimal dipole. The total field resulting from the reflected rays is given by

$$E_r(R_r) = \frac{(1-\sin^2\theta\cos^2\phi)\Gamma_r \tau_{1_r} \tau_{2_r}}{4\pi(R_r)} e^{-(\alpha_2 R_{2_r} + j(\beta_o(R_{1_r} + R_{3_r}) + \beta_2 R_{2_r}))} \quad (3.32)$$

4. Beam Shaping

The effect of the antenna pattern is easily included in this model. The 3dB beamwidth, which varies with wavelength (λ) and antenna diameter (d), is approximately

$$\theta_{3dB} = \frac{65\lambda}{d} \text{ (deg)} \quad (3.33)$$

for uniform excitation. To account for the decreasing beamwidth with increasing frequency, a cosine taper function was used which is raised to the n^{th} power

$$\cos^n(\theta_{3dB}) = \cos^n(65\frac{\lambda}{d}\frac{\pi}{180}) = .707 \quad (3.34)$$

where the exponent is given by

$$n = \frac{\log(.707)}{\log(65\frac{\lambda}{d}\frac{\pi}{180})} \quad . \tag{3.35}$$

Thus, the direct and reflected fields are $E_d \cos^n \theta_i$ and $E_r \cos^n \theta_r$ where E_d and E_r are defined in Equation (3.22) and (3.32), respectively. The direct and floor reflected fields are now a function of antenna beamwidth, which varies with frequency. The beamshape has very little effect on the direct term, but significant effect on the floor reflected term.

5. Total Received Field

The complex field of the direct and reflected rays are summed to determine the total resultant field E_T. From aperture theory [Ref. 6] the total far field received is an integral of the aperture fields

$$\vec{E}_T = \frac{jke^{-jkr}}{2\pi r} \iint_{S_A} \left[\vec{E}_A\right]_{tan} e^{j\vec{k}\bullet\vec{d}} ds_A \tag{3.36}$$

where S_A is the aperture surface, $\vec{k}$ is the incident ray propagation vector and $\vec{d}$ the position vector to the point of integration. Neglecting constants and writing Equation (2.36) in terms of previously defined quantities for a discretized grid

$$E_T = \sum_m \sum_n \left(E_{d_{mn}} + E_{r_{mn}}\right) \bullet \Delta x \Delta y \quad . \tag{3.37}$$

C. MODELING RESULTS

1. Overview

The spherical wave propagation model was programmed in MATLAB (a code listing is provided in Appendix B). If a single frequency is input, the program calculates and plots the magnitude and phase of the direct, reflected, and total fields on the surface of the antenna and provides a loss in dB to that of free space for the user specified wall parameters. If more than one frequency point is input, the program calculates the loss in dB for each frequency and plots the resulting loss versus frequency over the band specified. The program variables specified by the user are:

d1, d2 = distance from antenna to wall (ft)

L = thickness of wall (ft)

h = height of antennas from floor (ft)

e2 = dielectric constant of wall

lt = loss tangent of wall

ef = dielectric constant of floor

ltf = loss tangent of floor

2. Comparison of Computed and Measured Data

Using the wall loss data from the measurements described in Chapter II, Section B, comparisons were made to the data computed using the model in Chapter III, Section B. The wall characteristics are summarized in Table 2. The electrical characteristics of the walls were not known precisely, so parametric calculations were performed. The quantities ε_r and $\tan\delta$ were varied until the best match with measured data was obtained. Comparisons of the measured

and computed insertion loss data are given in Figures 17 through 21. A summary of the dielectric and loss tangents are given in Table 3.

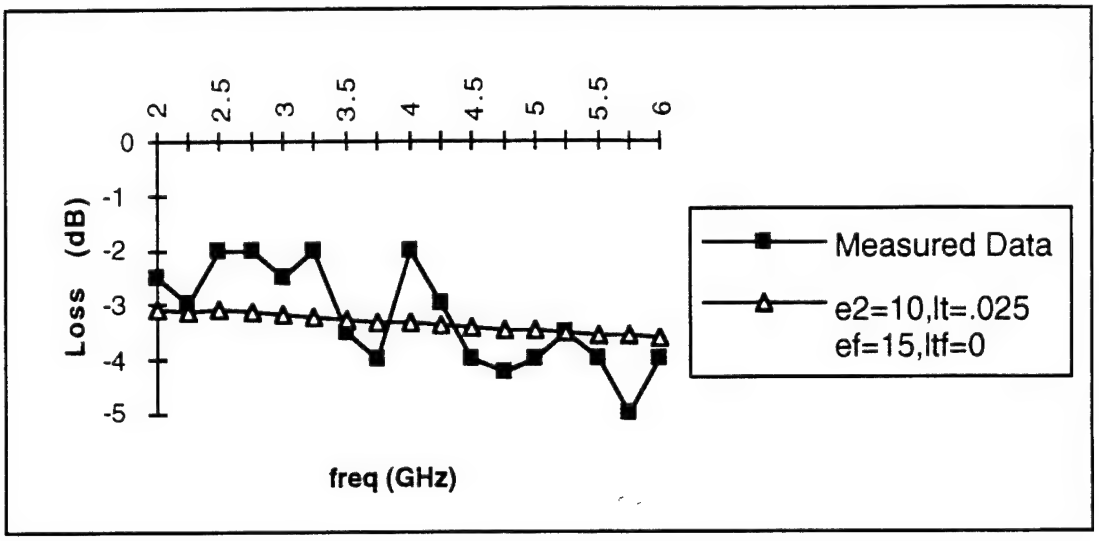

Figure 17. Insertion loss of .25" glass pane

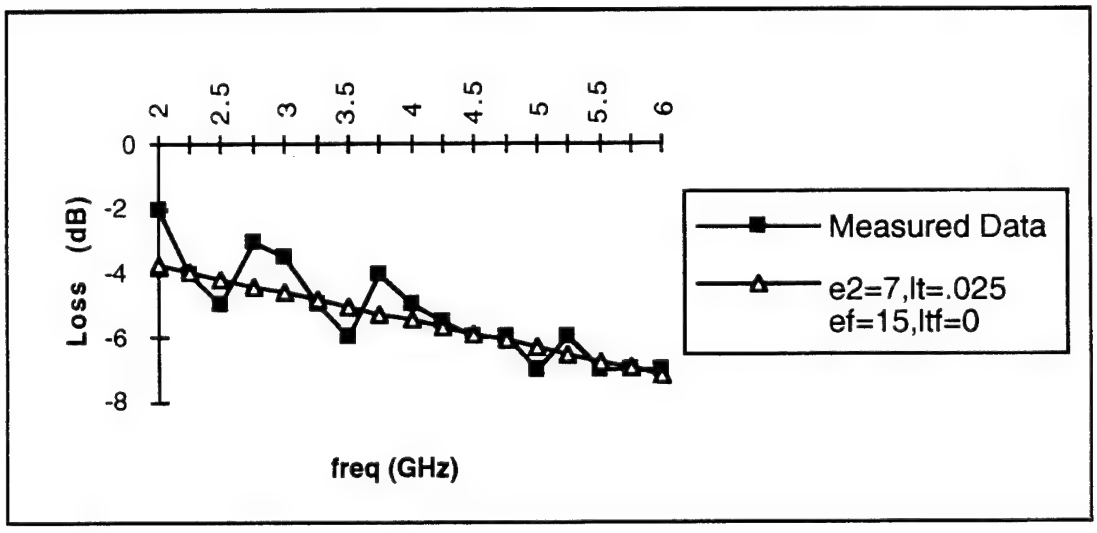

Figure 18. Insertion loss of 1.75" wood doors

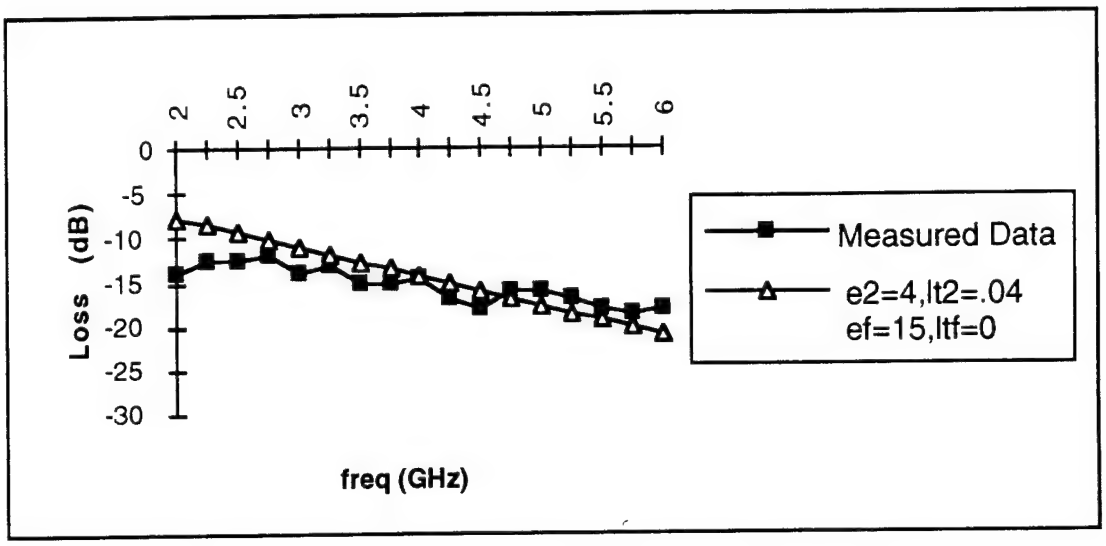

Figure 19. Insertion loss of 5.5" wall w/ chalkboard

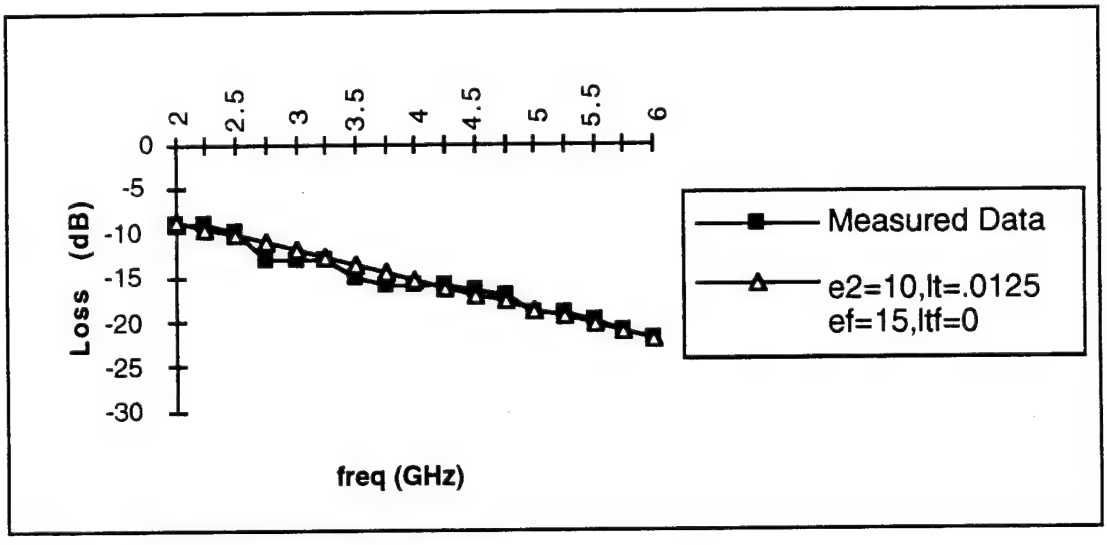

Figure 20. Insertion loss of 10.75" cement wall

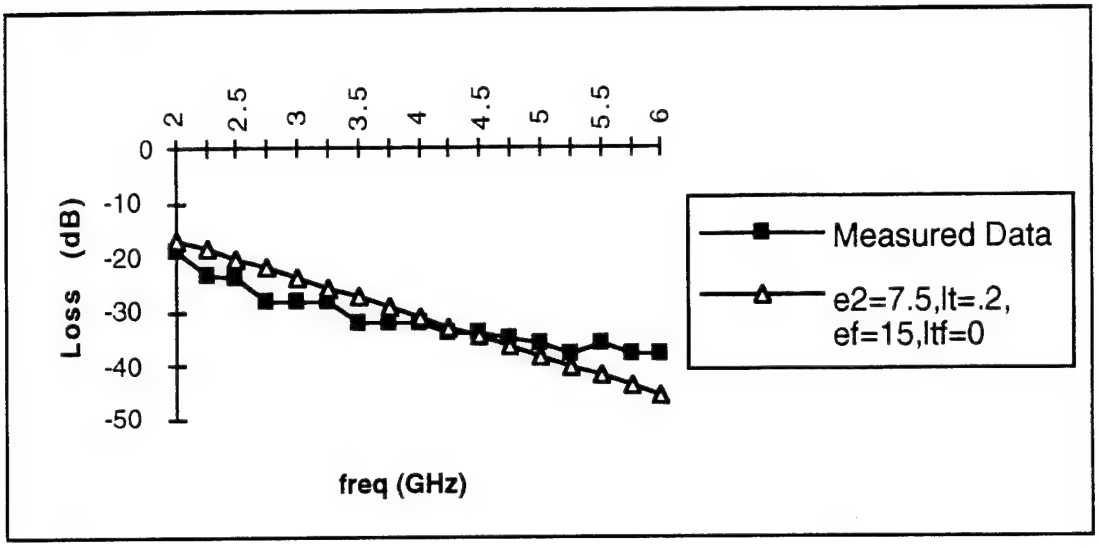

Figure 21. Insertion loss of 1.75" metal doors

The outputs for the single frequency calculations are provided in Appendix C. These plots include the calculations of field values over the grid of points for the direct, reflected, and combined terms.

	d_1 (ft)	L (ft)	h (ft)	e2	lt	ef	ltf
Fig 17	.25" glass pane, front entrance, King Hall						
Actual	7.5	.46	3	unknown	unknown	unknown	unknown
Model	7.5	.46	3	7.5	.2	15	0
Fig 18	1.75" wood doors, Rm 429, Spanagel Hall						
Actual	5	.46	3	unknown	unknown	unknown	unknown
Model	5	.46	3	7	.025	15	0
Fig 19	5.5" wall w/ chalkboard, Rm 408, Spanagel Hall						
Actual	7.5	.46	3	unknown	unknown	unknown	unknown
Model	7.5	.46	3	4	.04	15	0
Fig 20	10.75" cement wall, Rm 421, Spanagel Hall						
Actual	5	.89	3	unknown	unknown	unknown	unknown
Model	7.5	.46	3	10	.0125	15	0
Fig 21	1.75" metal covered doors, roof, Spanagel Hall						
Actual	7.5	.46	3	unknown	unknown	unknown	unknown
Model	7.5	.46	3	7.5	.2	15	0

Table 3. Summary of propagation loss measurements and calculations

3. Summary

A mathematical model was developed to approximate the propagation of a spherical electromagnetic wave front through a wall. Discrepancies between the measured and computed data can be attributed to the limitations of the

model and possible inaccuracies in the measured data. The assumptions inherent in the model are as follows:

1) the polarization of the source and receive antennas is vertical,
2) surface roughness of the wall is neglected and the faces are parallel,
3) loss tangent and dielectric are constant throughout the wall,
4) a frequency independent dielectric constant and loss tangent are used in the equations for impedance, phase, and attenuation, and
5) multiple reflections within the wall are neglected.

Based on the data in Figures 17 through 21 several conclusions can be made. First, it does not appear that the effects of mulitpath are significant. The ripple at lower frequencies is at most 4 dB peak to peak for low loss materials such as wood (Figure 19). For lossy materials the multipath effect is even less noticeable. Secondly, one can conclude that this simple model provides a relatively accurate estimate of wall losses if the dielectric constant and loss tangent can be determined from visual inspection of the wall.

With regard to the MRPV, the smaller wall losses at lower frequencies indicate that the 2.45 GHz scientific and commercial frequency band is preferable to the 5.5 GHz band. However, the antenna design also enters into the frequency selection tradeoff. As the frequency decreases, the gain decreases for a fixed antenna size. This effect favors the higher frequency. The wall loss is probably the more important of the two, because the beam may pass through several walls.

IV. ANTENNA DESIGN

A. BACKGROUND

The transmission of beamed microwave power for the MRPV is designed such that a substantial amount of pitch and roll can be tolerated without significant power collection loss. This is accomplished with a highly directional transmitter and a near omni-directional receiver. Therefore, the reception of power for the MRPV is based on an antenna design that provides maximum coverage in space. This coverage is attained through a design that approximates the far-field pattern of an ideal dipole.

1. Configurations

In determining the antenna design for the MRPV, several configurations exist for both horizontal and vertical polarizations. Given consideration of the effect of ground returns on the total received field, the polarization of the antenna is of importance. The multi-path effect that is present when operating near the ground can cause an undesired cancellation of the direct and reflected paths of the transmitted microwave beam. This would result in a reduction in the total received field at the antenna. A wave with horizontal polarization has a large ground reflection coefficient while a wave with vertical polarization has a smaller ground reflection. Thus multi-path favors vertical polarization. However, multi-path is only of secondary concern because the transmit antenna beam is very narrow. The major reason for using vertical polarization is the most efficient and compact antennas that conform to the vehicle shape are vertically polarized. Two such antenna configurations for the MRPV are shown in Figure 22.

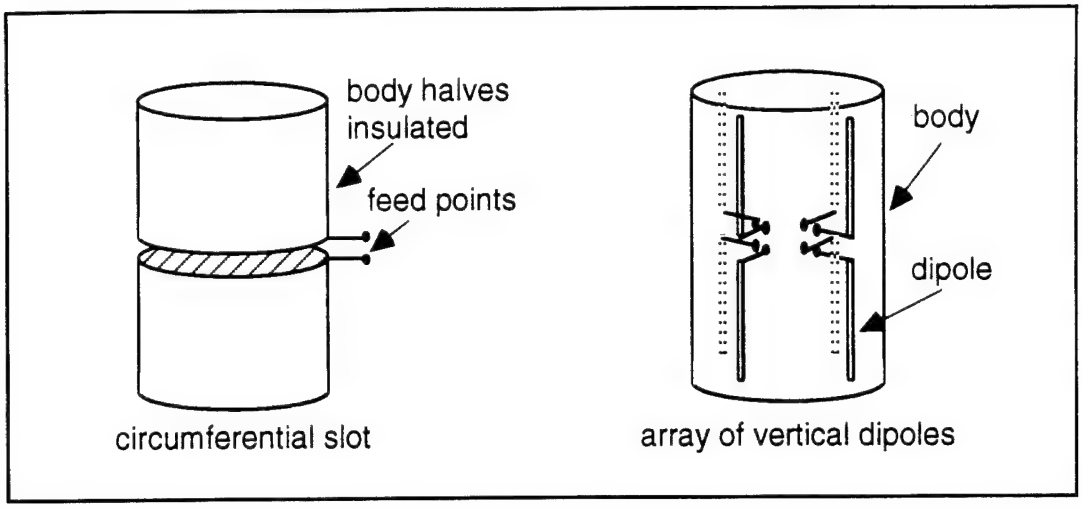

Figure 22. Possible antenna configurations

2. Circumferential Slot

The preferred configuration for vertical polarization is the circumferential slot antenna. As shown in Figure 22, the design uses direct excitation of the body with feed points on each of the insulated body halves. The primary advantage of the slot antenna over the array of vertical dipoles is the simplicity of the feed. The vertical array of dipoles would consist of at least four dipoles requiring some feed circuitry. The complexity of the design would also increase based on the number of dipoles chosen in the array. The radiation pattern of the dipole array will also be affected by the mutual coupling between the dipoles themselves as well as with the vehicle body. The results of the propagation loss study (Chapter III, Section C) indicate that the 2.45 GHz scientific and commercial frequency band is preferable to the 5.5 GHz band. At 2.45 GHz the circumferential slot with a cylinder length of approximately 6 cm corresponds to an excitation of $(1/2)\lambda$. At 5.5 GHz the slot antenna with a cylinder length of 6 cm corresponds to an excitaion of $(1)\lambda$.

Although the electric field pattern is optimized for maximum coverage (i.e. has a dipole pattern) at frequencies where the body is less than a wavelength, the efficiency of the antenna favors the lower frequency. Antennas that are electrically small have a large input reactance. In the case of the MRPV, this problem is avoided because, although the antenna is electrically short, it is not electrically thin. The antenna impedance is important in the transfer of power from the receiver to the battery. Since the final dimensions of the MRPV are not yet chosen, the design of the circumferential slot is centered around a full wavelength excitation. Due to the limitations of testing in the NPS anechoic chamber, a scaled version of the antenna prototype was designed to operate at X-band, whereas the actual antenna will operate at S-band.

B. SIMULATION

1. Method of Moments

The calculations of far-field patterns for the prototype antenna designs were done using the PATCH computer code developed at the Sandia National Laboratories [Ref. 7]. PATCH is a frequency domain electromagnetic scattering code based on a method-of-moments solution to the Electric Field Integral Equation (EFIE). The objects in PATCH are modeled by planar triangular patches, which easily conform to surfaces and boundaries of general shape and allow variable patch densities over the surface of the object. Although the EFIE has been formulated in terms of a scattering problem, the PATCH code has the ability to treat both plane wave and voltage source excitations. Therefore, PATCH is capable of handling antenna problems if the terminals across which a voltage drop can be defined are identified. The voltage drop can be represented by cutting a thin slot along the edge of two adjoining

patches to create a potential difference between the two triangular patches. This is shown in Figure 23 where the two adjoining triangular patches, A and B, are specified to have a potential difference of V_S with a surface current $\bar{J}_s$ across the slot. To model a structure effectively, the density of the triangular patches must be sufficient to accurately represent variations in surface geometry and surface current density. The edge lengths of each triangular patch used are 1/10 of a wavelength.

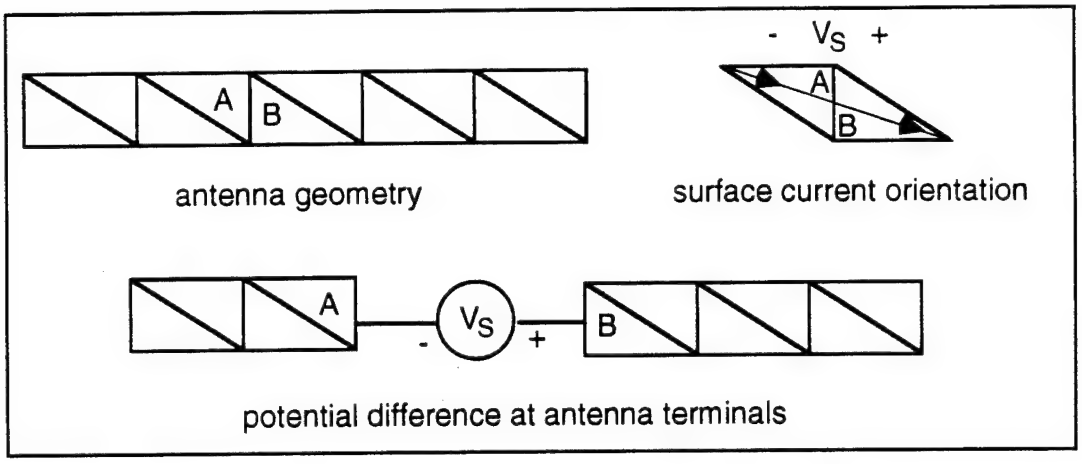

Figure 23. Voltage source excitation with PATCH

2. Antenna Model

Two models are constructed for the circumferential slot antenna: 1) an edge fed slot antenna, and 2) a center fed slot antenna. Both models were used to determine the effects of feed point location on the field pattern. In the first case, a triangular mesh structure is built for two unattached cylinders each closed on one end. The edge fed antenna model is shown in Figure 24, where the upper and lower cylinders are connected on the edge by a quadrilateral tab. The tab, as shown in Figure 25, serves as the feed point for the antenna

terminals. The units have arbitrarily been chosen so that the cylinder length is 500 m, and therefore a frequency of 0.6 MHz was used in the computation. This choice results in an overall antenna length that matches the desired (1)λ.

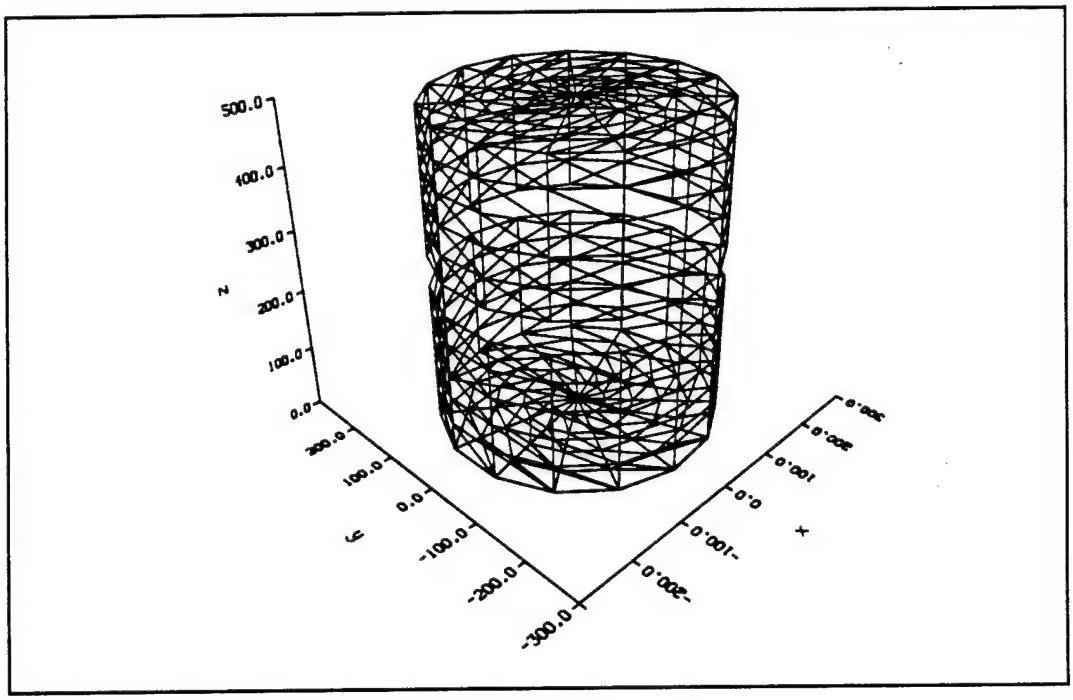

Figure 24. Edge fed slot antenna - isotropic view

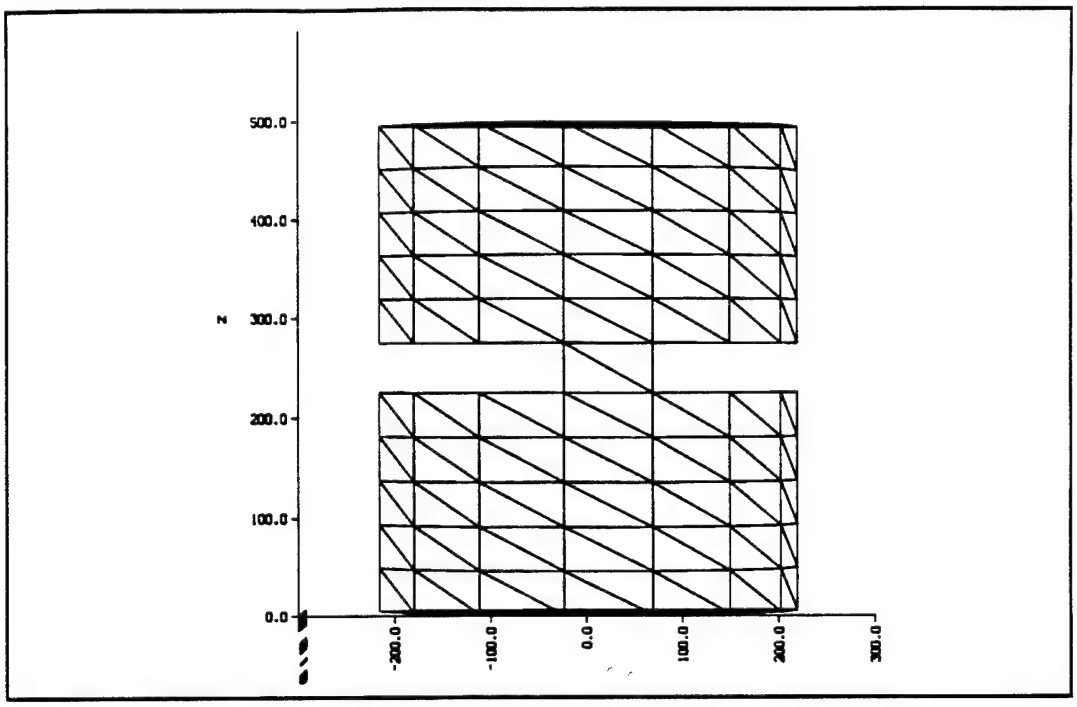

Figure 25. Edge fed slot antenna - profile view

The center-fed antenna model is shown in Figure 26. In this case, the upper and lower cylinders are closed on each end. A quadrilateral tab structure, which serves as the feed point for the antenna terminals, is located on the center point of each closed end as shown in Figure 27. The tab structure is constructed with a symmetrical center feed to provide a current with matching phases along the perimeter of the cylinders. Again, the excitation frequency is scaled relative to the overall antenna length to obtain the desired size in wavelengths.

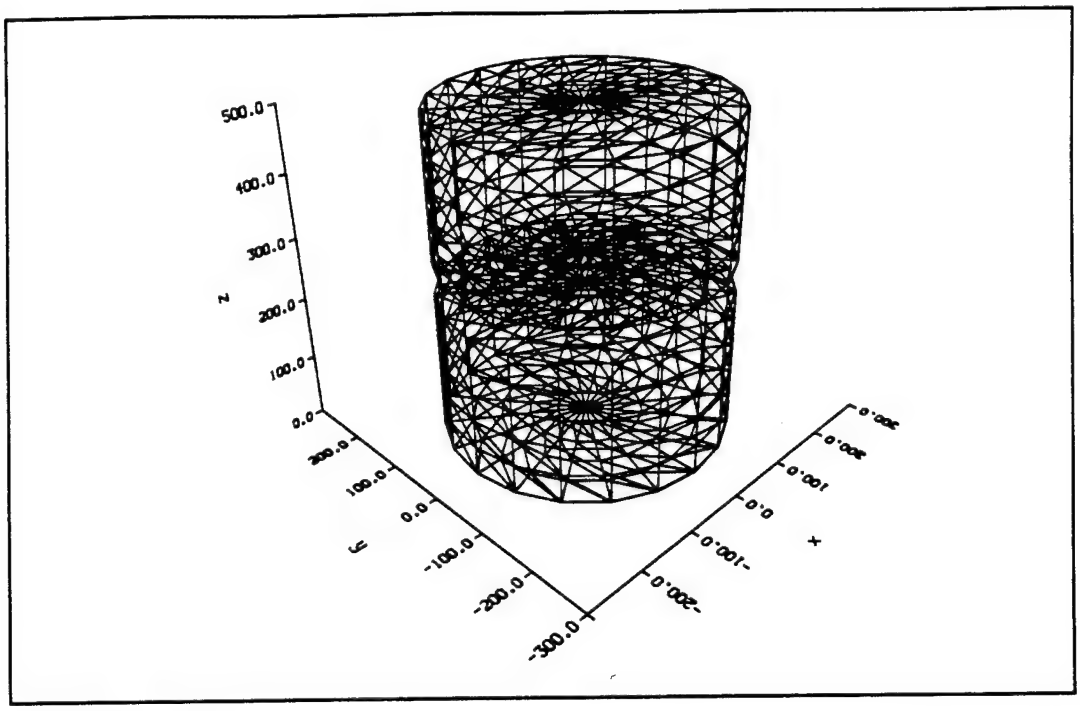

Figure 26. Center fed slot antenna - isotropic view

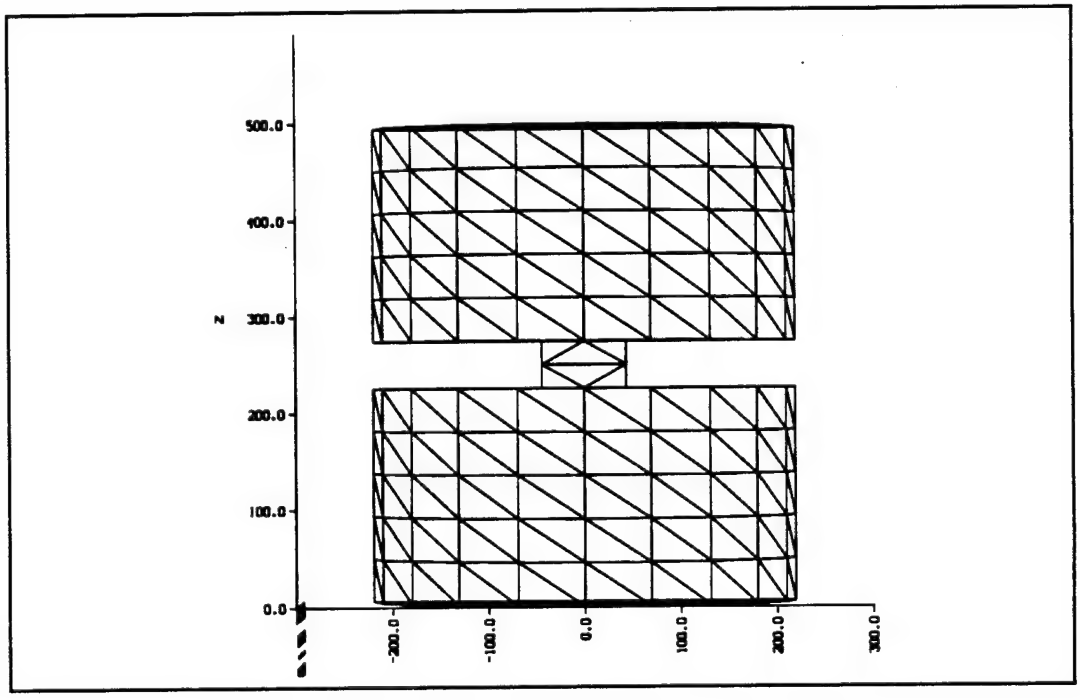

Figure 27. Center fed slot antenna - profile view

3. Results

The normalized computed patterns for the edge fed slot antenna are provided in Figures 28 and 29 for the E and H plane far field patterns, respectively. If the vehicle is flying straight and level, the E-plane (or vertical plane) is perpendicular to the ground; the H-plane (or horizontal plane) is parallel to the ground. As shown, the location of feed points results in a non-symmetric field pattern with nulls in both planes. This is caused by the surface currents being out of phase along the perimeter of the antenna. Therefore, the location of the feed point cannot be on the rim of the body, but must be centered on each cylinder interior cap to provide equal phasing of the surface currents. The normalized computed results for the center fed slot antenna are provided in Figures 30 and 31 for the E and H plane far field patterns, respectively. With a center feed point, the surface currents are flowing radially outward from the center of the body and arrive in equal phase along the perimeter of the body. As shown, this results in a symmetric field pattern in the E plane, and a near constant field pattern in the H plane. As a result of the PATCH simulation, a center fed circumferential slot antenna is chosen for the prototype design.

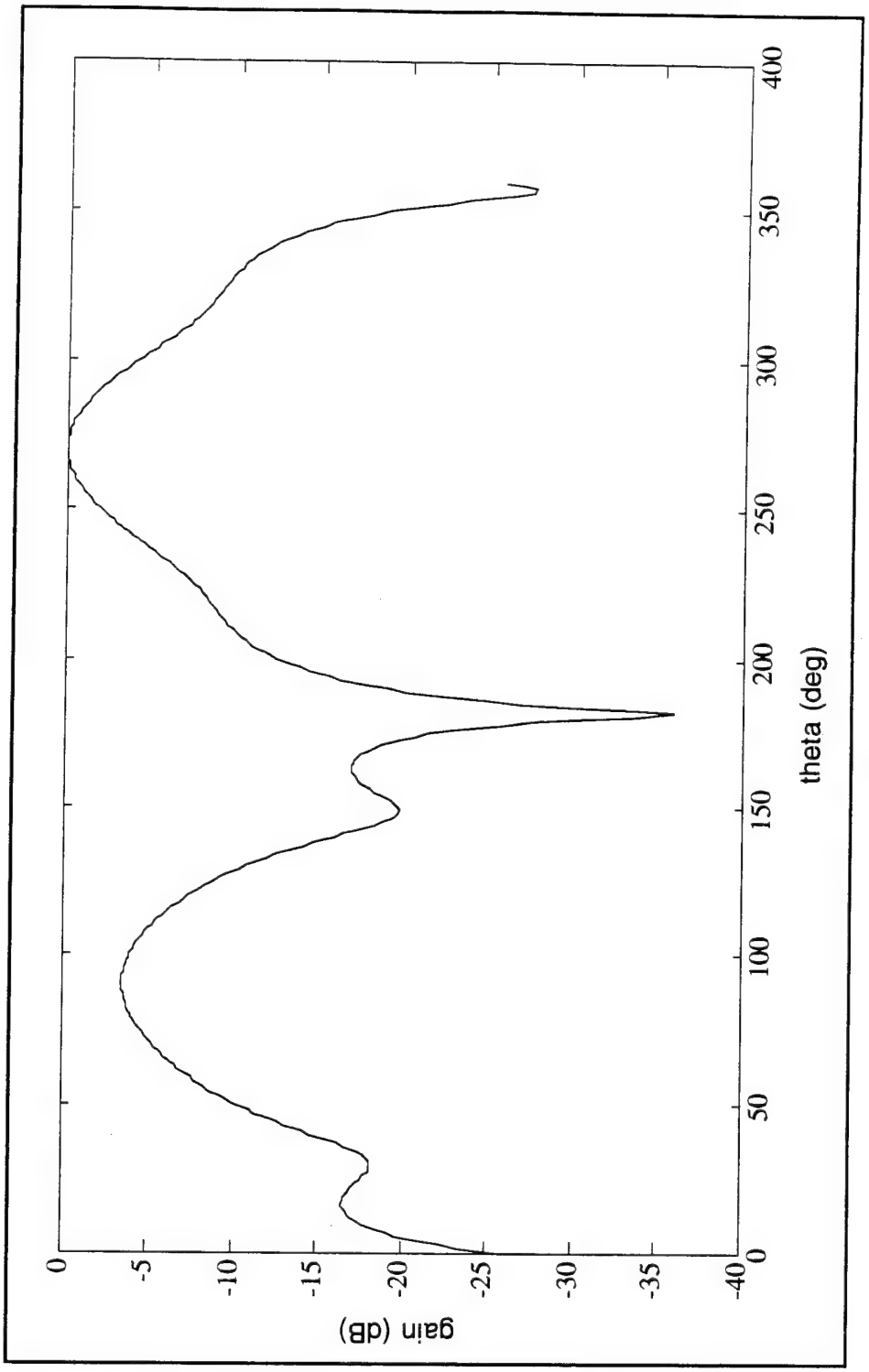

Figure 28. E-plane of edge fed slot antenna

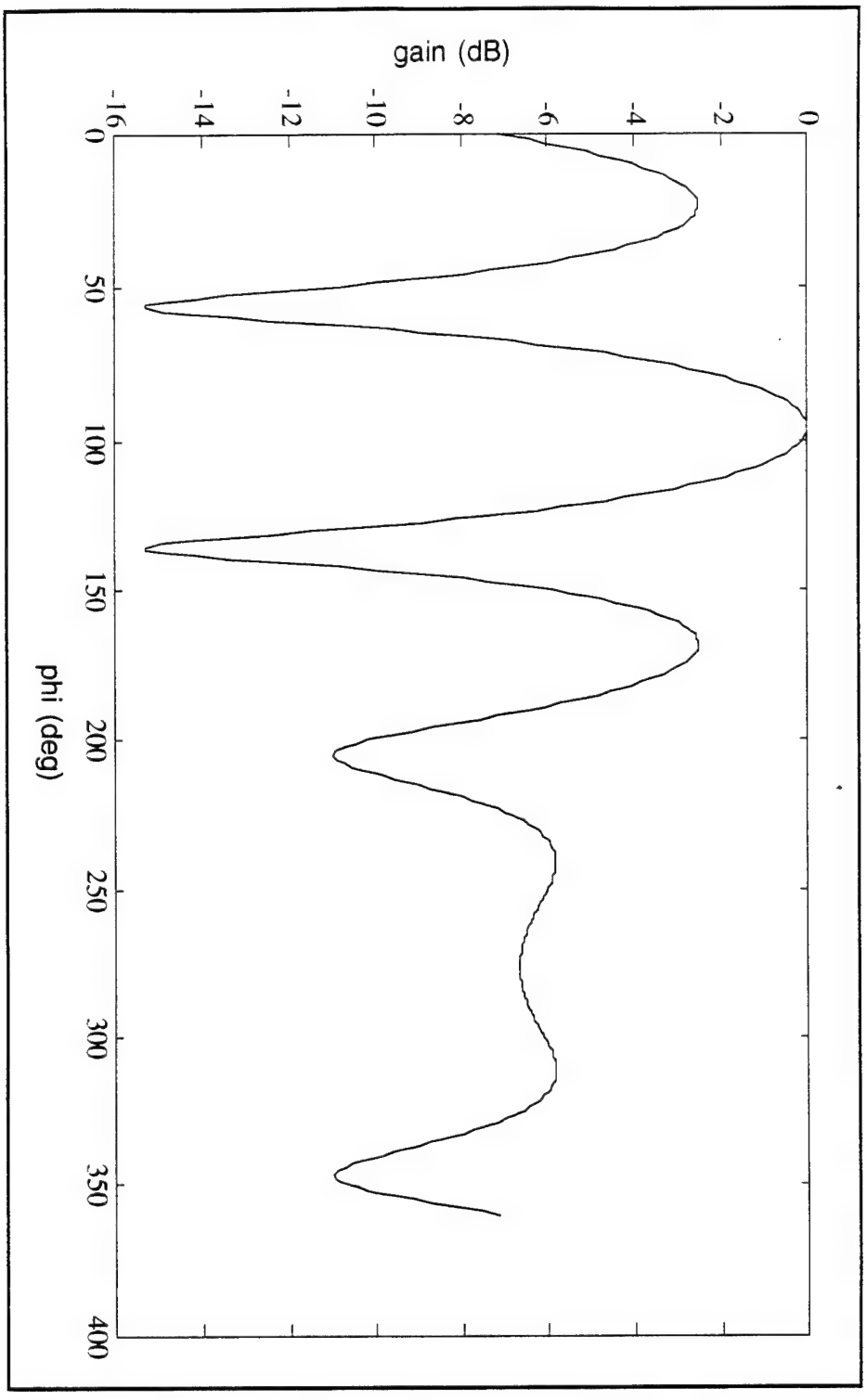

Figure 29. H-plane of edge fed slot antenna

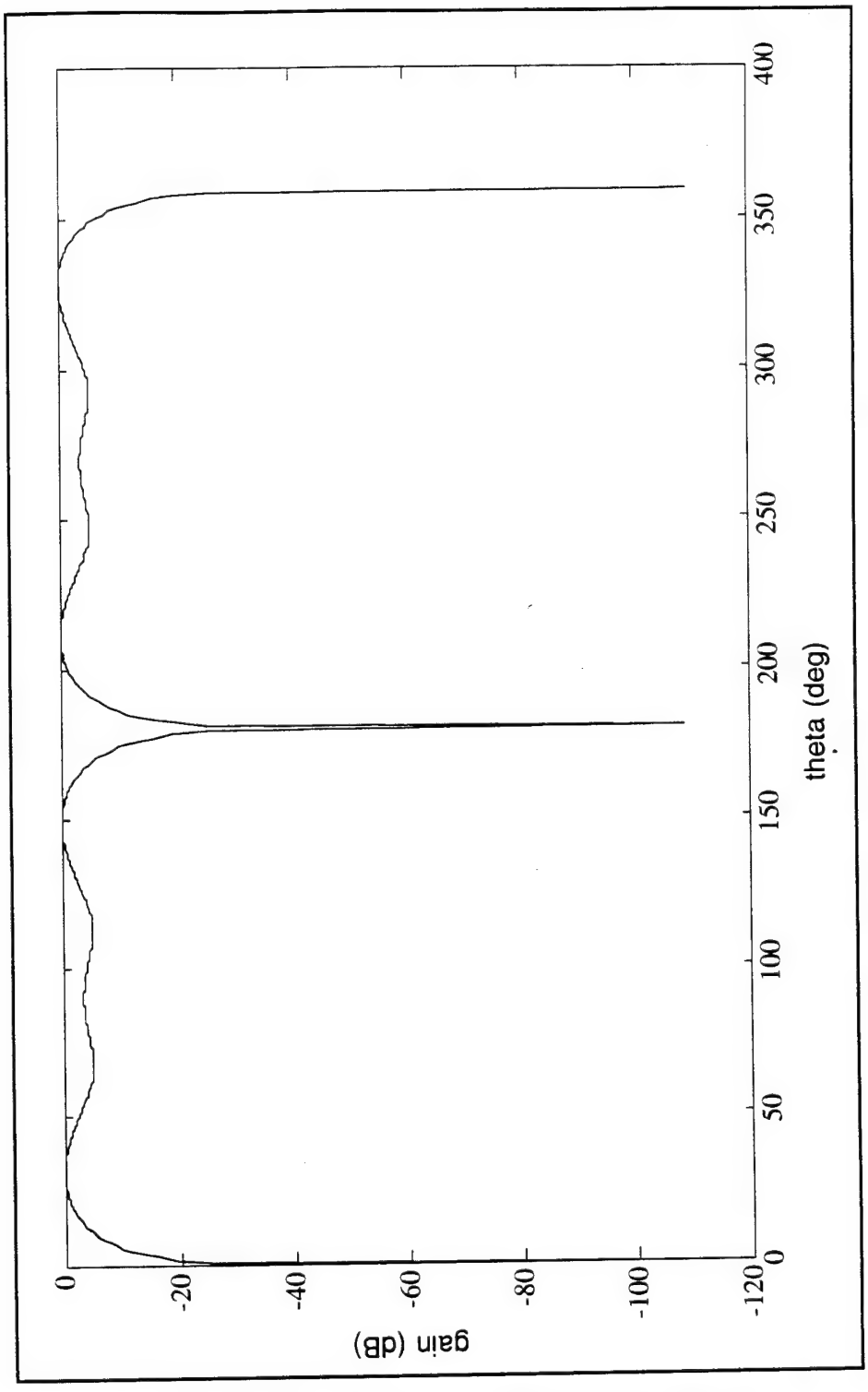

Figure 30. E-plane of center fed slot antenna

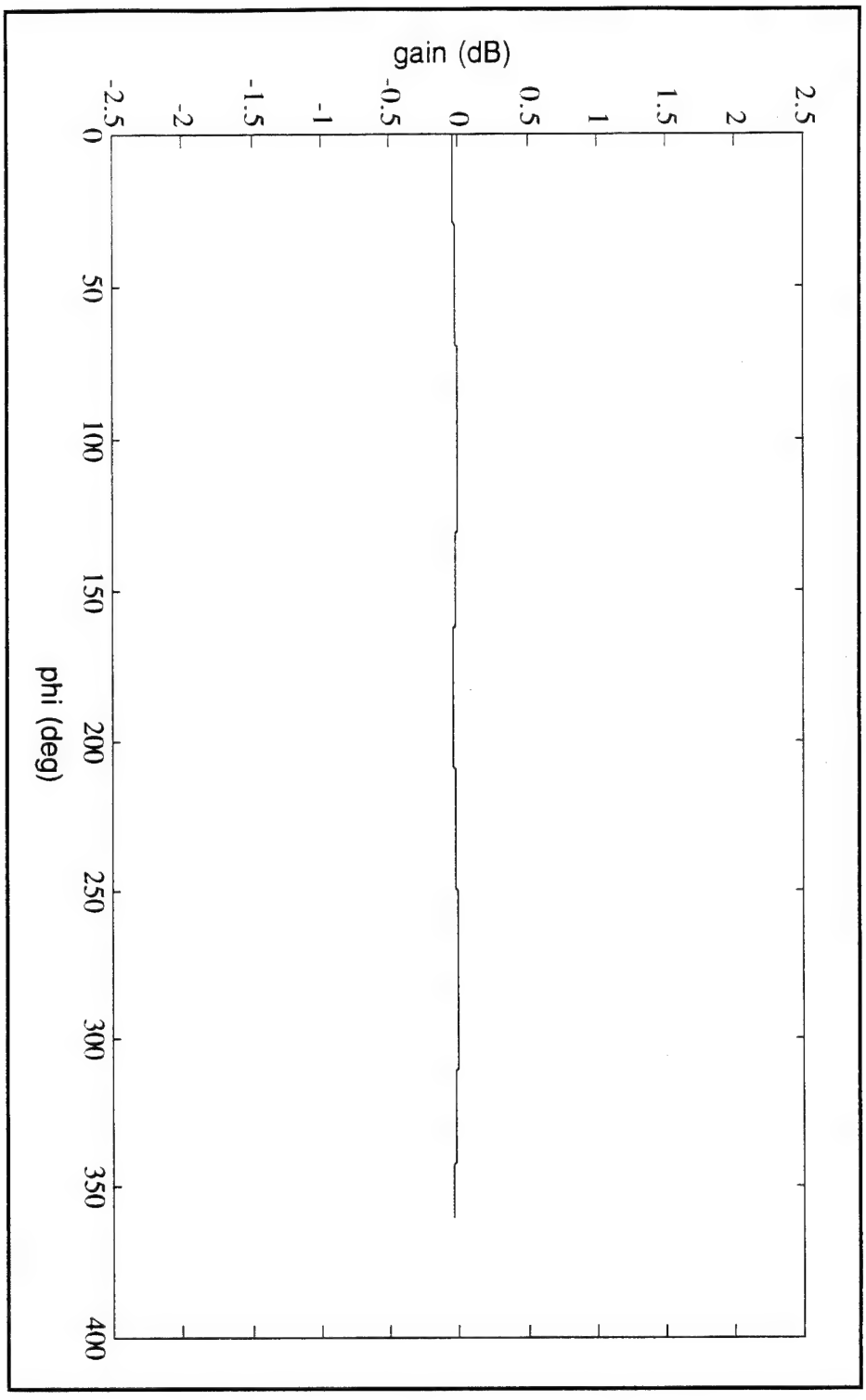

Figure 31. H-plane of center fed slot antenna

C. ANTENNA PROTOTYPE

A prototype of the center fed circumferential slot antenna was designed and tested. The antenna, depicted in Figure 32, consists of two cylindrical copper (Cu) caps attached to a 50 ohm RG 141 semi-rigid coaxial cable. The center and outer conductors are soldered to the caps, which are then closed on each of the ends with a Cu film to enclose each cylinder. Since the antenna is

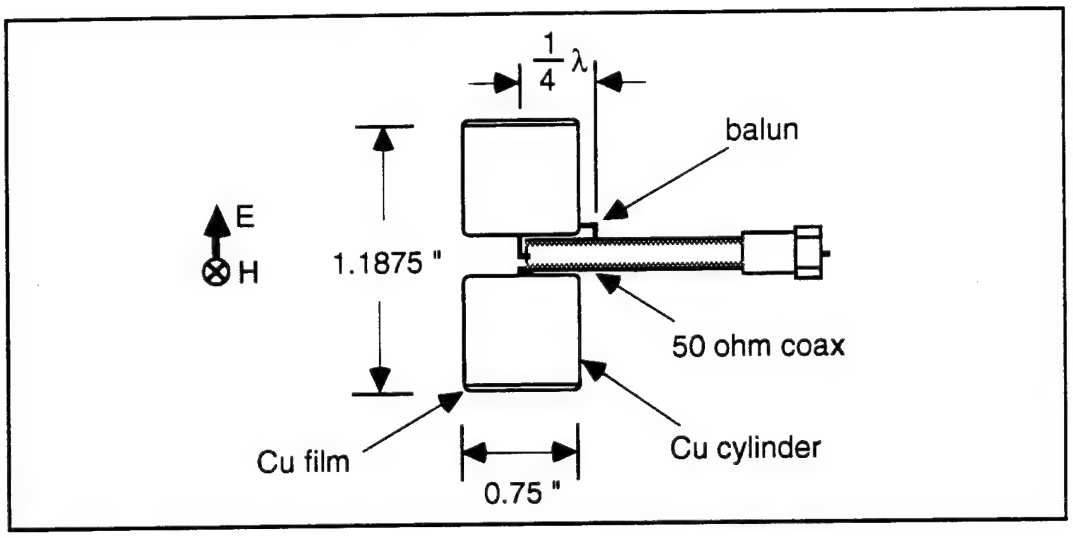

Figure 32. Prototype antenna

symmetrical in nature, the currents excited from an incident wave will also be symmetrical (or balanced). However, when an incident wave is launched down a coaxial line to a symmetrical antenna, a current will flow back on the outside of the outer conductor which unbalances the currents on the antenna and transmission line. The unbalanced currents will degrade the ability of the antenna to radiate and increase its input VSWR. In order to balance the currents on the coaxial line, a quarter wave balun is connected to the antenna. The balun, which is a contraction for "balanced to unbalanced," suppresses the

outside current which is causing the imbalance. The balun transforms the balanced input impedance of the slot antenna to the unbalanced coaxial line such that there is no net current on the outer conductor of the coax [Ref. 5]. A picture of the prototype slot antenna is shown in Figure 33.

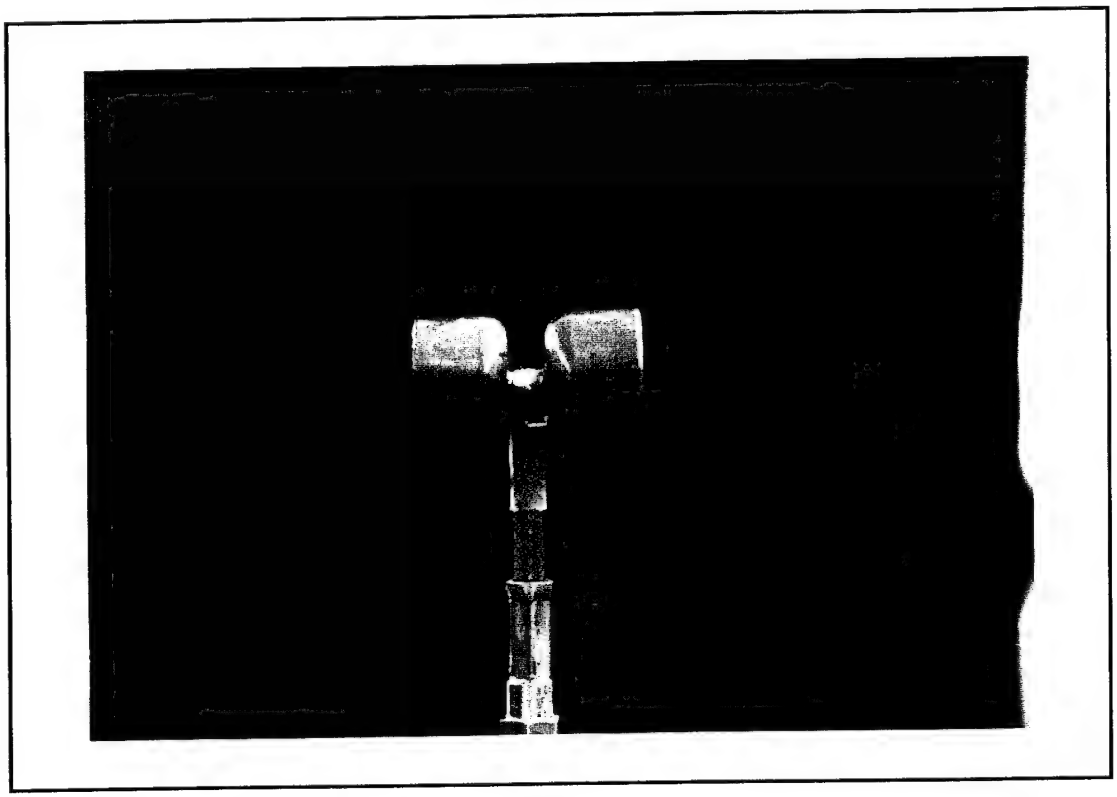

Figure 33. Circumferential slot antenna - prototype

V. ANTENNA MEASUREMENTS

A. ANTENNA PARAMETERS

The antenna parameters were measured using an HP 8510C network analyzer. The reflection parameters of the network were measured to determine the impedance, return loss, and Voltage Standing Wave Ratio (VSWR) of the slot antenna. Using the HP 8510C, a scattering parameter measurement was made to determine the S parameters S_{11} and S_{12} of the slot antenna. The measurement set-up is depicted in Figure 34 [Ref. 8]. As shown,

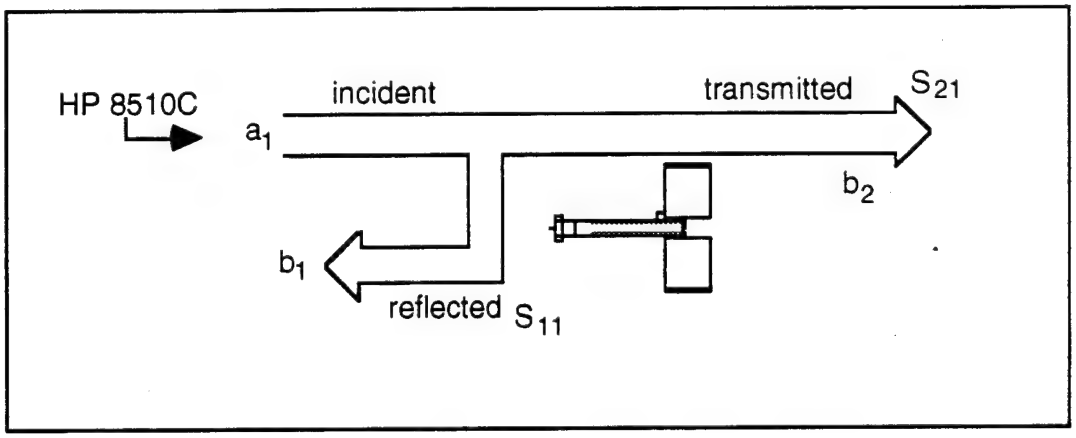

Figure 34. Scattering parameter measurement

the S_{11} parameter represents the reflection coefficient Γ, and the S_{12} parameter is the forward transmission coefficient τ. The measurements were taken from 9.5 to 10.5 GHz. The return loss is extracted from the S parameters and provided as a plot in Appendix D. A smith chart of the antenna impedance is included as Figure 35. The complex antenna impedance varies with frequency from $Z_{9.5GHz} = 23.2 - j9.3$ to $Z_{10.5GHz} = 98.6 + j36.8$. The optimum

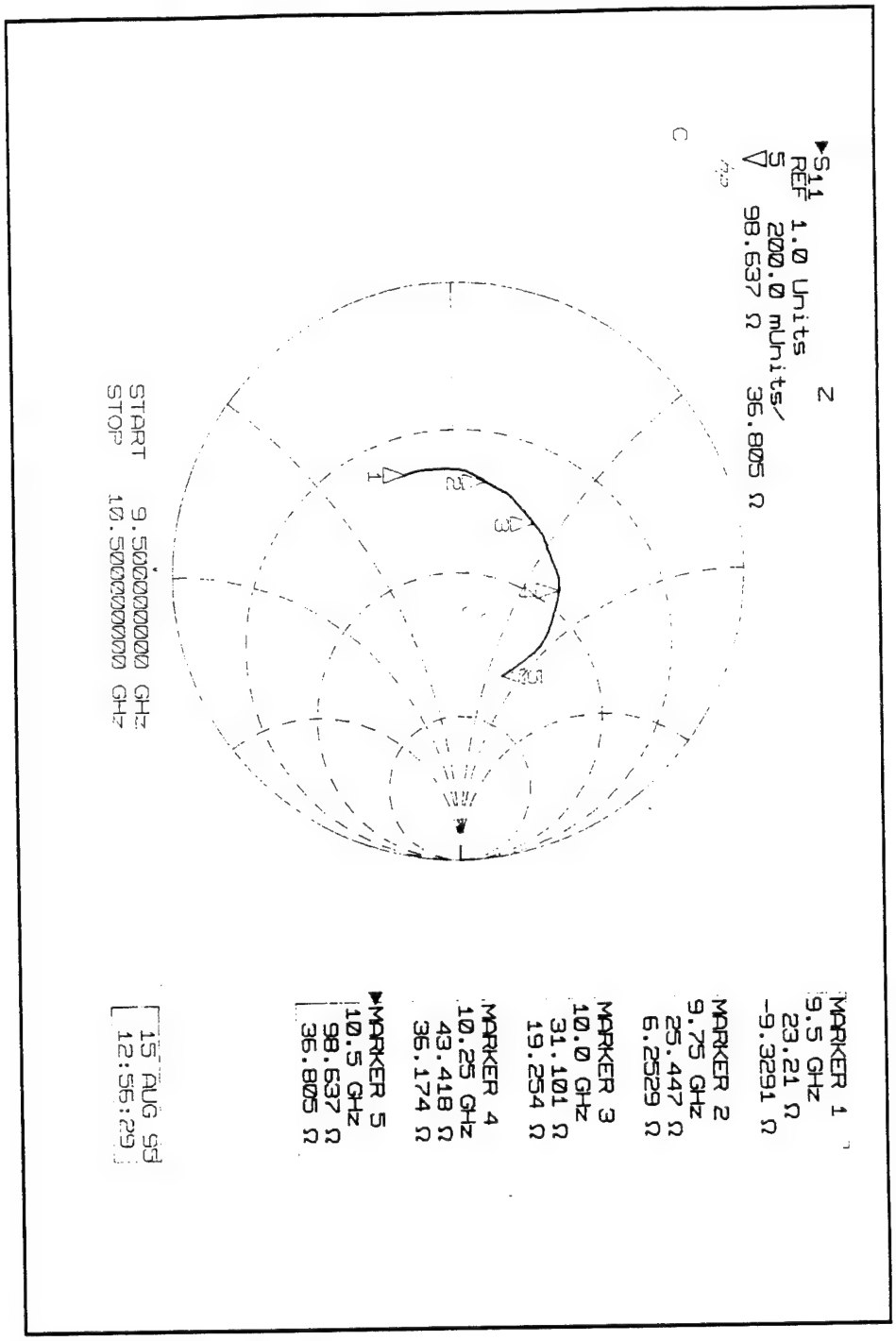

Figure 35. Smith chart of slot antenna

impedance for maximum transfer of power with a 50 ohm coaxial line is $Z_o = 50 + j0$. At a frequency of approximately 10.3 GHz, the complex impedance consists of a real 50 ohms with an inductive reactance. Thus, by tuning the antenna in frequency and matching it with a conjugate reactance, the antenna can be matched to the coaxial transmission line. The measured return loss at the full wavelength excitation of 9.9 GHz is -9.7 dB. Therefore, the power reflection coefficient is equal to

$$|\Gamma|^2 = 10^{(\text{Loss}/10)} = 10^{(-9.7/10)} = 0.107 \quad . \tag{5.1}$$

Thus about 89% of the power delivered to the antenna is radiated, and 10% is reflected. This is a mismatch loss of about .45 dB. The VSWR of the antenna at 9.9 GHz is

$$\text{VSWR} = \frac{1+|\Gamma|}{1-|\Gamma|} = \frac{1+|0.327|}{1-|0.327|} = 1.97 \quad . \tag{5.2}$$

B. PATTERN MEASUREMENT

The far-field patterns of the prototype slot antenna were measured in the NPS anechoic chamber. A general layout of the X-band anechoic facility is provided as Figure 36. As indicated in Chapter IV, Section A, the antenna prototype is designed at a scaled version to operate at X-band.

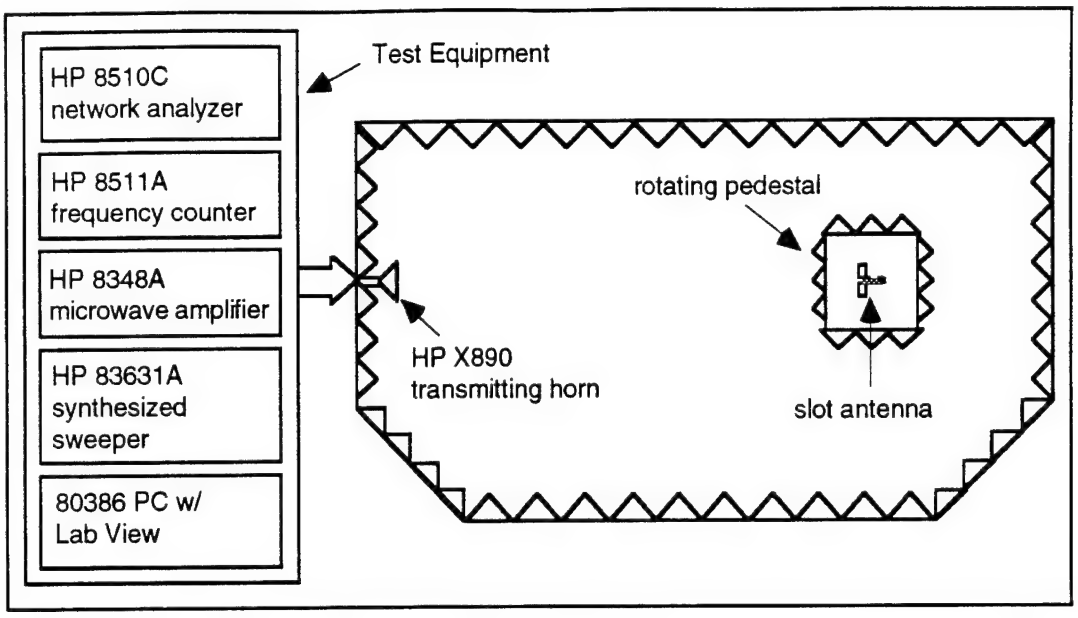

Figure 36. NPS X-band anechoic chamber

1. Test Set-Up

The test set-up for the far-field pattern measurements is shown in Figure 37. The HP X890 transmitting horn is oriented for horizontal transmission for the electromagnetic wave. For an E plane measurement, the slot antenna is centered over the pedestal with a horizontal orientation. The transmitting horn is oriented with a horizontal E plane and the pedestal then rotated with measurements taken for the specified angular increment. The H plane measurement is taken in the same manner, with the transmitting H plane horizontal, and the slot antenna centered over the pedestal with a vertical orientation. A 386 PC with the test equipment software Lab View is used to operate the test equipment.

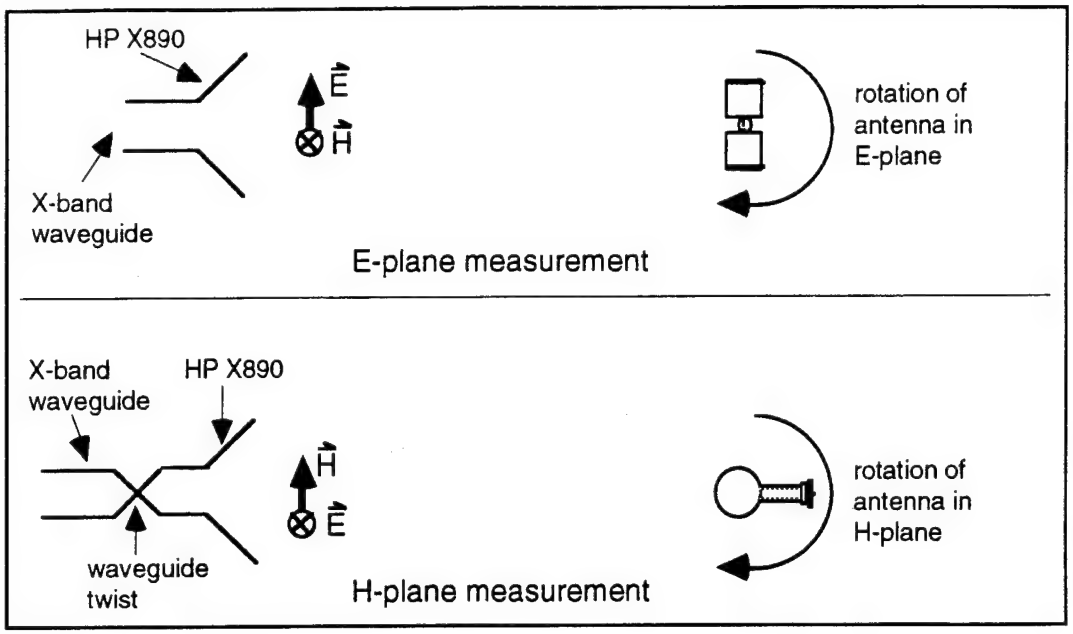

Figure 37. Far-field pattern measurements

2. Far-Field Measurements

The normalized far-field patterns for the E and H planes of the slot antenna were measured and are provided in Figures 38 and 39, respectively. The E plane measurement from 0^{o} to 180^{o} is shown to have a half power beamwidth HPBW=102^{o}. The portion of the pattern from 180^{o} to 360^{o} is affected by the exposure of the balun and cable blockage of the incident field, thereby corrupting the pattern. The H plane measurement contains a ripple with a maximum value of 8 dB. Figure 38 indicates that the pattern is also affected by the exposure of the balun and shadowing of the incident field by the feed cable.

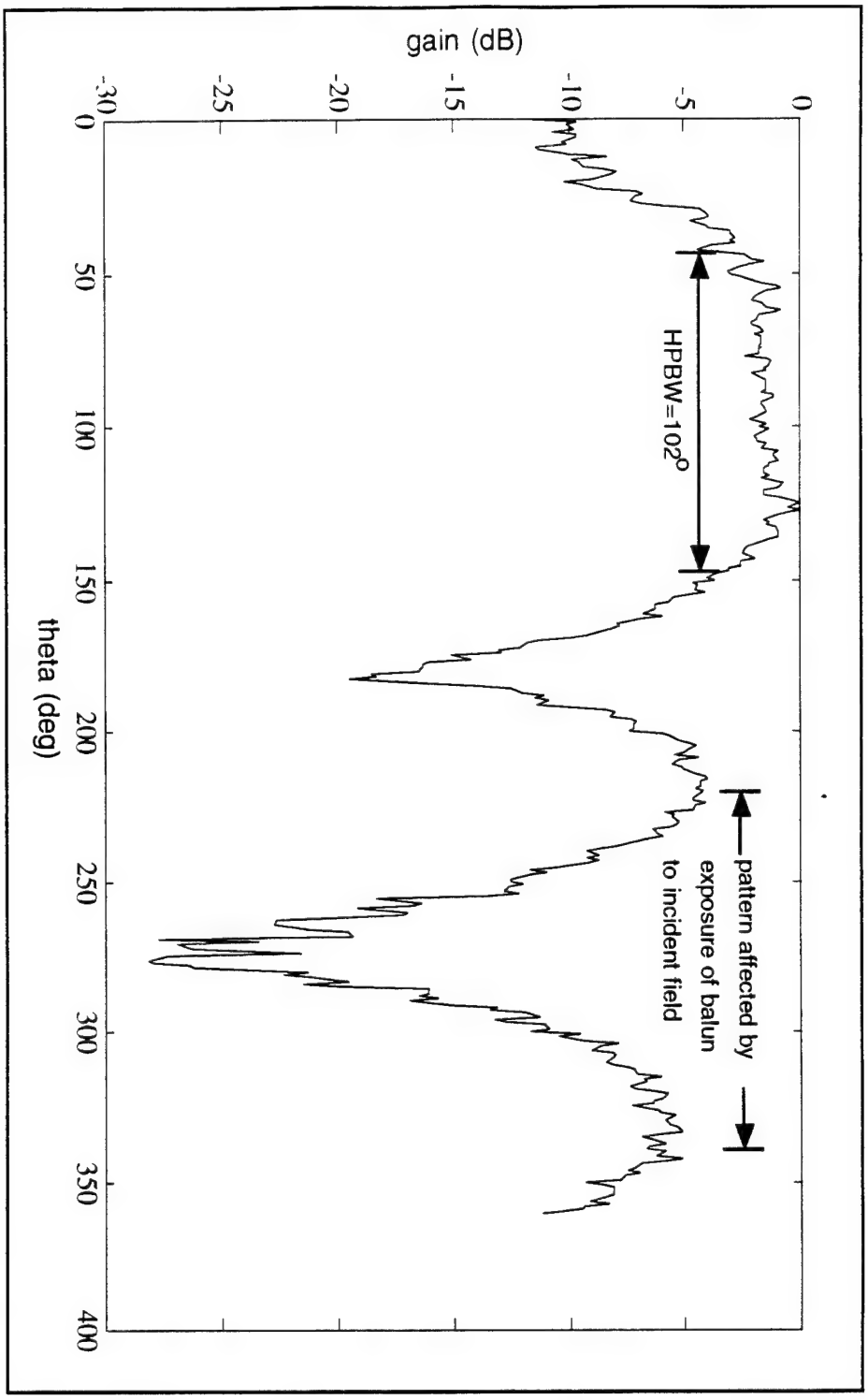

Figure 38. Measured E-plane pattern

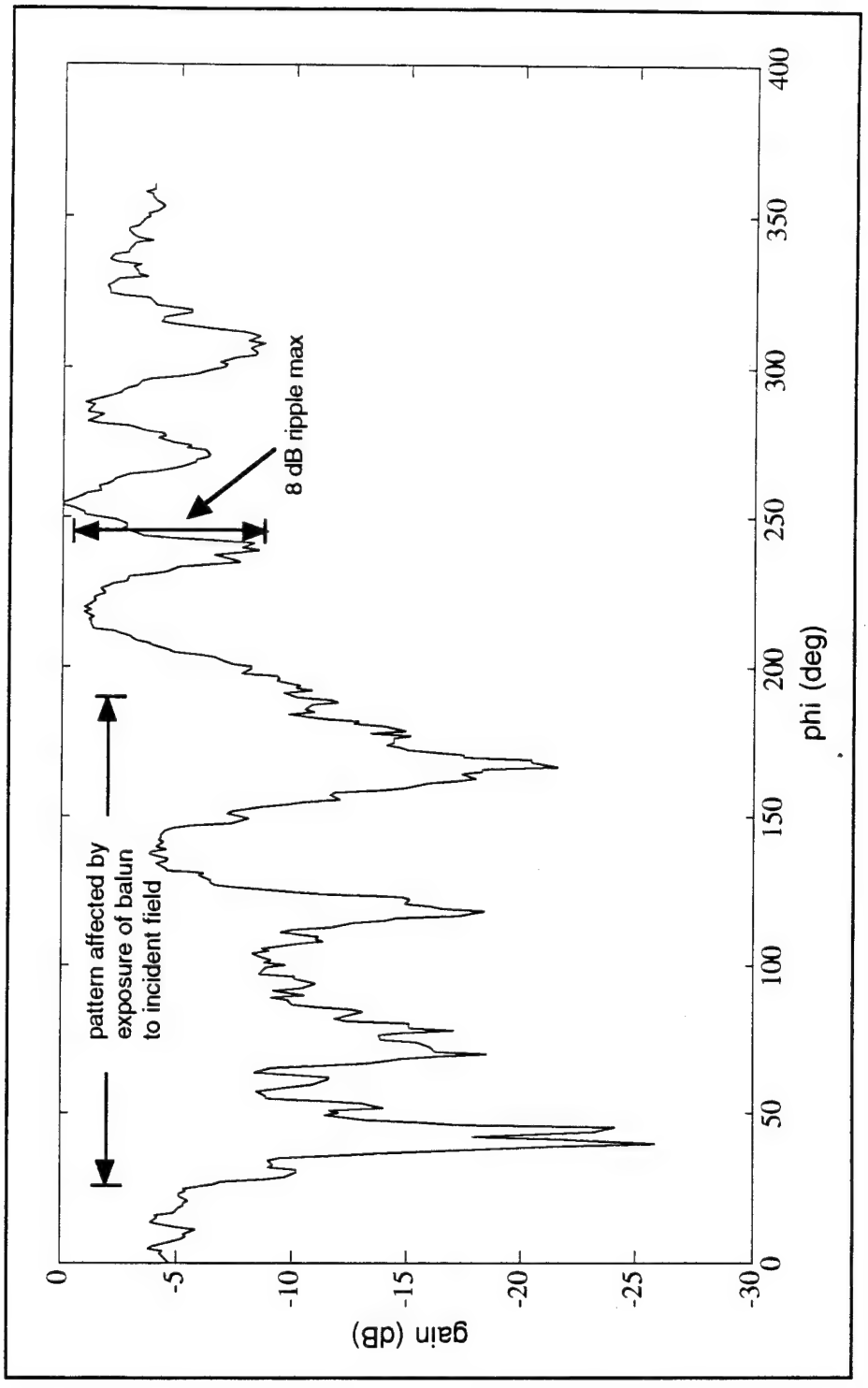

Figure 39. Measured H-plane pattern

C. RF TO DC POWER CONVERSION

The final section of measurements deals with the conversion of the microwave signal to usable dc power. The device that accomplishes this is known as the rectenna and consists of the slot antenna and a diode rectifier. The antenna collects the incident field and delivers microwave power to the feed point. The rectifier converts the microwave power to a dc signal. In order to determine the rectenna's ability to convert power, the efficiencies of the antenna and rectifier are estimated.

1. Antenna Efficiency

The efficiency of the slot antenna is determined by measuring the gain of the antenna and comparing it to the directivity. The antenna efficiency is defined by

$$e = \frac{G}{D} \tag{5.3}$$

where G is the antenna gain and D is the directivity. The directivity represents the power gain an antenna would have if all received power appeared as output power. The gain of the slot antenna is measured using a constant power transmitter and a reference antenna with known gain. Using the known standard gain of the reference antenna, the absolute maximum power gain of the slot antenna is calculated from the differences in the measured receive powers. The ratio P_t/P_s is the increase in received power from the test antenna over that of the standard gain antenna. Therefore, the measured gain of the test antenna is given by [Ref. 5]

$$G_t = \frac{P_t}{P_s} G_s \quad . \tag{5.4}$$

The Microline 56x1 antenna is used as the standard gain horn antenna with a specified nominal gain G_s = 17 dB at X-band. The measured power gain of each antenna for a constant transmitted power is P_t = -38.25 dB and P_s = -21.75 dB. Writing equation (5.4) in terms of dB, yields

$$G_t(dB) = P_t(dB) - P_s(dB) + G_s(dB) \quad . \tag{5.5}$$

The gain of the slot antenna is determined from

$$G_t = -38.25\ dB - (-21.75\ dB) + 17\ dB = .5\ dB \quad . \tag{5.6}$$

This measurement of gain was taken at $\theta = 90^o$ in the E plane and $\phi = 0^o$ in the H plane. At $\phi = 0^o$, a gain of -4.7 dB is measured in the H plane with an average gain of -3.7 dB. The accuracy of the measurement is $\pm$ .5 dB. Therefore, the gain of the slot antenna is now given by

$$G_t = .5\ dB + (\ -3.7 - (\ -4.7\ )\ )\ dB \pm .5\ dB = 1.5 \pm .5\ dB \quad . \tag{5.7}$$

The directivity of an antenna is the maximum value of directive gain given by

$$D = \frac{U_m}{U_{ave}} \tag{5.8}$$

where U_{ave} is the average radiation intensity defined as

$$U_{ave} = \frac{1}{4\pi}\iint U(\theta,\phi)d\Omega = \frac{P_r}{4\pi} \tag{5.9}$$

and U_m is the maximum radiation intensity given by

$$U_m = \frac{P_r}{\Omega_A} \tag{5.10}$$

where the term P_r is the total radiated power and Ω_A is the antenna beam solid angle. The antenna beam solid angle is the solid angle through which all the power would be radiated if the power per unit solid angle (radiation intensity) equaled the maximum value over the beam area. The directivity can now be defined as

$$D = \frac{U_m}{U_{ave}} = \frac{P_r/\Omega_A}{P_r/4\pi} = \frac{4\pi}{\Omega_A} \quad . \tag{5.11}$$

The antenna beam solid angle is given by

$$\Omega_A = \iint |F(\theta,\phi)|^2 d\Omega \tag{5.12}$$

where the term $|F(\theta,\phi)|^2$ is the normalized field pattern replaced by two fourth order polynomials $f_{n1}(\theta)$ and $f_{n2}(\theta)$ which approximate the E plane data of Figure 38 in a least squares sense. The approximation is shown in Figure 40 where the normalized E plane data is linearized and taken from 0 to 2π. The polynomial $f_{n1}(\theta)$ exists from 0 to π given by

$$f_{n1}(\theta) = -.0064\theta^4 - .0262\theta^3 - .0999\theta^2 + .7368\theta - .0068 \tag{5.13}$$

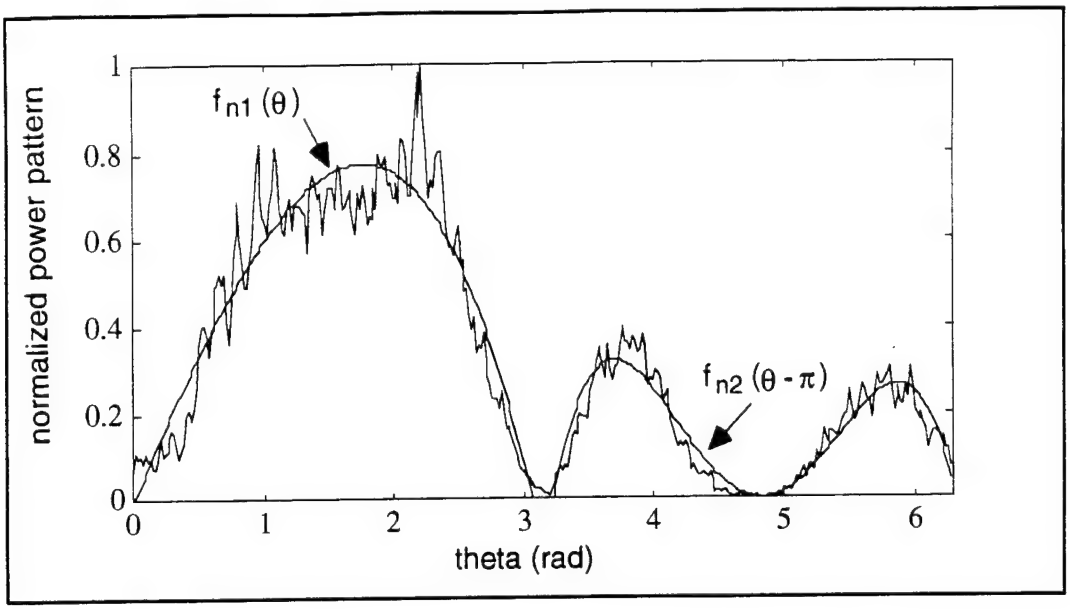

Figure 40. Polynomial approximation to E plane data

and the polynomial $f_{n2}(\theta)$ exists from π to 2π given by

$$f_{n2}(\theta) = -.1998(\gamma)^4 + 1.3188(\gamma)^3 - 2.7836(\gamma)^2 + 1.9771(\gamma) - .1237 \quad (5.14)$$

where the term $\gamma = \theta - \pi$. The beam solid angle is now written as

$$\Omega_A = \int_0^{2\pi}\int_0^{\pi} \frac{f_n(\theta)}{f_{max}} \sin\theta d\theta d\phi = \int_0^{\pi}\int_0^{\pi} \frac{f_{n1}(\theta)}{f_{max}} \sin\theta d\theta d\phi + \int_{\pi}^{2\pi}\int_0^{\pi} \frac{f_{n2}(\theta - \pi)}{f_{max}} \sin\theta d\theta d\phi \quad (5.15)$$

where each polynomial is normalized by the maximum value f_{max}. With work, the integral of Equation (5.15) results in

$$\Omega_A = \Omega_1 + \Omega_2 = 4.92 + 1.08 = 6.0 \text{ sr} \ . \quad (5.16)$$

Using the calculated beam solid angle, the directivity of the slot antenna is given by

$$D = \frac{4\pi}{6.0} = 2.09 = 3.21 \text{ dB} . \qquad (5.17)$$

The efficiency of the slot antenna is now calculated with the measured gain and directivity as

$$e = \frac{G_t}{D} = \frac{10^{(1.5/10)}}{10^{(3.21/10)}} = .675 = 67.5\% . \qquad (5.18)$$

However, there is a $\pm$ .5 dB gain measurement error. Therefore the efficiency could be as low as 60% or as high as 76%.

2. Rectenna Efficiency

The combined capture and rectification efficiency of the rectenna can be estimated using the antenna efficiency and a known rectifier efficiency. The efficiency of diode rectifiers have been measured as high as 80% [Ref. 9]. Assuming a rectifier efficiency e_r=.80 as demonstrated in earlier experiments, the maximum overall power efficiency for the circumferential slot used as a rectenna device is

$$e_{pwr} = e_{slot} \bullet e_r = (0.76)(.80) = 0.608 = 61\% . \qquad (5.19)$$

VI. CONCLUSIONS

A. SUMMARY

A propagation loss study and antenna design were presented for the MRPV. The concept of beamed microwave power transmission was shown to be limited by conversion efficiencies and propagation loss due to spreading of the electromagnetic wave and any blockage encountered. The reception and conversion from beamed microwave power to dc is performed by a device known as the rectenna which consists of an antenna and a rectifier.

The insertion loss of typical building walls was measured using the system described in Chapter II, Section A. The walls tested consisted of low loss materials such as wood doors to high loss materials such as metal covered doors. An approximate model was developed for the propagation of a spherical electromagnetic wave front through a building wall of known material properties. The model is based on the method of images and geometrical optics. Using locally plane wave approximations and ray tracing techniques, the signal strength of each plane wave was determined at the receive antenna. Combining the direct and reflected paths, the total resultant field strength was calculated through summation and complex integration. The model was shown to provide relatively accurate results. The measurements and modeling were performed over a band from 2 to 6 GHz. Two primary frequency bands of interest were looked at for overall system design: 1) the 2.45 GHz scientific and commercial band, and 2) the 5.5 GHz satellite uplink frequency band. The smaller wall losses at the lower frequencies indicate that the 2.45 GHz frequency band is preferable to the 5.5 GHz band. The gain of an antenna with

a fixed size decreases with lower frequency, thereby favoring the higher frequency. However, the wall loss was determined to be the more important of the two because the beam may pass through several walls. Thus the 2.45 GHz band (S-band) was used for overall system design.

The transmission of beamed microwave power for the MRPV requires a highly directional transmitter and a near omni-directional receiver. The design of the receive antenna provides maximum coverage in space. Two possible configurations were presented for a vertically polarized antenna - the circumferential slot and the vertical array. Due to the simplicity of a single feed point, the slot antenna was the selected approach. Using the PATCH computer code, simulations were performed on two slot antennas - the edge fed slot, and the center fed slot. The far-field patterns were calculated and the center fed slot antenna was shown to be the preferred design. A prototype of the circumferential slot antenna was designed, built and tested. Antenna parameters and far-field patterns were provided, with an estimated antenna efficiency between 60 and 76%. The sources of loss are feed point mismatch, feed cable loss, and ohmic losses due to the imperfectly conducting antenna surfaces.

B. FUTURE CONSIDERATIONS

The continuing research efforts for the MRPV should concentrate on the areas of microwave to dc power conversion (rectenna), improvements to propagation loss model, and transmitter design. The microwave to dc power conversion includes the design of a diode rectifier with sufficient conversion efficiency to supply power for operation of a dc motor. The diode rectifiers looked at during the course of this study were the HP 8471E series. These

diodes were designed as a measuring device and were not intended for power conversion. Improvements to the propagation loss model can be made in the areas listed as assumptions in Chapter III, Section 3. The inclusion of mulitple reflections and frequency dependent dielectric constants and loss tangents will improve the accuracy of the results. Finally, with the results of the propagation loss study and rectenna design, the performance requirements of a highly directional transmitter and antenna can be specified.

APPENDIX A
WALL LOSS DATA

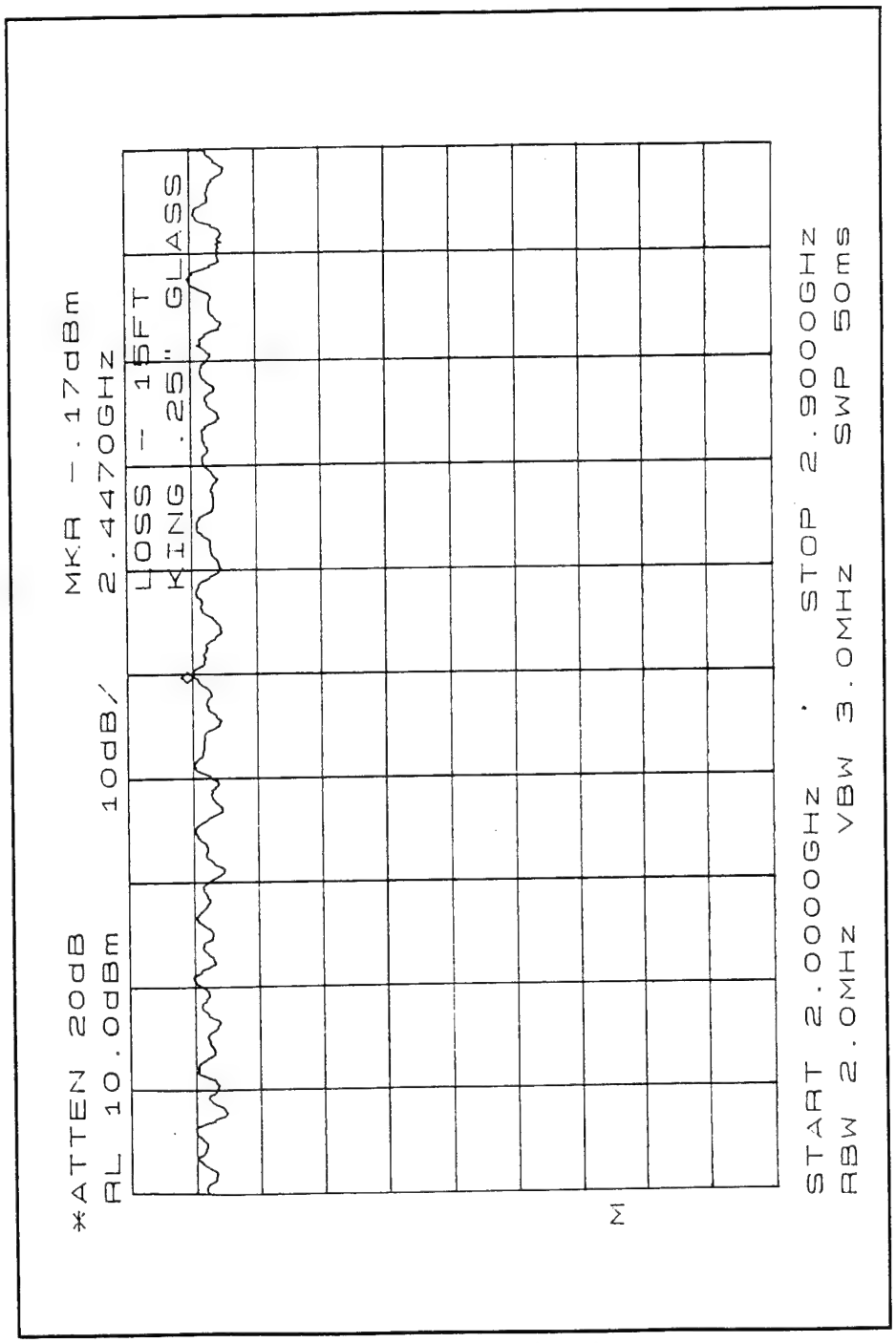

Figure 41. Loss measurement of .25" glass pane, 2 to 2.9 GHz

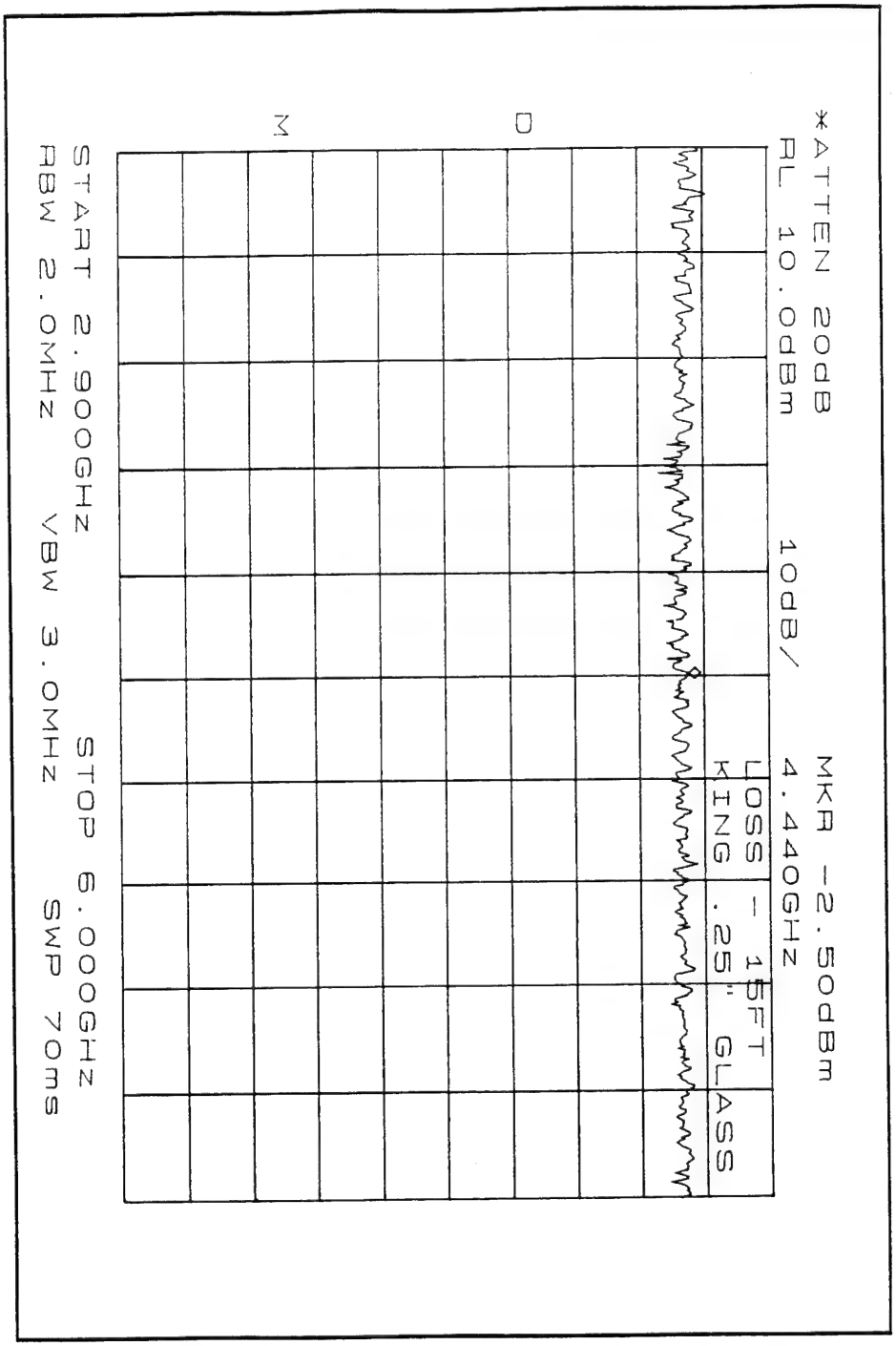

Figure 42. Loss measurement of .25" glass pane, 2.9 to 6 GHz

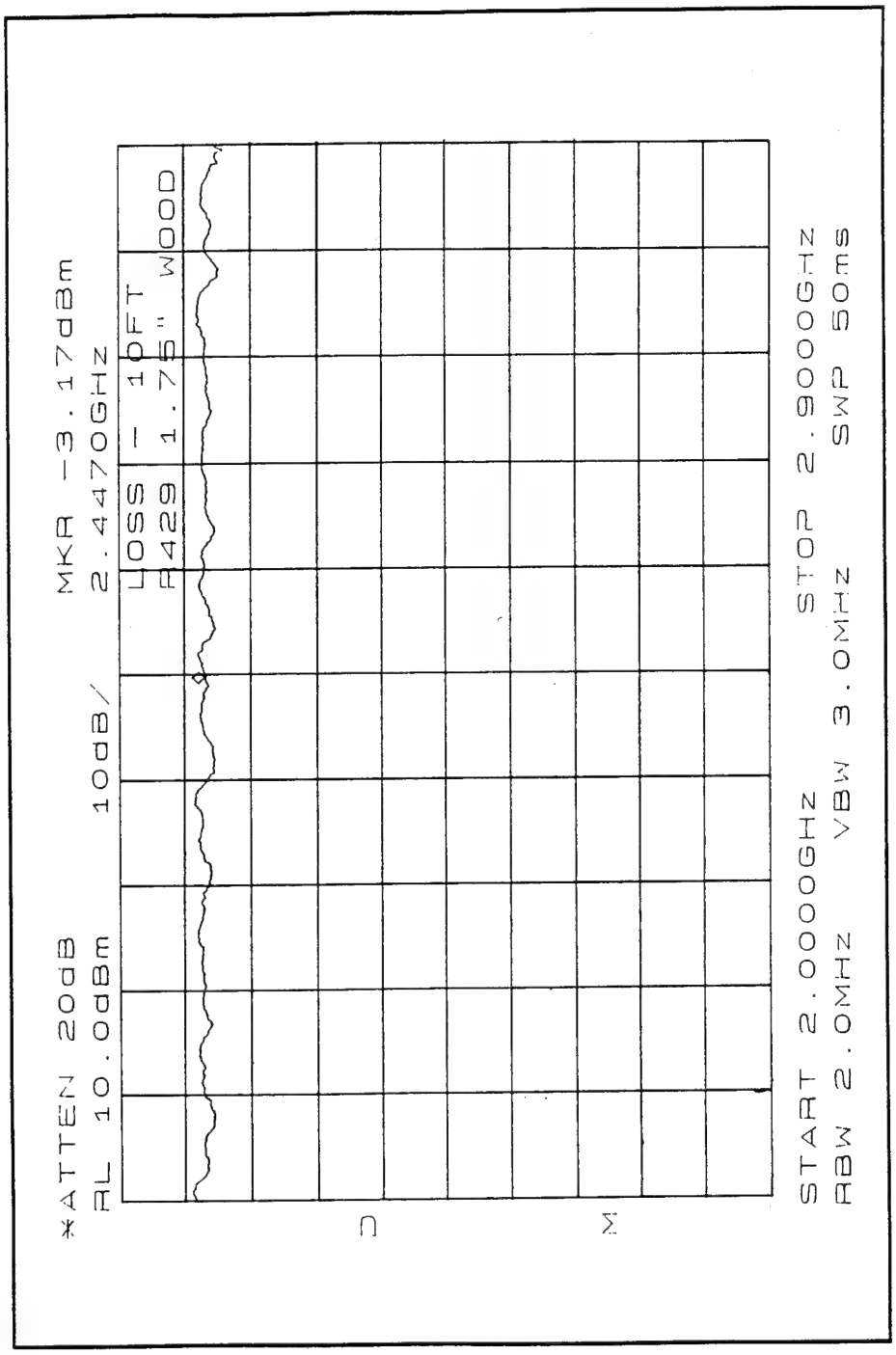

Figure 43. Loss measurement of 1.75" wood doors, 2 to 2.9 GHz

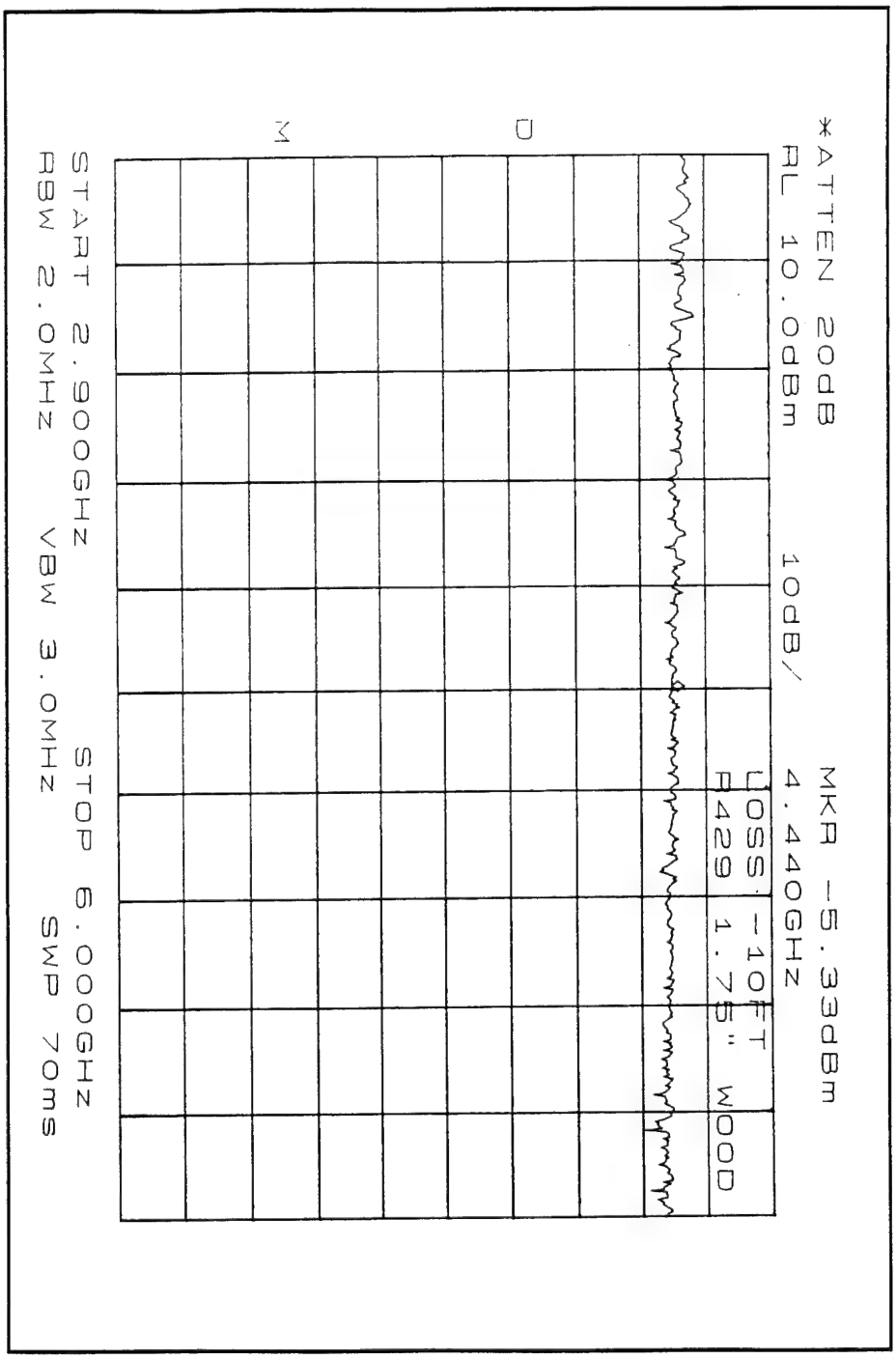

Figure 44. Loss measurement of 1.75" wood doors, 2.9 to 6 GHz

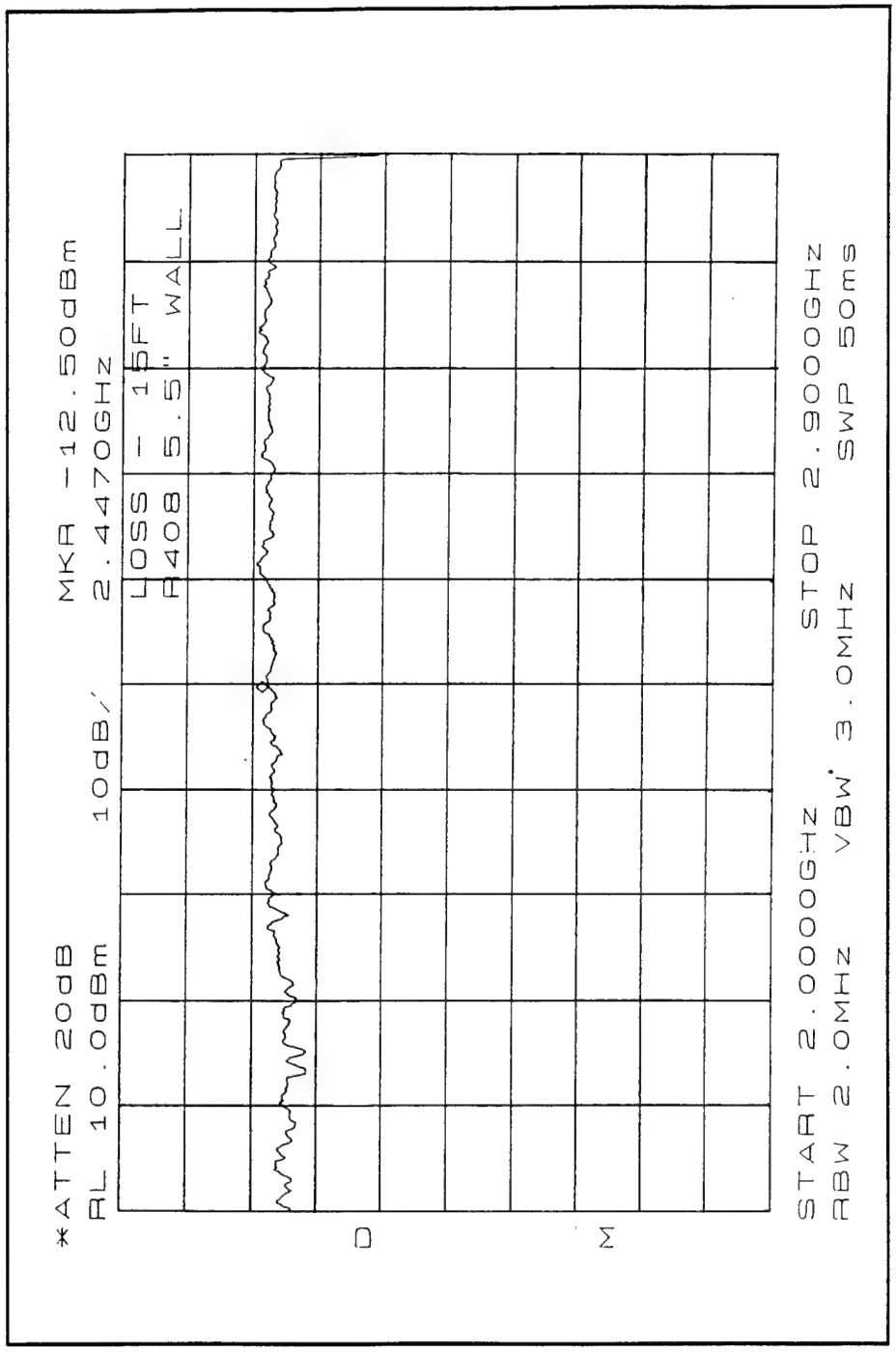

Figure 45. Loss measurement of 5.5" wall w/ chalkboard, 2 to 2.9 GHz

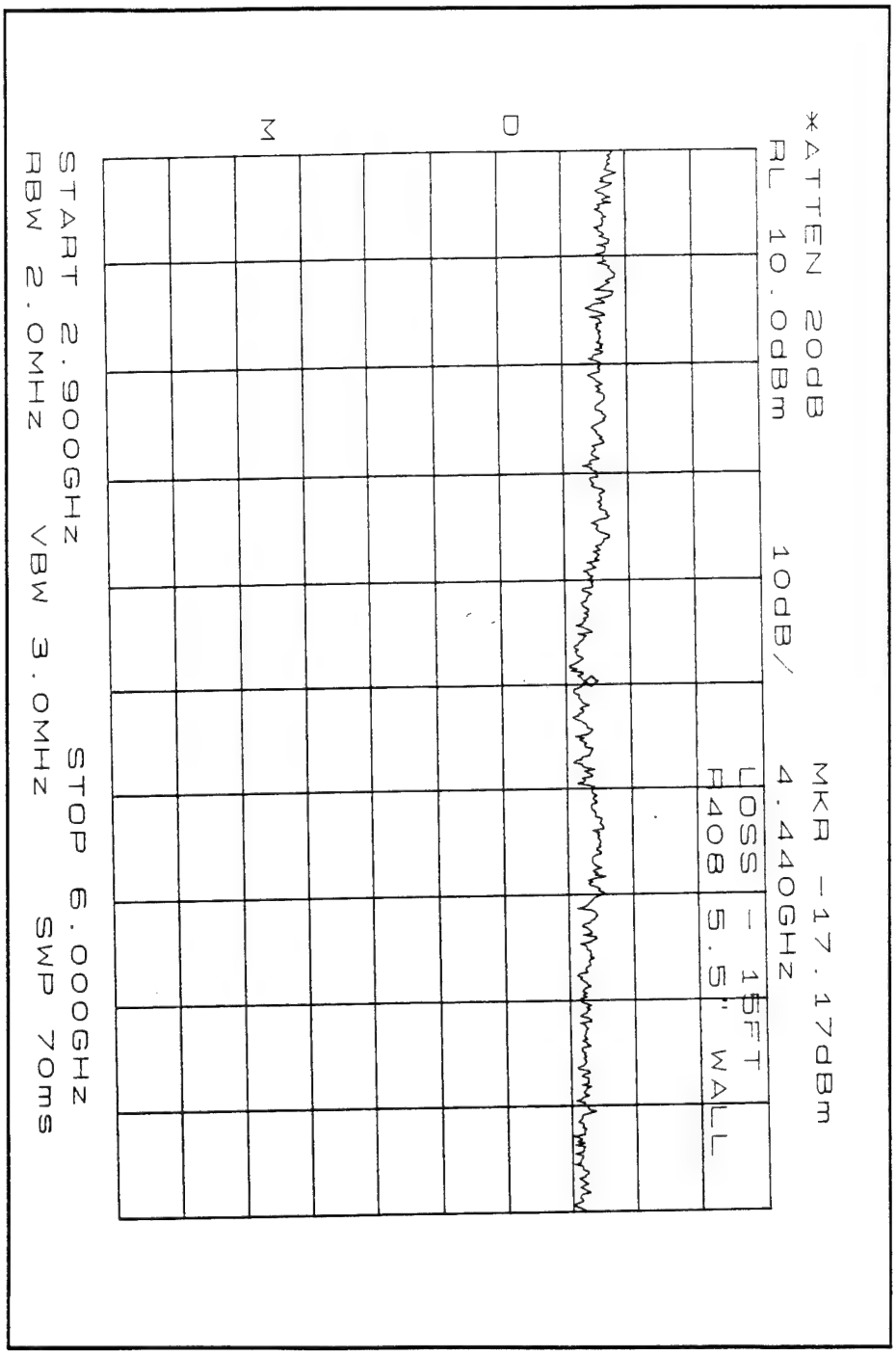

Figure 46. Loss measurement of 5.5" wall w/ chalkboard, 2.9 to 6 GHz

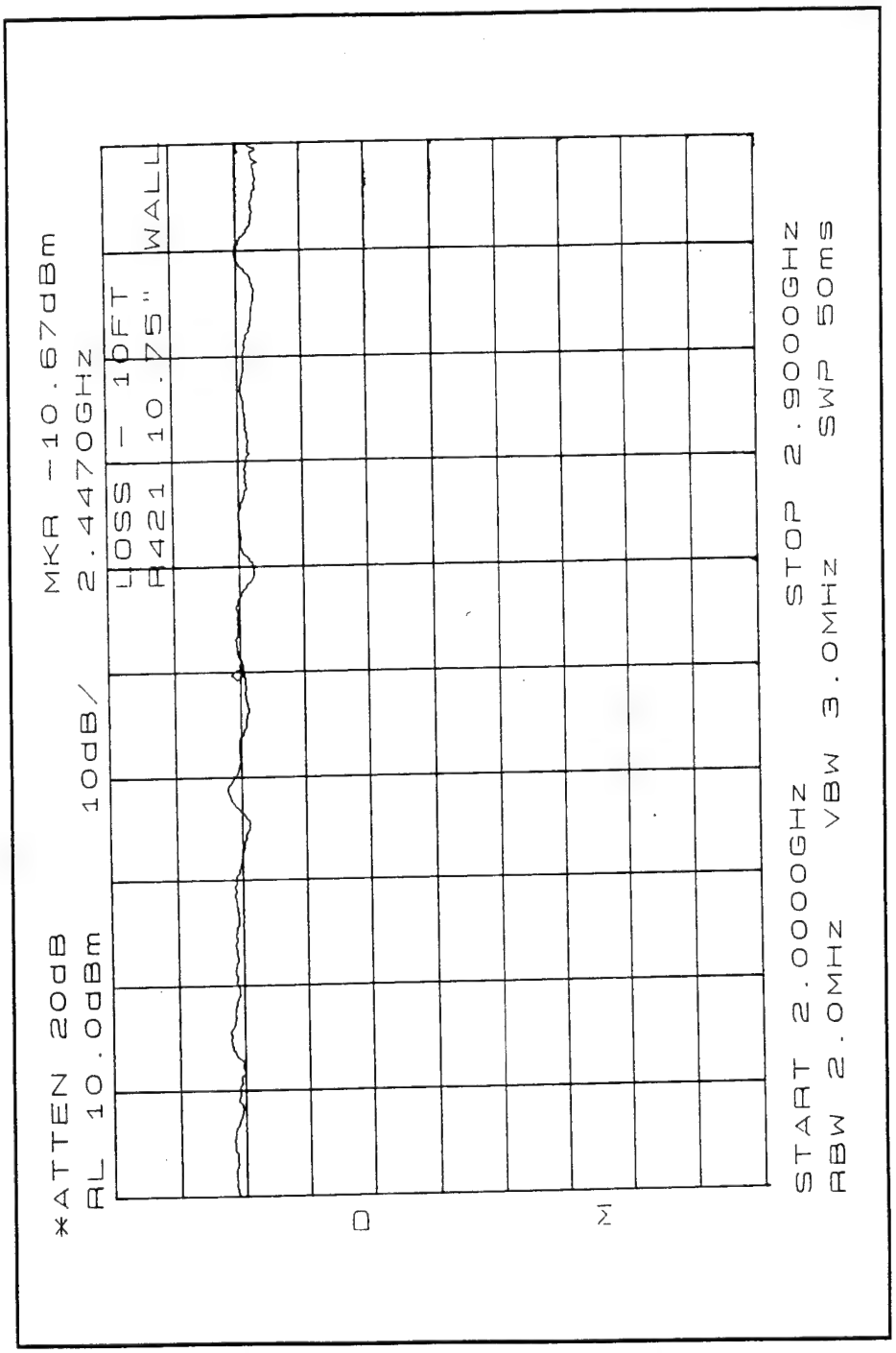

Figure 47. Loss measurement of 10.75" cement wall, 2 to 2.9 GHz

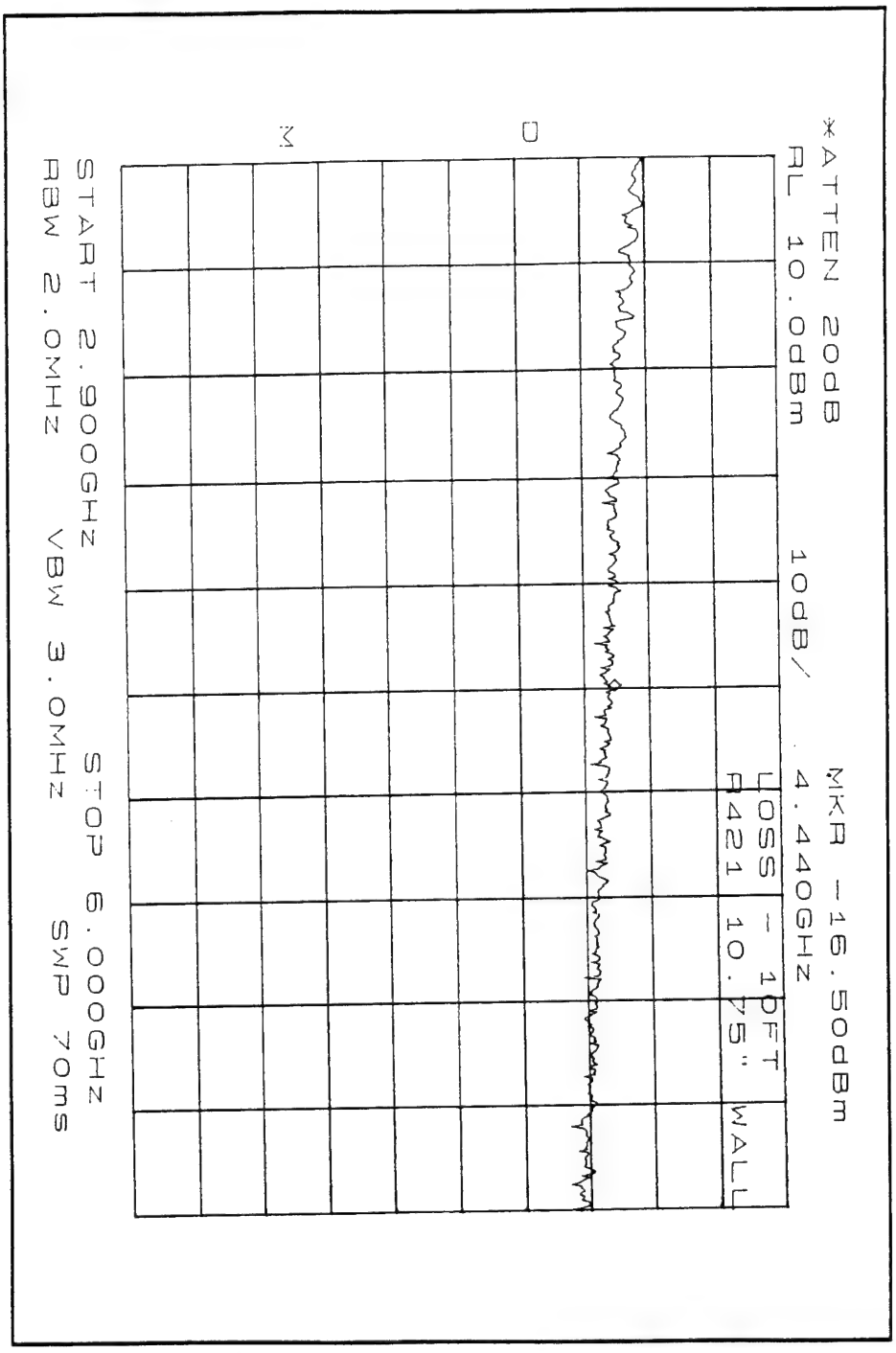

Figure 48. Loss measurement of 10.75" cement wall, 2.9 to 6 GHz

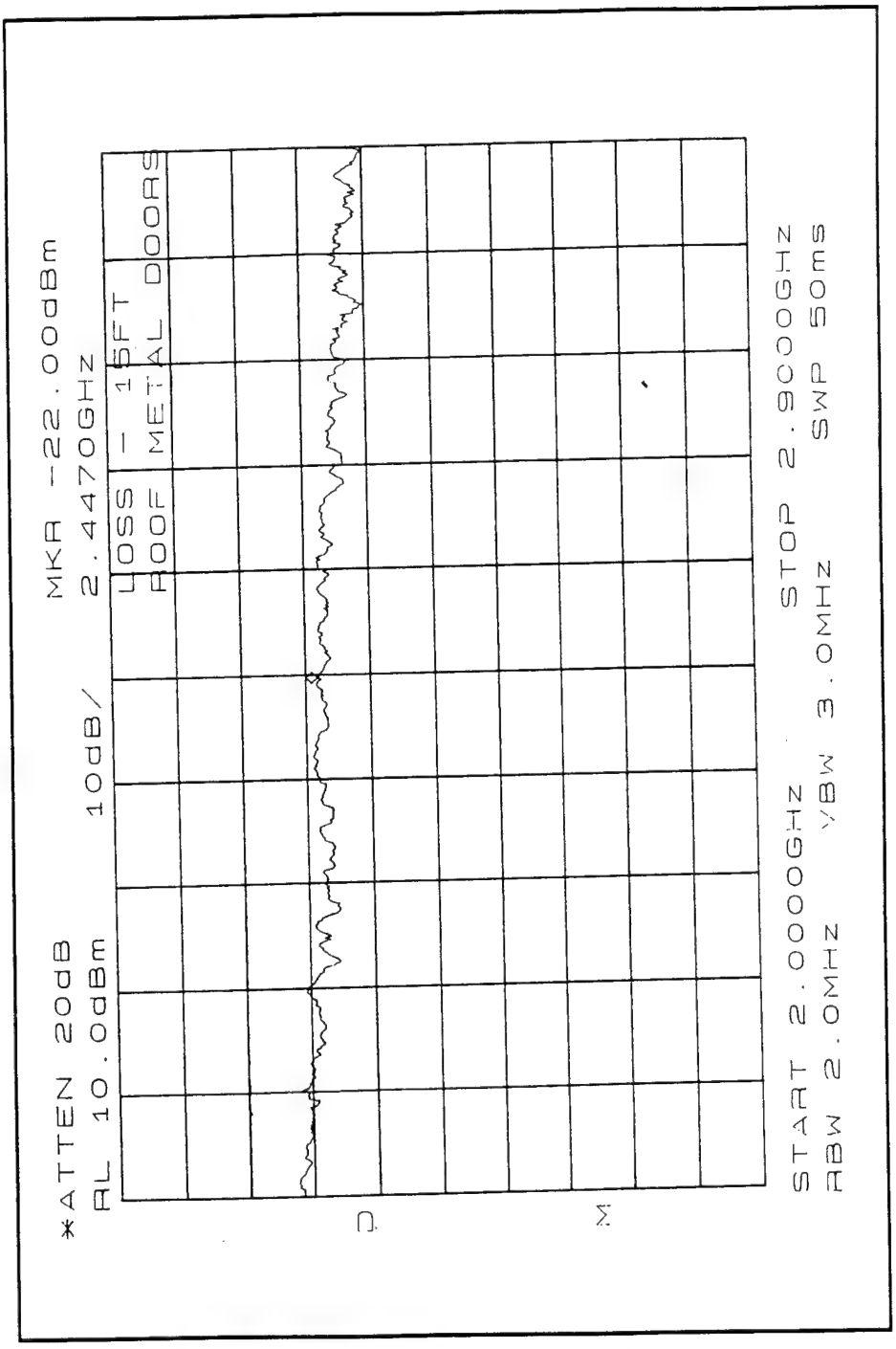

Figure 49. Loss measurement of 1.75" metal doors, 2 to 2.9 GHz

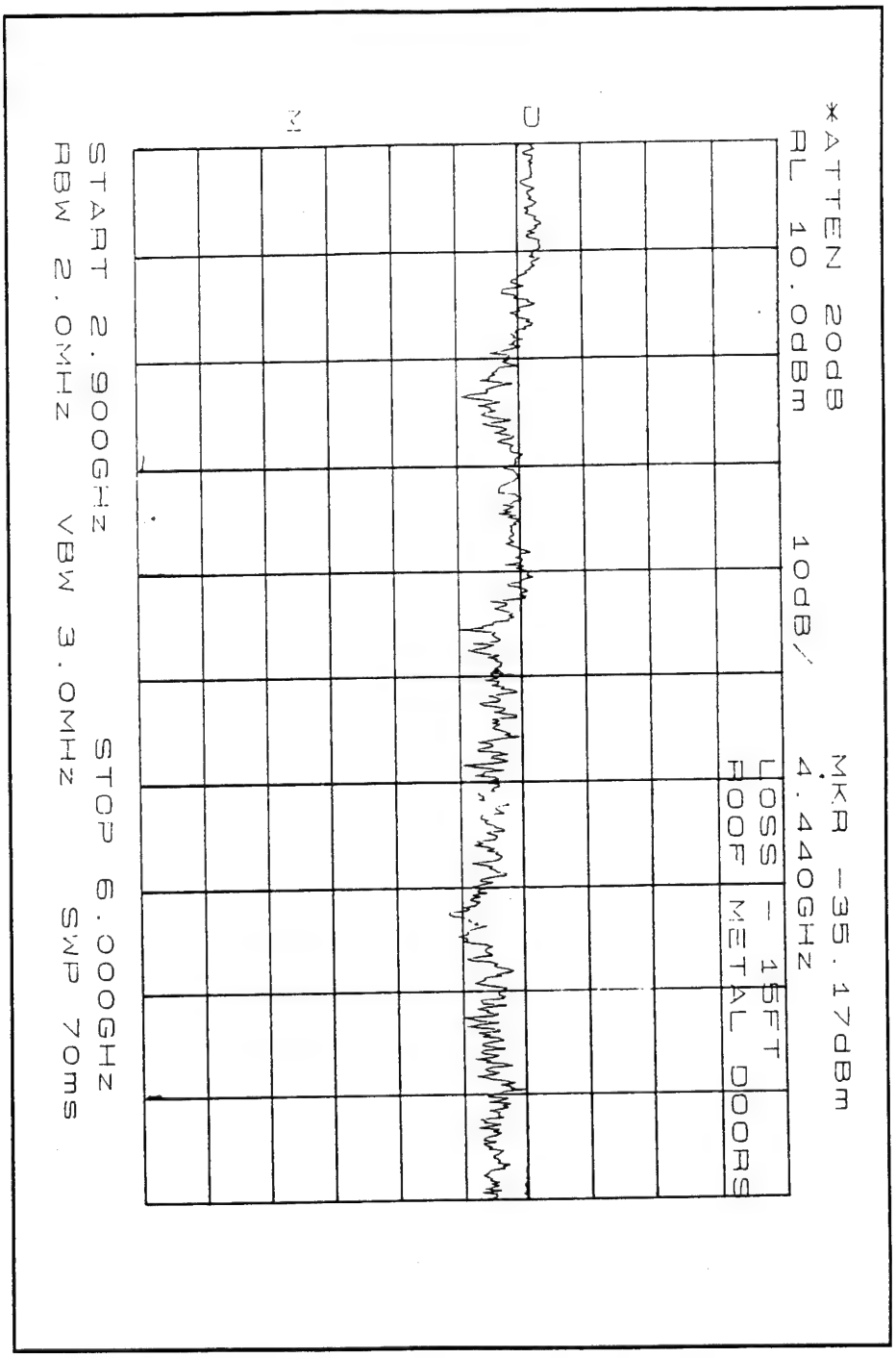

Figure 50. Loss measurement of 1.75" metal doors, 2.9 to 6 GHz

APPENDIX B
MATLAB PROGRAM

```
% Thad B Gibson
%
% RAY4.m - BUILDING WALL PROPAGATION LOSS MODEL
%
% This program models the propagation of a spherical electromagnetic
% wave front through a wall. The program will calculate an equivalent
% replacement source for the DIRECT and an equivalent image of the
% REFLECTED portions of a spherical wave. If a single frequency is chosen, it
% will calculate and then plot the magnitude and phase of the DIRECT,
% REFLECTED, and COMBINED rays on the surface of the antenna and
% provide a Loss in dB to that of free space.  If morethan one frequency point is
% chosen, it will calculate the Loss in dB for eachfrequency and then plot the
% resulting Loss vs. frequency.
%
%
clear; clg; format compact;
%
%
% ********************************************************************************
% **                    INPUT - SET UP ALL INPUT VALUES                          **
% ********************************************************************************
%
pflag=input('Do you want hardcopy?(y/n) ','s');
fstart=input('Enter the start frequency (GHz) ');
fstop=input('Enter the stop frequency (GHz) ');
count=input('Enter # of points to calculate between fstart and fstop ');
        if fstart == fstop,
        count = 1;
        ptest=input('Do you want plots of phase as well as magnitude?','s');
        end;
d1=input('Enter the distance from antenna to wall (ft) '); d2=d1;
l=input('Enter length of wall (ft) ');
h=input('Enter height of antennas from floor (ft) ');
erx=input('Enter the dielectric constant of wall ');
tandx=input('Enter the loss tangent of the wall');
erfx=input('Enter the dielectric constant of the floor ');
tandfx=input('Enter the loss tangent of the floor');
fstart=fstart*1e9;
fstop=fstop*1e9;
%
% **                              END INPUT                                      **
% --------------------------------------------------------------------------------
%
%
```

```
%
%
% ********************************************************************************
% **       OUTER LOOP - SETS FREQUENCY BEING CALCULATED                         **
% ********************************************************************************
%
%
frange=linspace(fstart,fstop,count);
for freq=1:count,
        f=frange(freq);
        c=3e8; d=1.5;
        er=erx; erf=erfx; tand=tandx; tandf=tandfx;
        incr=round((d/3.281)/(.1*c/f));
%
%
% ********************************************************************************
% **   INNER LOOP - USED TO DETERMINE A LOSS FOR A GIVEN                        **
% **   FREQUENCY BY CALCULATING WITH WALL AND SUBTRACTING                       **
% **   FROM WITHOUT WALL (FREE SPACE)                                           **
% ********************************************************************************
%
%
for loop=1:2,
        if loop == 2,
                er=1; erf=1; tand=0; tandf=0;
        end
%
% Calculate material constants
%
eo=8.84e-12; uo=12.56e-7;
w=2*pi*f;
alphad=w*sqrt((uo*eo*er/2)*(sqrt(1+tand^2)-1));
alphaf=w*sqrt((uo*eo*er/2)*(sqrt(1+tandf^2)-1));
bo=w*sqrt(eo*uo);
b2=w*sqrt((uo*eo*er/2)*(sqrt(1+tand^2)+1));
bf=w*sqrt((uo*eo*er/2)*(sqrt(1+tandf^2)+1));
no=sqrt(uo/eo); n2=sqrt(uo/(er*eo))/sqrt(1-j*tand);
nf=sqrt(uo/(erf*eo))/sqrt(1-j*tandf);
%
% Initialize arrays
%
Ei=zeros(incr); Er=zeros(incr); Et=zeros(incr);
theta=zeros(size(1:incr));
phi=zeros(size(1:incr));
thetar=zeros(size(1:incr));
phir=zeros(size(1:incr));
dxi=linspace(-d/2,d/2,incr); dyi=dxi;
```

```
dxr=linspace(2*h-d/2,2*h+d/2,incr); dyr=dxi;
%
%
% ********************************************************************************
% **  DIRECT RAYS - FIND MIN AND MAX INCIDENT ANGLES TO FIND      **
% **  THE EQUIVALENT REPLACEMENT SOURCE LOCATION - diz             **
% ********************************************************************************
%
%
acc=200;
ang=linspace(0,pi/4,acc);
for k=1:acc,
        y1=(d1+d2)*tan(ang(k))+l*tan(asin(bo/b2*sin(ang(k))));
        if y1 > d/2,
                break;
        end
end
angimax=ang(k-1);
angimin=-angimax;
%
diz=d1+l+d2-((d/2)/tan(angimax));
%
%
% **                          END DIRECT RAY                              **
% --------------------------------------------------------------------------------
%
%
%
%
% ********************************************************************************
% **  REFLECTED RAYS - FIND MIN AND MAX INCIDENT ANGLES TO        **
% **  FIND THE EQUIVALENT IMAGE SOURCE LOCATION - drx,drz          **
% ********************************************************************************
%
%
acc=400;
ang=linspace(0,pi,acc);
for k=1:acc,
        y2=(d1+d2)*tan(ang(k))+l*tan(asin(bo/b2*sin(ang(k))));
        if y2 > 2*h-d/2,
                break;
        end
end
angrmin=ang(k-1);
%
for k=1:acc,
        y2=(d1+d2)*tan(ang(k))+l*tan(asin(bo/b2*sin(ang(k))));
```

```
        if y2 > 2*h+d/2,
                break;
        end
end
angrmax=ang(k-1);
%
% Calculate drmin and drmax -the min & max deviation (z) from the original
% source to the image
%
drmin=d1+d2+l-((2*h-d/2)/tan(angrmin));
drmax=d1+d2+l-((2*h+d/2)/tan(angrmax));
%
% The relfected rays do not trace back to the z axis, so must determine
% where they cross in (z,x) coordinates. Calculate equation of line for
% max and min angles and find intersection in (drx,drz)
%
bmin=-tan(angrmin)*drmin;
bmax=-tan(angrmax)*drmax;
mmin=tan(angrmin);
mmax=tan(angrmax);
%
% Now find the point where the two lines cross (drx,drz)
drz=(bmin-bmax)/(mmax-mmin);
drx=mmin*drz+bmin;
%
% Now find distance from point (drx,drz) to center of antenna
Rc=sqrt((2*h-drx)^2+(d2+l+d1-drz)^2);
%
%
% **                    END REFLECTED RAY                                **
% ------------------------------------------------------------------------
%
%
%
%
% ************************************************************************
% **   EFFECT OF A TYPICAL ANTENNA BEAMWIDTH WHICH VARIES               **
% **   WITH FREQUENCY                                                   **
% ************************************************************************
%
%
% Now account for beamwidth of antenna which is approximated by (65*(c/f)/d)
p=log10(.707)/log10((65*(c/f)/d)*(pi/180));
%
%
% **                END OF EFFECT OF BEAMWIDTH                           **
% ------------------------------------------------------------------------
```

```
%
%
%
%
% ********************************************************************************
% **  DIRECT RAYS - FIND Ei FOR EACH GIVEN ANGI, THEN STORE                     **
% **  EACH VALUE OF Ei IN A SQUARE MATRIX                                       **
% ********************************************************************************
%
%
for m=1:incr,
 for n=1:incr,
   rho=sqrt(dxi(n)^2+dyi(m)^2);
    if rho < d/2,
       theta=atan(dxi(n)/(d2+l+d1-diz));
       phi=atan(dyi(m)/(d2+l+d1-diz));
       angi=atan(rho/(d2+l+d1-diz));
       R1=d1/cos(angi);
       R2=l/cos(asin(bo/b2*sin(angi)));
       R3=d2/cos(angi);
       Ri=(d2+l+d1-diz)/cos(angi);
       angt=asin(bo/b2*sin(angi));
       t1=(2*n2*cos(angt))/(n2*cos(angt)+no*cos(angi));
       t2=(2*no*cos(angi))/(no*cos(angi)+n2*cos(angt));
       E=[t1*t2/(4*pi*Ri)]*exp(-alphad*R2-j*(bo*(R1+R3)+b2*R2));
       Ei(incr+1-n,m)=cos(angi)^p*(1-sin(theta)^2*cos(phi)^2)*E;
    end
 end
end
%
%
% **                  END DIRECT RAY CALCULATION OF Ei                          **
% --------------------------------------------------------------------------------
%
%
%
%
% ********************************************************************************
% **  REFLECTED RAYS - FIND Er FOR EACH ANGLE ANGR, THEN                        **
% **  STORE EACH VALUE OF Er IN A SQUARE MATRIX                                 **
% ********************************************************************************
%
for m=1:incr,
 for n=1:incr,
   grid=sqrt(dxi(n)^2+dyi(m)^2);
    if grid < d/2,
       thetar=atan((dxr(n)-drx)/(d2+l+d1-drz));
```

```
        phir=atan(dyr(m)/Rc);
        rhor=sqrt((dxr(n)-drx)^2+dyr(m)^2);
        angr=atan(rhor/(d2+l+d1-drz));
        R1r=d1/cos(angr);
        R2r=l/cos(asin(bo/b2*sin(angr)));
        R3r=d2/cos(angr);
        Rir=rhor/sin(angr);
        angtr=asin((bo/b2)*sin(angr));
        t1r=(2*n2*cos(angtr))/(n2*cos(angtr)+no*cos(angr));
        t2r=(2*no*cos(angr))/(no*cos(angr)+n2*cos(angtr));
        angf=pi/2-angr;
        angtf=asin((bo/bf)*sin(angf));
        Gr=(nf*cos(angtf)-no*cos(angf))/(nf*cos(angtf)+no*cos(angf));
        E=[Gr*t1r*t2r/(4*pi*Rir)]*exp(-alphad*R2r-j*(bo*(R1r+R3r)+b2*R2r));
        Er(incr+1-n,m)=cos(angr)^p*(1-sin(thetar)^2*cos(phir)^2)*E;
    end
  end
end
%
%
% **              END REFLECTED RAY CALCULATION OF Er                    **
% ------------------------------------------------------------------------------------------
%
%
%
%
% ********************************************************************************
% **   DETERMINE MAGNITUDE AND PHASE OF DIRECT, REFLECTED       **
% **   AND TOTAL                                                **
% ********************************************************************************
%
%
% Now determine the magnitude and phase across the antenna for both the
% DIRECT and REFLECTED rays
%
magi=abs(Ei); phas=phase(Ei).*(180/pi);
magr=abs(Er); phasr=phase(Er).*(180/pi);
%
% Determine magnitude and phase of COMBINED direct and relfected across
% the antenna
%
Et=Ei+Er;
magt=abs(Et); phast=phase(Et).*(180/pi);
if loop == 1,
        magihold=magi; magrhold=magr; magthold=magt;
        phashold=phas; phasrhold=phasr; phasthold=phast;
end
```

```
%
%
% **                    END OF MAGNITUDE AND PHASE                    **
% ------------------------------------------------------------------------------
%
%
%
%
% ********************************************************************************
% **                    COMPLEX INTEGRATION OF mag(Et)                **
% ********************************************************************************
%
for m=1:incr,
        for n=1:incr,
        value(n)=Et(m,n)*(d/incr)*(d/incr);
        end
temp1(m)=sum(value);
end
field=sum(temp1);
field=abs(field);
Total(loop)=20*log10(field);
end
%
Loss(freq)=Total(1)-Total(2);
end
%
%
% **                    END OF COMPLEX INTEGRATION                    **
% ------------------------------------------------------------------------------
%
%
%
%
% ********************************************************************************
% **                                PLOTTING                          **
% ********************************************************************************
%
%
er=num2str(erx);
erf=num2str(erfx);
tand=num2str(tandx);
tandf=num2str(tandfx);
h=num2str(h);
l=num2str(l);
d1=num2str(d1);
d2=num2str(d2);
%
```

```
% If range of frequencies were specified plot Loss vs. frequency
%
if count > 1,
        freq=linspace(fstart/1e9,(fstop+1e9)/1e9,count);
        plot(freq,Loss,'*',freq,Loss)
        xlabel('freq (GHz)')
        ylabel('Loss (dB)')
        title(['er= ',er,', erf= ',erf,', tand= ',tand,', tandf= ',tandf,...
        ', h= ',h,', d1=d2= ',d1,', l= ',l])
        if pflag == ('y'), print; end
end
%
% If one frequency was specified mesh the magnitude and phase
% of DIRECT,REFLECTED and COMBINED rays.
if count == 1,
        fig=1;
        fs=num2str(f);
        figure(fig);
        meshc(magihold);
        title(['Magnitude of DIRECT rays wall - f = ',fs]);
        xlabel('Antenna (incr)'); ylabel('Antenna (incr)');
        zlabel('abs(Ei)');
        text(.5,1,['er=',er,', erf=',erf,', tand=',tand,', tandf=',tandf,...
        ', h=',h,', d1=d2=',d1,', l=',l],'units','normalized','horiz','center');
%       print -depsc plot1_25
        if pflag == ('y'), print; end
%
        if ptest ~= 'n',
          fig=fig+1;
          figure(fig);
          meshc(phashold);
          title(['Phase of DIRECT rays - f = ',fs]);
          xlabel('Antenna (incr)'); ylabel('Antenna (incr)'); zlabel('phase(Ei)');

          text(.5,1,['er=',er,', erf=',erf,', tand=',tand,', tandf=',tandf,...
          ', h=',h,', d1=d2=',d1,', l=',l],'units','normalized','horiz','center');
%         print -depsc plot2_25
          if pflag == ('y'), print; end
        end
%
        fig=fig+1;
        figure(fig);
        meshc(magrhold);
        title(['Magnitude of REFLECTED rays - f = ',fs]);
        xlabel('Antenna (incr)'); ylabel('Antenna (incr)'); zlabel('abs(Er)');
        text(.5,1,['er=',er,', erf=',erf,', tand=',tand,', tandf=',tandf,...
          ', h=',h,', d1=d2=',d1,', l=',l],'units','normalized','horiz','center');
```

```
%       print -depsc plot3_25
        if pflag == ('y'), print; end
%
        if ptest ~= 'n',
          fig=fig+1;
          figure(fig);
          meshc(phasrhold);
          title(['Phase of REFLECTED rays - f = ',fs]);
          xlabel('Antenna (incr)'); ylabel('Antenna (incr)'); zlabel('phase(Er)');
          text(.5,1,['er=',er,', erf=',erf,', tand=',tand,', tandf=',tandf,...
          ', h=',h,', d1=d2=',d1,', l=',l],'units','normalized','horiz','center');
%         print -depsc plot4_25
          if pflag == ('y'), print; end
        end
%
        if ptest ~= 'n',
          fig=fig+1;
          figure(fig);
          meshc(phasthold);
          title(['Phase of COMBINED rays - f = ',fs]);
          xlabel('Antenna (incr)'); ylabel('Antenna (incr)'); zlabel('phase(Et)');
          text(.5,1,['er=',er,', erf=',erf,', tand=',tand,', tandf=',tandf,...
          ', h=',h,', d1=d2=',d1,', l=',l],'units','normalized','horiz','center');
%         print -depsc plot5_25
          if pflag == ('y'), print; end
        end
%
        fig=fig+1;
        figure(fig);
        meshc(magthold);
        Loss=num2str(Loss(freq));
        title(['Magnitude of COMBINED rays - f = ',fs])
        text(.5,.9,['Loss w/r free space= ',Loss,'dB'],'units','normalized',...
        'horiz','center');
        text(.5,1,['er=',er,', erf=',erf,', tand=',tand,', tandf=',tandf,...
          ', h=',h,', d1=d2=',d1,', l=',l],'units','normalized','horiz','center');
        xlabel('Antenna (incr)'); ylabel('Antenna (incr)'); zlabel('abs(Et)');
%       print -depsc plot6_25
        if pflag == ('y'), print; end
end
%
%
% **                          END PLOTTING                                    ***
% ------------------------------------------------------------------------------------------
%
% ***************************      END PROGRAM      ******************************
% ********************************************************************************
```

APPENDIX C
SINGLE FREQUENCY PLOTS

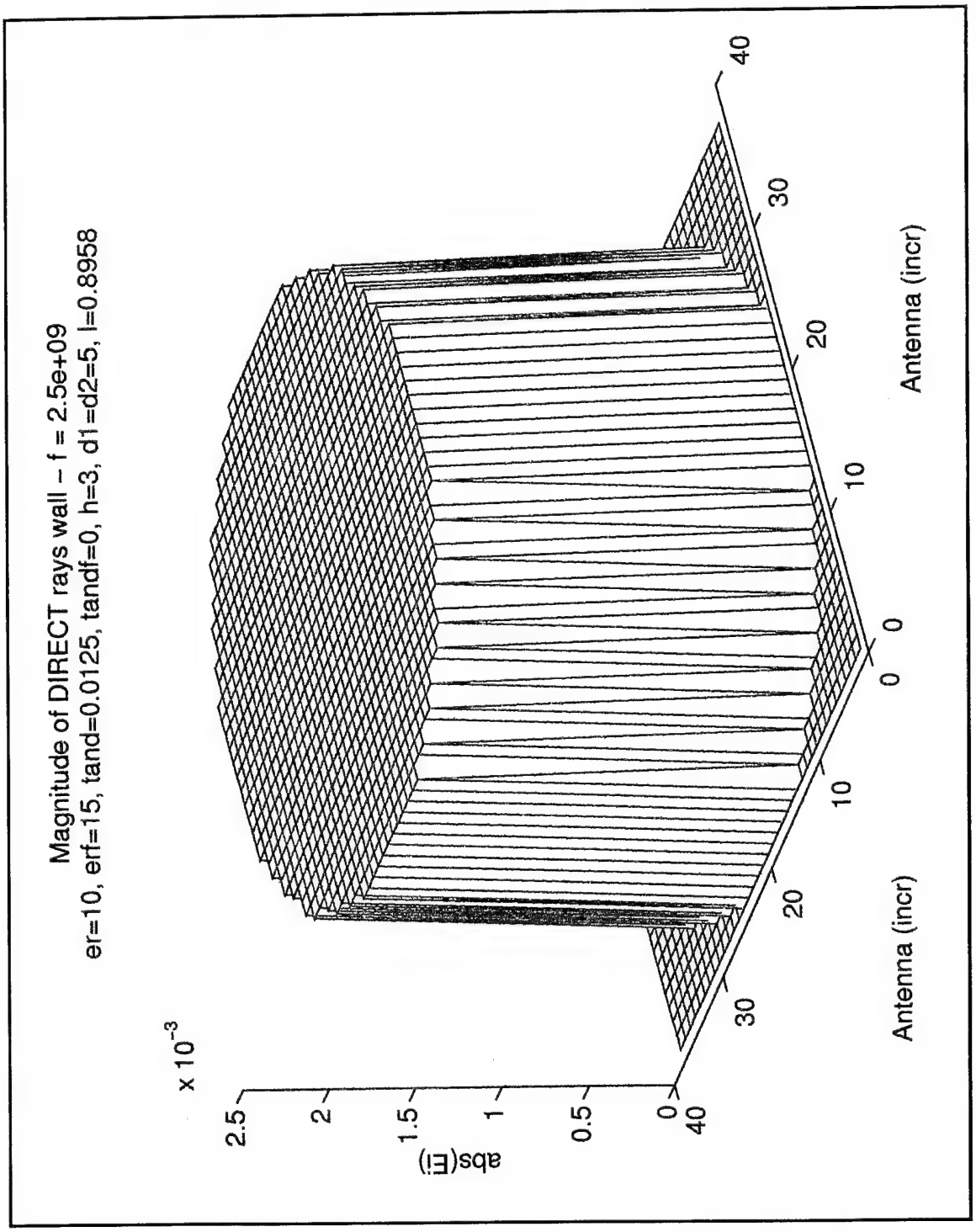

Figure 51. Magnitude of direct rays at 2.5 GHz

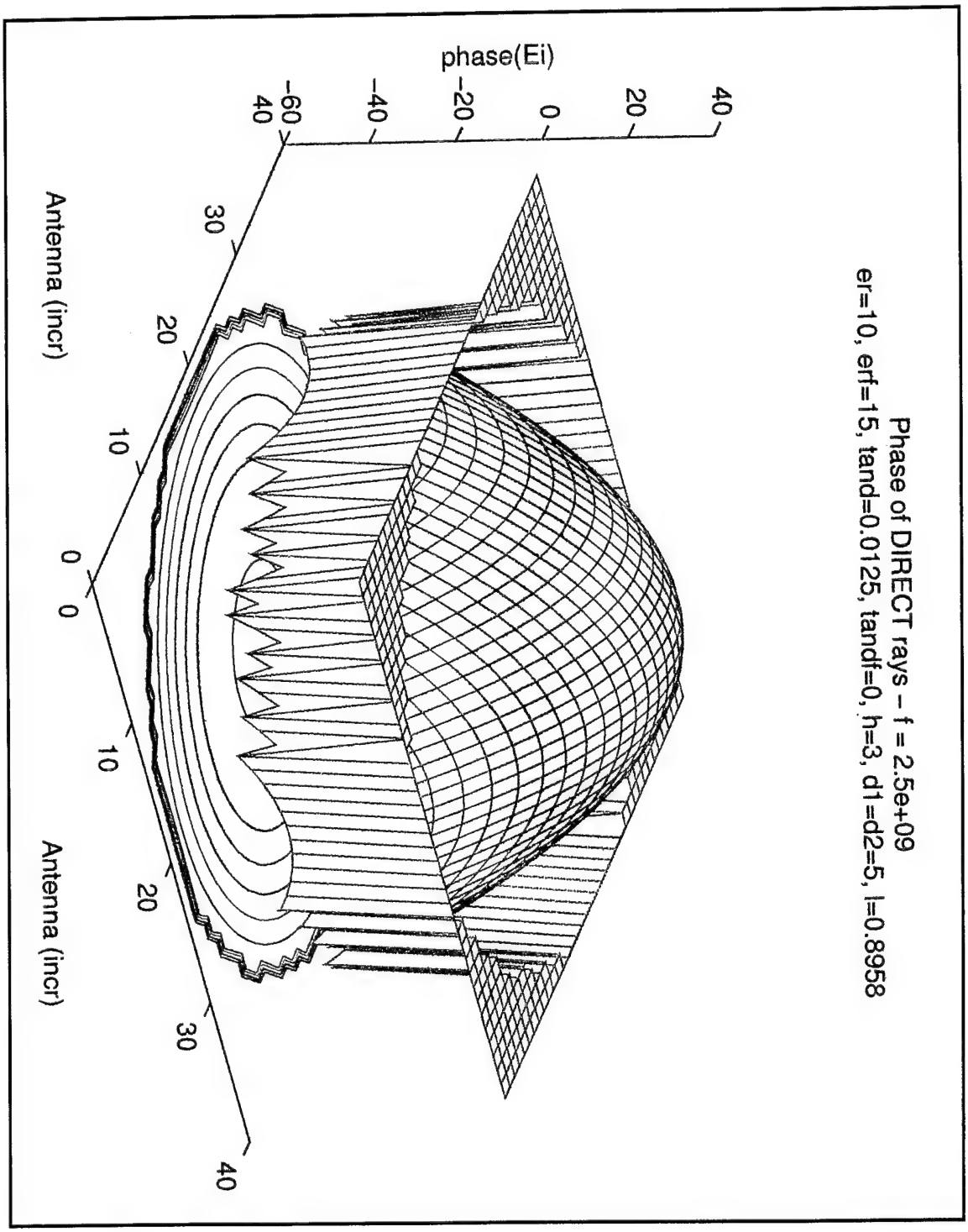

Figure 52. Phase of direct rays at 2.5 GHz

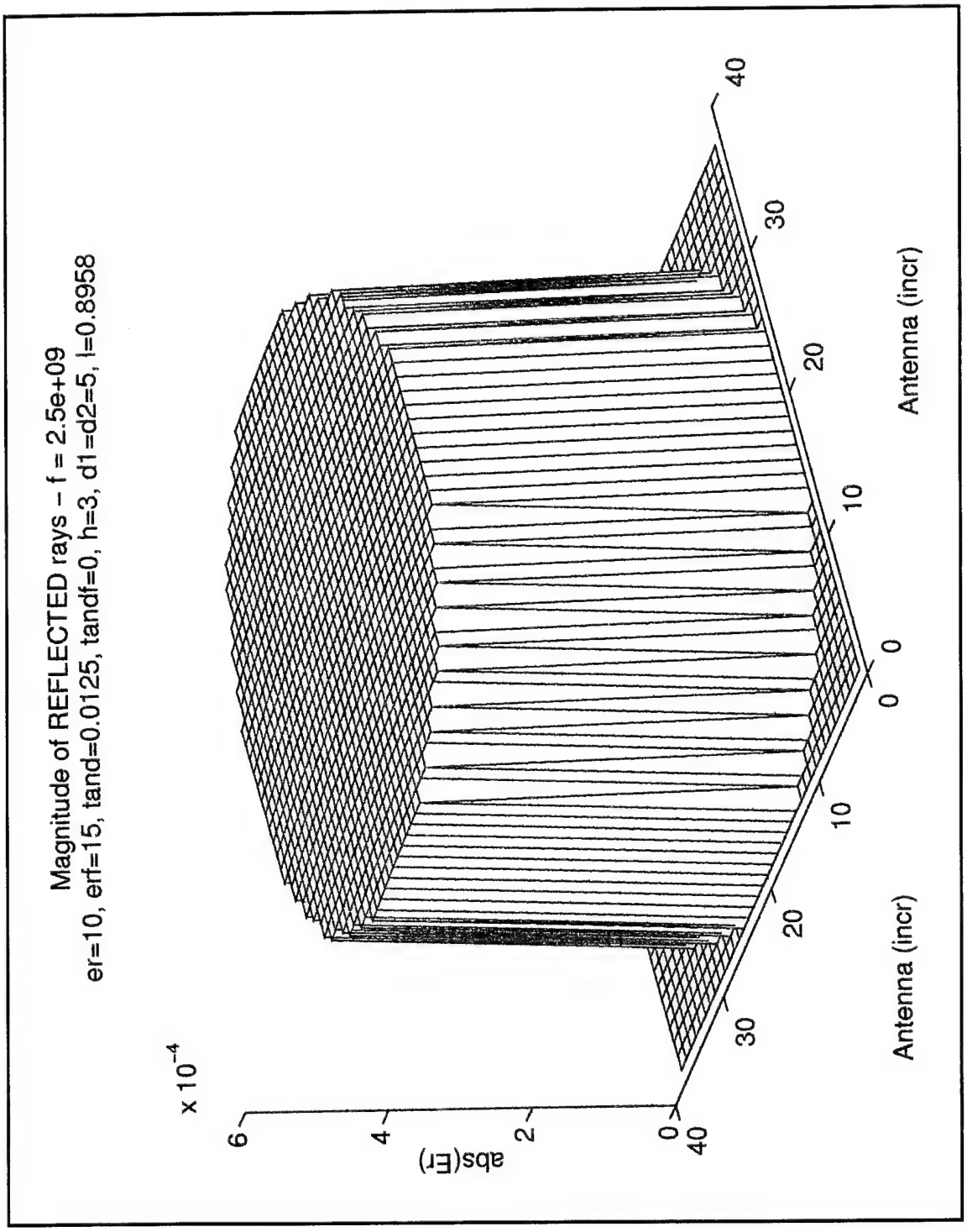

Figure 53. Magnitude of reflected rays at 2.5 GHz

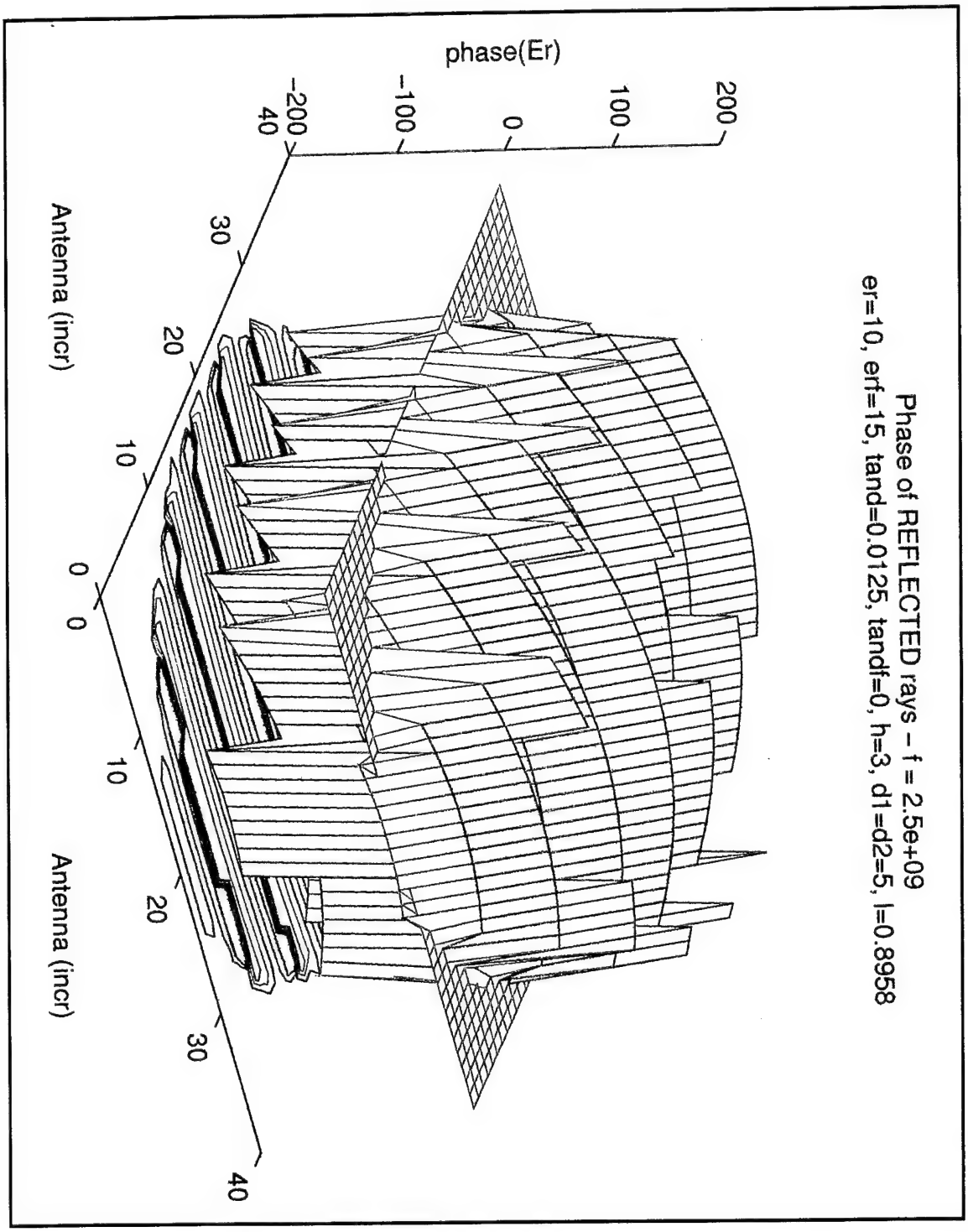

Figure 54. Phase of reflected rays at 2.5 GHz

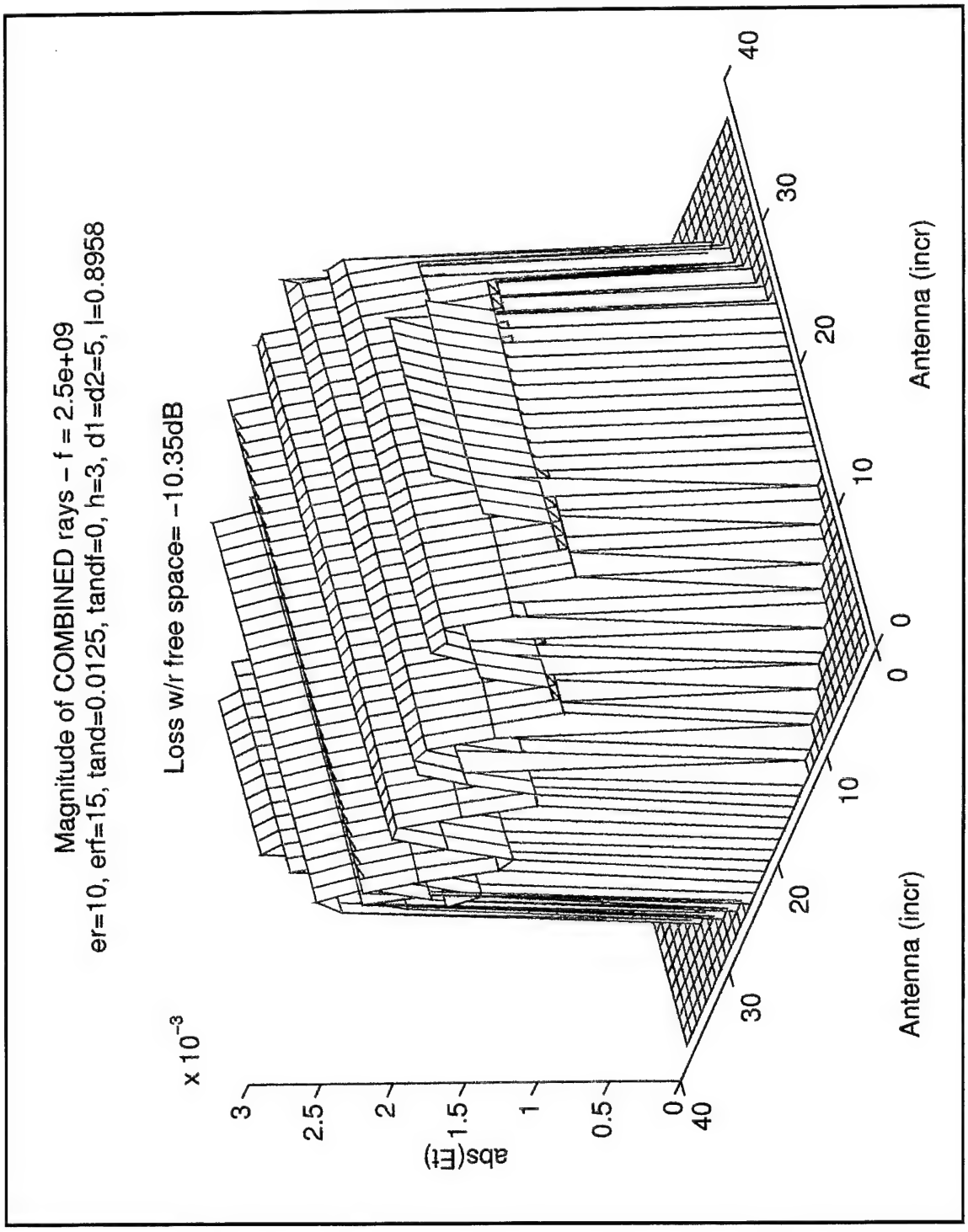

Figure 55. Magnitude of combined rays at 2.5 GHz

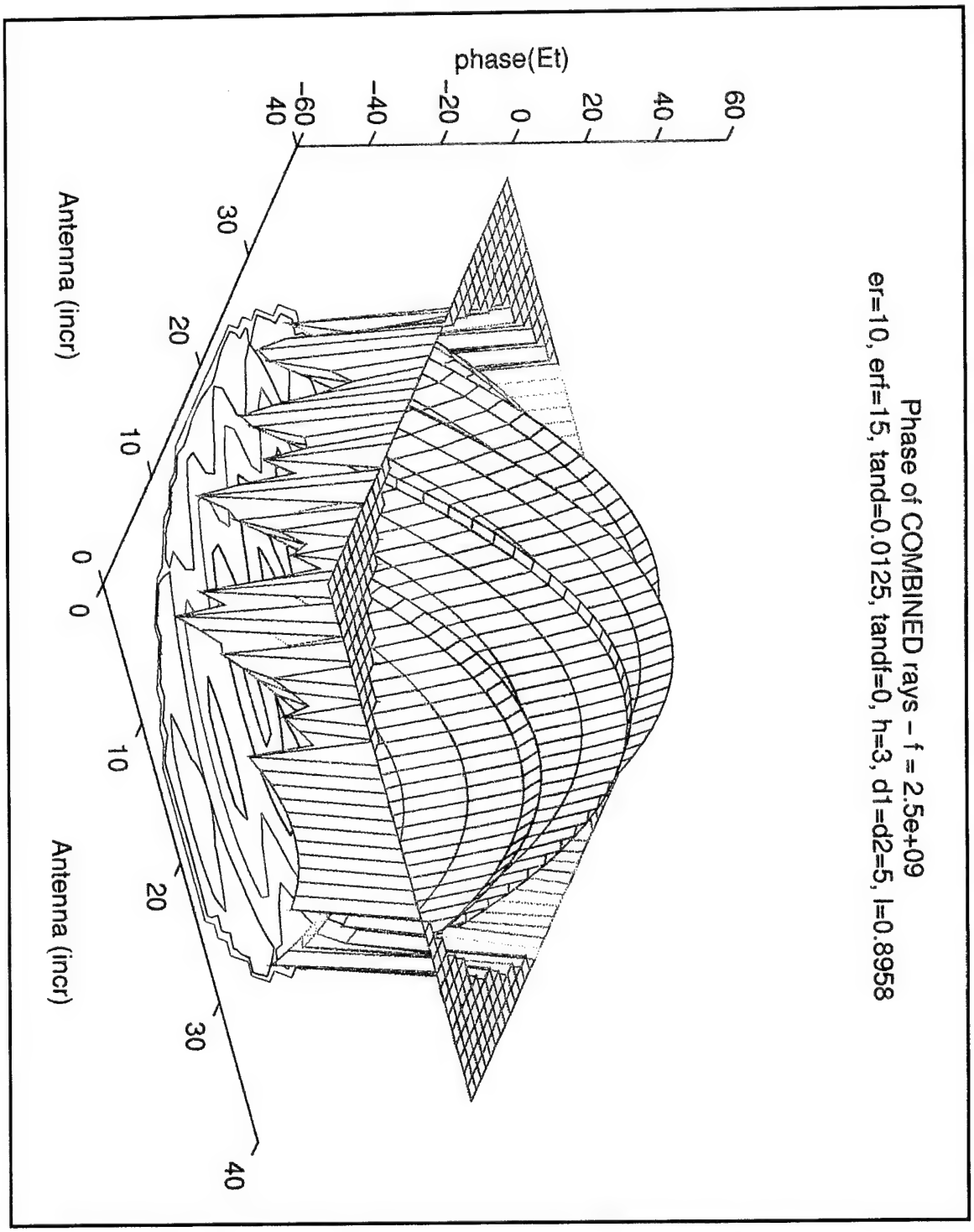

Figure 56. Phase of combined rays at 2.5 GHz

APPENDIX D
ANTENNA PARAMETER PLOTS

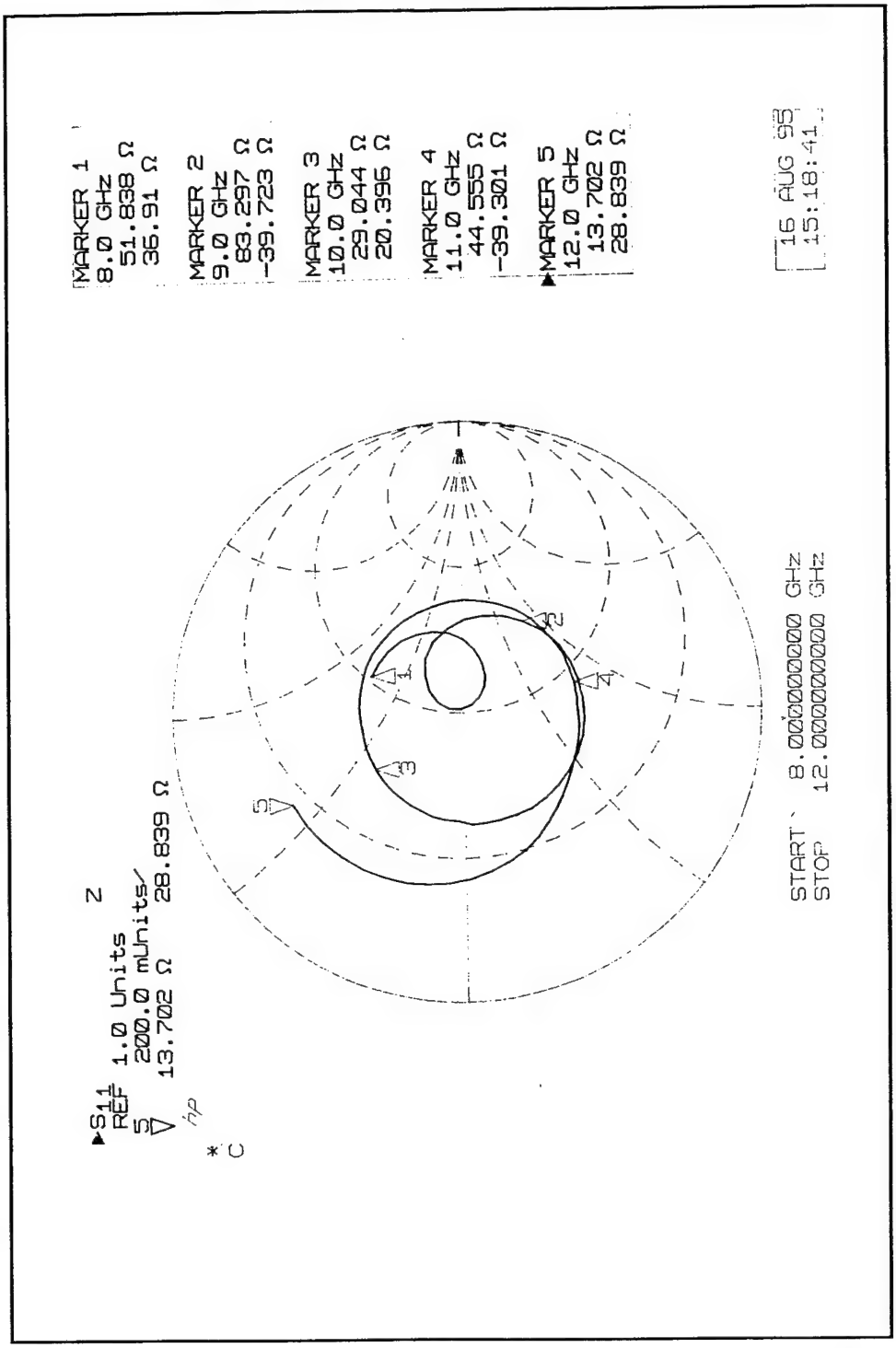

Figure 57. Slot antenna impedance measurement - 8 to 12 GHz

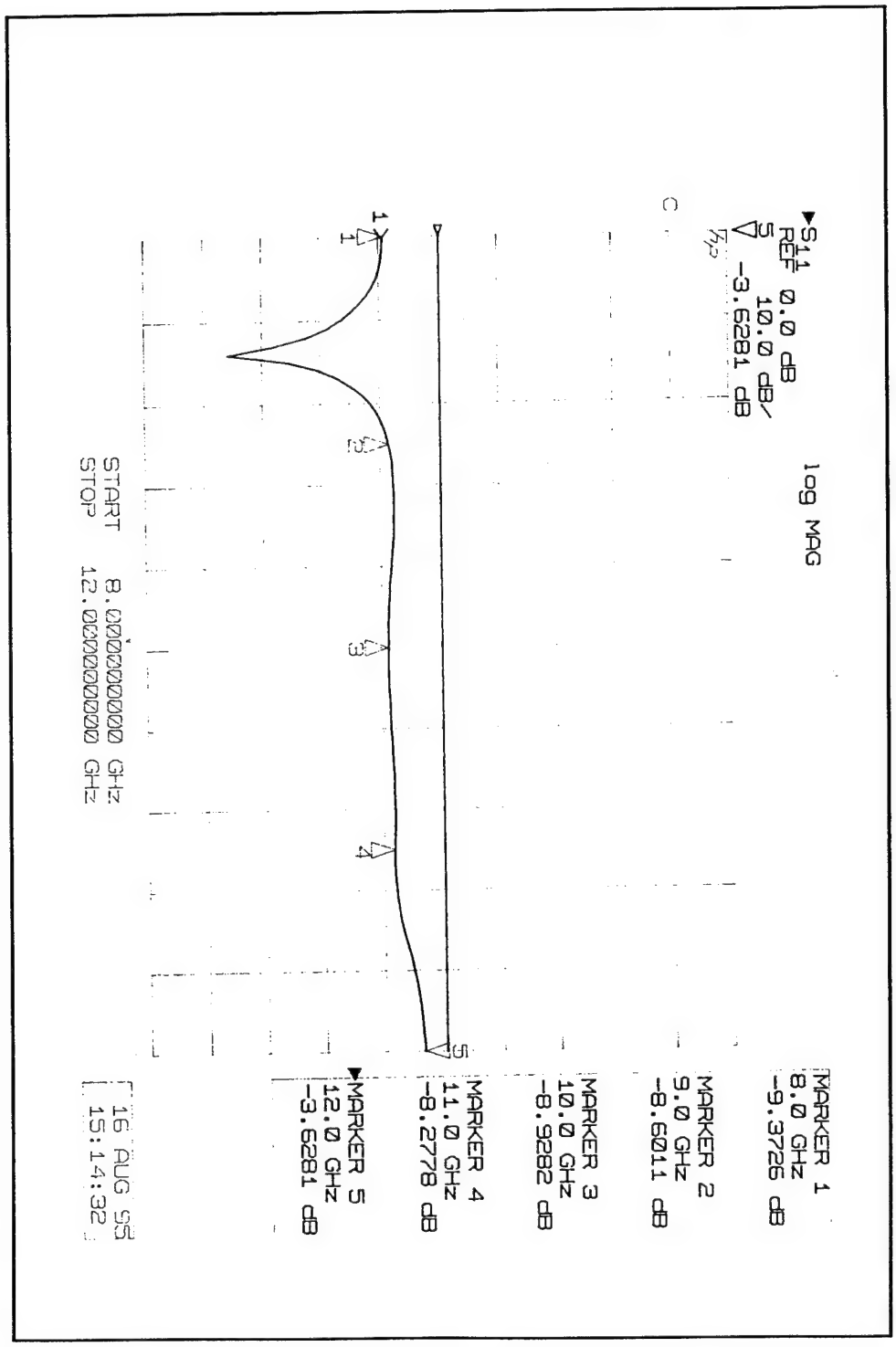

Figure 58. Slot antenna reflection loss measurement - 8 to 12 GHz

LIST OF REFERENCES

1. Koert, Peter, and Cha, James T., "Millimeter Wave Technology for Space Power Beaming," IEEE Transactions on Microwave Theory and Techniques, Vol. 40, No. 6, June 1992.

2. Brown, William C., and Eves, Eugene E., "Beamed Microwave Power Transmission and its Application to Space," IEEE Transactions on Microwave Theory and Techniques, Vol. 40, No. 6, June 1992.

3. Liao, S., *Microwave Devices and Circuits*, Prentice Hall Publishing, Englewood Cliffs, NJ, 1980.

4. Jenn, David C., *Radar and Laser Cross Section*, American Institute of Aeronautics and Astronautics (AIAA), New York, NY, 1995.

5. Stutzman, Warren L., and Thiele, Gary A., *Antenna Theory and Design*, John Wiley and Sons, New York, NY, 1981.

6. Balanis, Constantine A., *Antenna Theory Analysis and Design*, Harper and Row, Dallas, TX, 1982.

7. Johnson, W. A., Wilton, D. R., and Sharpe, R. M., "Patch Code Users' Manual," Technical Report SAND87-2991, Sandia National Laboratories, Albuquerque, NM, May 1988.

8. *Microwave network analyzer applications*, Application Note 117-1, Hewlett Packard Company, Jan 1978.

9. Brown, William C., "Experiments Involving a Microwave Beam to Power and Position a Helicopter," IEEE Transactions on Aerospace and Electronic Systems, Vol. AES-5, No. 5, September 1969.

INITIAL DISTRIBUTION LIST

1.	Defense Technical Information Center Cameron Station Alexandria, VA 22304-6145	2
2.	Library, Code 013 Naval Postgraduate School Monterey, CA 93943-5101	2
3.	Department Chairman, Code EC Department of Electrical and Computer Engineering Naval Postgraduate School Monterey, CA 93943-5121	1
4.	Professor David C. Jenn, Code EC/Jn Department of Electrical and Computer Engineering Naval Postgraduate School Monterey, CA 93943-5121	3
5.	Professor Rama Janaswamy, Code EC/Js Department of Electrical and Computer Engineering Naval Postgraduate School Monterey, CA 93943-5121	1
6.	Professor Gurnam Gill, Code EC/Gl Department of Electrical and Computer Engineering Naval Postgraduate School Monterey, CA 93943-5121	1
7.	Dr. Gary Lee Lutronix Corporation,13627 Portofino Dr. Del Mar, CA 92014	1
8.	Technical Library, Code 474710E Naval Air Warfare Center - Weapons Division Point Mugu, CA 93042-5000	1
9.	Col. William L. Gibson (Ret) Science Applications International Corporation (SAIC) 2301 Yale Blvd S.E., Suite F Albuquerque, NM 87106	1
10.	Professor John M. Levosky 51 Cypress Point Wimberley, TX 78676	1

11. Betty L. Gibson
429 Chermont
El Paso, TX 79912 1

12. Thad B. Gibson
5467 Camino Compadre
Camarillo, CA 93012 2